Universiteit
Leiden
The Netherlands

Cancer detection and visualization : molecular diagnostics and imaging techniques in pancreatic cancer and metastases

Sibinga Mulder, B.G.

Citation
Sibinga Mulder, B. G. (2019, November 20). *Cancer detection and visualization : molecular diagnostics and imaging techniques in pancreatic cancer and metastases*. Retrieved from https://hdl.handle.net/1887/80690

Version:	Publisher's Version
License:	Licence agreement concerning inclusion of doctoral thesis in the Institutional Repository of the University of Leiden
Downloaded from:	https://hdl.handle.net/1887/80690

Note: To cite this publication please use the final published version (if applicable).

Cover Page

Universiteit Leiden

The handle http://hdl.handle.net/1887/80690 holds various files of this Leiden University dissertation.

Author: Sibinga Mulder, B.G.
Title: Cancer detection and visualization : molecular diagnostics and imaging techniques in pancreatic cancer and metastases
Issue Date: 2019-11-20

Cancer detection & visualization

Molecular diagnostics and imaging techniques in pancreatic cancer and metastases

ISBN 978-94-6361-338-5
Design: Esther van Lierop
Lay-out and printing: Optima Drukkers

All rights reserved. No parts of this thesis may be reproduced, distributed, stored in a retrieval system or transmitted in any form or by any means, without prior written permission of the author.

The research in this thesis was financially supported by Dutch Cancer Society, European Research Council and National Institutes of Health.

Financial support by LI-COR, SurgVision, Quest Medical Imaging, Alphatron Medical, Vital Images, Erbe Nederland B.V., Servier Nederland Farma, KARL STORZ Endoscopie Nederland B.V., Blaak&Partners, Sysmex, Stöpler Medical, Mirada Medical, Canon Medical Systems, ChipSoft for the printing of this thesis is gratefully acknowledged.

Cancer detection & visualization

Molecular diagnostics and imaging techniques in pancreatic cancer and metastases

PROEFSCHRIFT

Ter verkrijging van de graad van Doctor
Aan de universiteit Leiden, op gezag van
Rector Magnificus prof. mr C.J.J.M. Stolker,
volgens besluit van het College voor Promoties
te verdedigen op woensdag 22 november 2019
Klokke 16:15 uur

DOOR

Babs Gianna Sibinga Mulder
geboren te Leiden
in 1992

PROMOTOR

Prof. dr. C.J.H. van de Velde

CO-PROMOTORES

Dr. A.L. Vahrmeijer
Dr. J.S.D. Mieog

LEDEN PROMOTIECOMMISSIE

Prof dr. J. Burggraaf
Prof. dr. C. Verhoef (Erasmus Medisch Centrum, Rotterdam)
Prof. dr. S. Hernot (Vrije Universiteit, Brussel)

TABLE OF CONTENT

1.	General introduction and thesis outline	7
Part I.	**Molecular diagnostics**	
2.	Targeted Next-Generation Sequencing of FNA-derived DNA in pancreatic cancer	19
3.	Diagnostic value of Targeted Next-Generation Sequencing in patients with suspected pancreatic or periampullary cancer	31
4.	Accuracy of Targeted Next-Generation Sequencing in the diagnostic process for pancreatic cancer: A multi-center prospective cohort study	49
Part II.	**Preoperative imaging techniques**	
5.	Gadoxetic acid-enhanced magnetic resonance imaging significantly influences the clinical course in patients with colorectal liver metastases	65
6.	A dual-labeld cRGD-based PET/optical tracer for preoperative staging and intraoperative treatment of colorectal cancer	79
Part III.	**Intraoperative imaging techniques**	
7.	Staging laparoscopy with ultrasound and near-infrared fluorescence imaging to detect occult metastases in pancreatic and periampullary cancer	99
8.	Real-time surgical margin assessment using ICG-Fluorescence during minimally invasive resections of colorectal liver metastases	113
9.	Intraoperative optical fluorescent detection of pancreatic cancer tissue targeting vascular endothelial growth factor (VEGF): A multicenter feasibility dose-escalation study	129
10.	A prospective clinical trial to determine the effect of intraoperative ultrasound on surgical strategy and resection outcome in patients with pancreatic cancer	145
11.	Quantitative margin assessment of radiofrequency ablation of a solitary colorectal hepatic metastasis using Mirada RTx: A feasibility study	163
Part IV.	**Summary and appendices**	
12.	Summary and future perspectives	179
13.	Nederlandse samenvatting	193
	List of publications	199
	Curriculum vitae	203
	Dankwoord	205

1

General introduction and thesis outline

PANCREATIC CANCER

Patients with pancreatic cancer have a poor prognosis, only patients fit for surgery and whose tumor is resected completely, tend to live longer.(1) Unfortunately, 80-85% from the patients have either a locally advanced tumor or metastatic spread at time of diagnosis, and will no longer benefit from surgery.(2) In case surgery is indicated, radical resection of the tumor yields an 5-year overall survival rate of 26%, whereas 5-year survival rates are only 8% for patients with irradical resections of their tumor.(3)

The peri-operative process in patients with a suspicion of pancreatic cancer consists of several parts: diagnosis, staging, treatment proposal, including neoadjuvant therapy or palliation, and possible resection of the cancer. During the diagnostic work-up, only patients fit for surgery and with resectable tumors should be selected for surgery or neoadjuvant therapy. Importantly, hazardous surgery in patients with a benign condition, like focal pancreatitis, or in patients with an locally extensive or metastasized disease should be prevented.(4, 5)

Imaging, mostly CT-scanning and if indicated endoscopic ultrasound (EUS) or MRI-scanning, plays a key role in the diagnosis and staging of patients with pancreatic cancer.(6) Despite technical improvements, small metastases or subtle local expansion of the tumor can still be missed, which ideally should be prevented.(7)

During EUS, cytology samples via fine-needle aspirations are taken from the suspect mass for morphological assessment.(8) However, morphologic assessment of cytology can be shortcoming and false or inconclusive results occur in 12-33% of the cases, which are mainly caused by sampling error, suboptimal sample quality, low cellular yield and the presence of an intense desmoplastic stromal reaction.(9-12) Due to shortcomings in imaging and pathology assessment, still 5-10% of the resections is performed for a benign lesion.(5) Molecular diagnostics, like Targeted Next-Generation Sequencing (NGS) could aid in reducing this number.(8, 13)

Staging laparoscopy can be performed immediately prior to surgery, this is not yet standardly performed worldwide. During this minimal-invasive procedure the abdominal cavity can be inspected to detect occult hepatic or peritoneal metastases, or locally advanced disease. In the presence of a metastasized or locally advanced disease further surgery should be renounced.(14)

Resection can be performed in patients with proven, non-metastasized, pancreatic cancer. The chance of obtaining a radical resection can be increased by optimal visualisation of the tumor. Several intraoperative techniques can contribute to this, for example intraoperative ultrasound or near-infrared fluorescence (NIRF) imaging.(15, 16) These techniques can aid in discriminating between peri-tumoral inflammation, fibrosis and vital cancer cells. In addition, they can be of special value for patients who are neoadjuvantly treated and aid in determining the degree of vascular involvement.(17)

COLORECTAL LIVER METASTASES

Patients with colorectal cancer liver metastases (CRLM) can experience long-term survival after surgery.(18) First choice of treatment for resectable CRLM is either surgical resection or ablation. Preoperative staging and surgical planning are key players in the achievement of prolonged survival and prevention of re-interventions.(19) Based on preoperative imaging the most suitable treatment plan should be proposed, consisting of either local therapy, conversion therapy, palliation or expectative treatment for benign conditions. For local therapy, complete and radical tumor removal is of importance for prognosis and disease free survival.(20, 21)

Several peri-operative techniques can aid the surgical team in localizing tumors and performing radical resections, of which improved MRI scanning and the use of intraoperative NIRF imaging are two.(22, 23) In case of ablation procedures, mostly no tissue is present for histopathological assessment and status about radicality cannot be determined. Success of complete tumor removal is currently determined mostly by visual post-procedural comparison of radiological images of the tumor and ablation zones.(24)

THESIS OUTLINE

The objective of this thesis is to improve the peri-operative process of patients with pancreatic cancer and colorectal liver metastases: from preoperative molecular diagnostics and imaging techniques to intraoperative imaging-guided resections and post-procedural evaluation of therapeutic success.

This thesis is divided in four parts:

Part I focuses on molecular diagnostics in patients with a suspect pancreatic lesion: targeted Next-Generation Sequencing, which sequences DNA to identify pathogenic variants in hot-spot genes. In **chapter 2 and 3** the validation of integrating NGS results into the diagnostic process for optimisation of treatment plan proposition is described. In **chapter 4** the results of a multicenter study are reported, in this study NGS is integrated in the diagnostic process of patients with an inconclusive diagnosis.

Part II focuses on preoperative imaging techniques. **Chapter 5** outlines the importance of preoperative imaging for staging, treatment proposition, surgical planning and surgical strategy. **Chapter 6** links pre-operative imaging to intraoperative imaging by describing the use of a hybrid tracer.

Part III discusses various intraoperative imaging techniques. In **chapter 7** the focus is on preventing surgery in patients with metastatic disease by performing staging laparoscopy with NIRF imaging, immediately prior to the laparotomy. **Chapter 8 and 9** focus on radical tumor removal by the use of NIRF imaging. In **chapter 8** a non-specific fluorescent dye is used for colorectal liver metastases detection and resection. In **chapter 9** the use of a tumor-specific fluorescent dye for detection and resection of pancreatic cancer is described. **Chapter 10** also focuses on pancreatic cancer visualisation and resection using intraoperative ultrasound. **Chapter 11** evaluates percutaneous radiofrequency ablations of CRLM and correlates the completeness of ablations to local recurrence.

The content of these three parts are visualized in Figure 1.

Part IV summarizes all results and discusses the future perspectives. This part focusses in particular on one of the most important and recurring described imaging technique in this thesis; near-infrared fluorescence imaging. This upcoming technique, quickly evolves and provides intraoperative guidance during various facets of surgery.

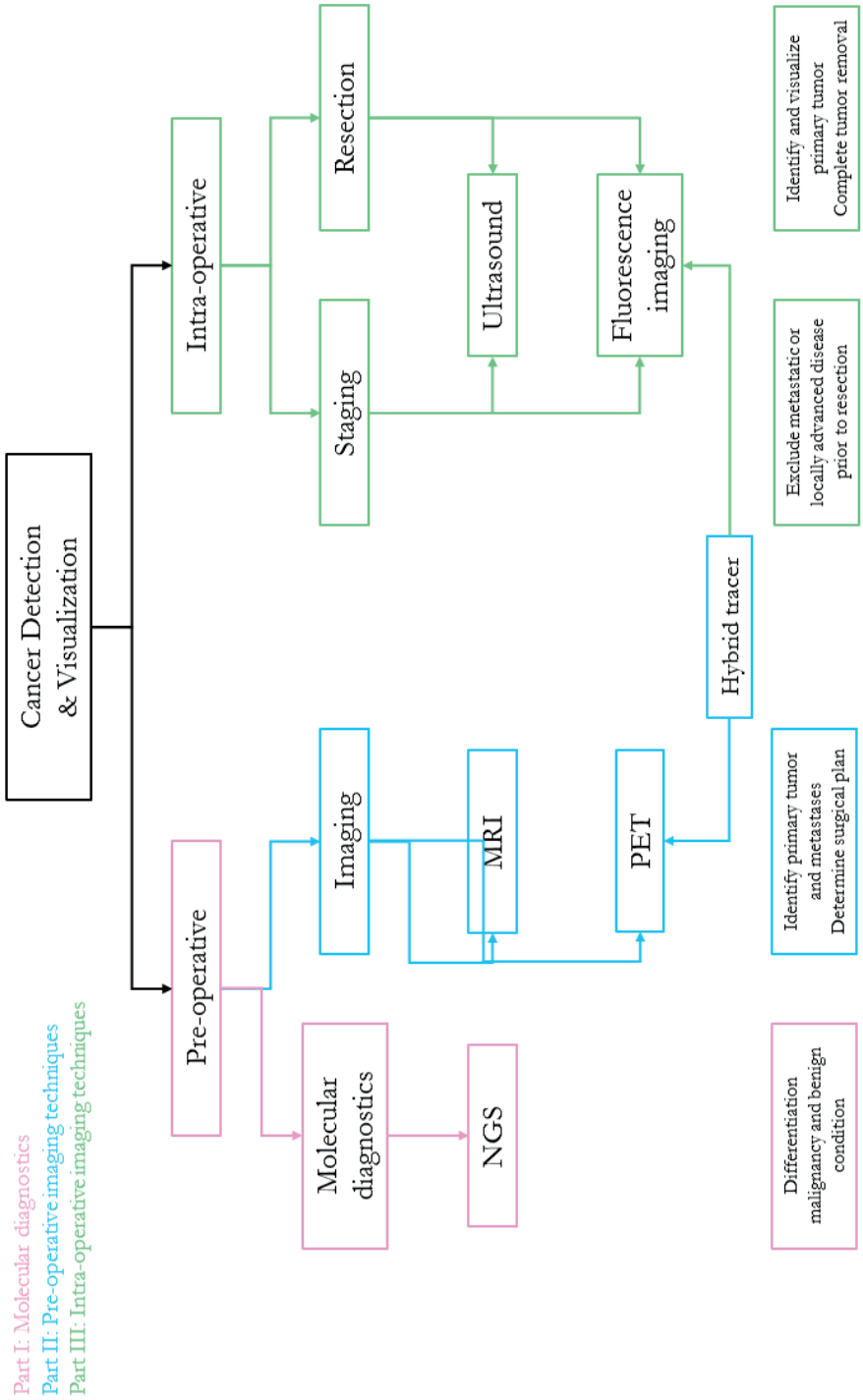

Figure 1. Thesis outline: Cancer Detection & Visualization

REFERENCES

1. Kim KS, Kwon J, Kim K, Chie EK. Impact of Resection Margin Distance on Survival of Pancreatic Cancer: a Systematic Review and Meta-Analysis. Cancer Res Treat. 2016.
2. Wray CJ, Ahmad SA, Matthews JB, Lowy AM. Surgery for pancreatic cancer: recent controversies and current practice. Gastroenterology. 2005;128(6):1626-41.
3. Konstantinidis IT, Warshaw AL, Allen JN, Blaszkowsky LS, Castillo CF, Deshpande V, et al. Pancreatic ductal adenocarcinoma: is there a survival difference for R1 resections versus locally advanced unresectable tumors? What is a "true" R0 resection? Ann Surg. 2013;257(4):731-6.
4. Abraham SC, Wilentz RE, Yeo CJ, Sohn TA, Cameron JL, Boitnott JK, et al. Pancreaticoduodenectomy (Whipple resections) in patients without malignancy: are they all 'chronic pancreatitis'? Am J Surg Pathol. 2003;27(1):110-20.
5. Kennedy T, Preczewski L, Stocker SJ, Rao SM, Parsons WG, Wayne JD, et al. Incidence of benign inflammatory disease in patients undergoing Whipple procedure for clinically suspected carcinoma: a single-institution experience. Am J Surg. 2006;191(3):437-41.
6. Feldman MK, Gandhi NS. Imaging Evaluation of Pancreatic Cancer. Surg Clin North Am. 2016;96(6):1235-56.
7. van der Geest LGM, Lemmens V, de Hingh I, van Laarhoven C, Bollen TL, Nio CY, et al. Nationwide outcomes in patients undergoing surgical exploration without resection for pancreatic cancer. Br J Surg. 2017;104(11):1568-77.
8. Iqbal S, Friedel D, Gupta M, Ogden L, Stavropoulos SN. Endoscopic-ultrasound-guided fine-needle aspiration and the role of the cytopathologist in solid pancreatic lesion diagnosis. Patholog Res Int. 2012;2012:317167.
9. Afify AM, al-Khafaji BM, Kim B, Scheiman JM. Endoscopic ultrasound-guided fine needle aspiration of the pancreas. Diagnostic utility and accuracy. Acta Cytol. 2003;47(3):341-8.
10. Woolf KM, Liang H, Sletten ZJ, Russell DK, Bonfiglio TA, Zhou Z. False-negative rate of endoscopic ultrasound-guided fine-needle aspiration for pancreatic solid and cystic lesions with matched surgical resections as the gold standard: one institution's experience. Cancer Cytopathol. 2013;121(8):449-58.
11. Brand B, Pfaff T, Binmoeller KF, Sriram PV, Fritscher-Ravens A, Knofel WT, et al. Endoscopic ultrasound for differential diagnosis of focal pancreatic lesions, confirmed by surgery. Scand J Gastroenterol. 2000;35(11):1221-8.
12. Fritscher-Ravens A, Brand L, Knofel WT, Bobrowski C, Topalidis T, Thonke F, et al. Comparison of endoscopic ultrasound-guided fine needle aspiration for focal pancreatic lesions in patients with normal parenchyma and chronic pancreatitis. Am J Gastroenterol. 2002;97(11):2768-75.
13. Saftoiu A, Vilmann P. Role of endoscopic ultrasound in the diagnosis and staging of pancreatic cancer. J Clin Ultrasound. 2009;37(1):1-17.
14. Gaujoux S, Allen PJ. Role of staging laparoscopy in peri-pancreatic and hepatobiliary malignancy. World J Gastrointest Surg. 2010;2(9):283-90.
15. de Werra C, Quarto G, Aloia S, Perrotta S, Del Giudice R, Di Filippo G, et al. The use of intraoperative ultrasound for diagnosis and stadiation in pancreatic head neoformations. Int J Surg. 2015;21 Suppl 1:S55-8.
16. Charlotte E.S. Hoogstins LSFB, Babs G. Sibinga Mulder, J. Sven D. Mieog, Rutger Jan Swijnenburg, Cornelis J.H. van de Velde, Arantza Farina Sarasqueta,

Bert A. Bonsing, Berenice Framery, André Pèlegrin, Marian Gutowski, Françoise Cailler, Jacobus Burggraaf, Alexander L. Vahrmeijer. Image-guided surgery in patients with pancreatic cancer: a clinical trial using SGM-101, a novel carcinoembryonic antigen-targeting, near-infrared fluorescent agent in process. 2017.

17. Katz MH, Fleming JB, Bhosale P, Varadhachary G, Lee JE, Wolff R, et al. Response of borderline resectable pancreatic cancer to neoadjuvant therapy is not reflected by radiographic indicators. Cancer. 2012;118(23):5749-56.
18. Creasy JM, Sadot E, Koerkamp BG, Chou JF, Gonen M, Kemeny NE, et al. Actual 10-year survival after hepatic resection of colorectal liver metastases: what factors preclude cure? Surgery. 2018;163(6):1238-44.
19. Jones RP, Kokudo N, Folprecht G, Mise Y, Unno M, Malik HZ, et al. Colorectal Liver Metastases: A Critical Review of State of the Art. Liver Cancer. 2016;6(1):66-71.
20. Hamady ZZ, Lodge JP, Welsh FK, Toogood GJ, White A, John T, et al. One-millimeter cancer-free margin is curative for colorectal liver metastases: a propensity score case-match approach. Ann Surg. 2014;259(3):543-8.
21. Margonis GA, Sergentanis TN, Ntanasis-Stathopoulos I, Andreatos N, Tzanninis IG, Sasaki K, et al. Impact of Surgical Margin Width on Recurrence and Overall Survival Following R0 Hepatic Resection of Colorectal Metastases: A Systematic Review and Meta-analysis. Ann Surg. 2018;267(6):1047-55.
22. Knowles B, Welsh FK, Chandrakumaran K, John TG, Rees M. Detailed liver-specific imaging prior to pre-operative chemotherapy for colorectal liver metastases reduces intra-hepatic recurrence and the need for a repeat hepatectomy. HPB (Oxford). 2012;14(5):298-309.
23. van der Vorst JR, Schaafsma BE, Hutteman M, Verbeek FP, Liefers GJ, Hartgrink HH, et al. Near-infrared fluorescence-guided resection of colorectal liver metastases. Cancer. 2013;119(18):3411-8.
24. Yedururi S, Terpenning S, Gupta S, Fox P, Martin SS, Conrad C, et al. Radiofrequency Ablation of Hepatic Tumor: Subjective Assessment of the Perilesional Vascular Network on Contrast-Enhanced Computed Tomography Before and After Ablation Can Reliably Predict the Risk of Local Recurrence. J Comput Assist Tomogr. 2017;41(4):607-13.

I

Molecular diagnostics

2

Targeted Next-Generation Sequencing of FNA-derived DNA in pancreatic cancer

B.G. Sibinga Mulder, J.S.D. Mieog, H.J.M. Handgraaf, A. Farina Sarasqueta, H. Vasen, T.P. Potjer, R.J. Swijnenburg, S.A.C. Luelmo, S. Feshtali, A. Inderson, A.L. Vahrmeijer, B.A. Bonsing, T. van Wezel, H. Morreau

Journal of Clinical Pathology, 2017 Feb.

ABSTRACT

To improve the diagnostic value of fine needle aspiration (FNA)-derived material, we perform Targeted Next-Generation Sequencing (NGS) in patients with a suspect lesion of the pancreas. NGS analysis can lead to a change in the treatment plan or supports inconclusive or uncertain cytology results. We describe the advantages of NGS using one particular patient with a recurrent pancreatic lesion seven years after resection of a pancreatic ductal adenocarcinoma (PDAC). Our NGS analysis revealed the presence of a presumed second primary cancer in the pancreatic remnant, which led to a change in treatment: resection with curative intend instead of palliation. Additionally, NGS identified an unexpected germline *CDKN2A* 19-base pair deletion, which predisposed the patient to developing PDAC. Preoperative NGS analysis of FNA-derived DNA can help identify patients at risk for developing PDAC and define future therapeutic options.

BACKGROUND

Cancer-causing genetic variations in human cells often cluster in predictable gene "hotspots". In lung cancer and pancreaticobiliary tract cancer, single-gene analysis of endoscopic ultrasound-guided fine needle aspiration (FNA)-derived DNA samples has yielded valuable diagnostic information(1, 2). Moreover, performing Targeted Next-Generation Sequencing (NGS) on these samples can identify multiple-gene variants in a limited quantity of material(3). NGS can indeed be reliably performed on FNAs from pulmonary and pancreatic tumors, as the gene variants identified correlated well with matched resected pancreatic tumors.(4, 5) The advantage of using a NGS panel that specifically targets hotspot mutations in 50 cancer genes is that robust ultra-deep sequencing results can be obtained from samples containing extremely low numbers of cancer cells, including DNA obtained from formalin-fixed paraffin-embedded tissue samples of neoplasms of the pancreas.(6)

In the past decade, the mutational landscape of PDAC has been well characterized.(7) Activated pathogenic variants in the proto-oncogene *Kirsten RAS* (*KRAS*) are present in 90% of patients with PDAC. Inactivated variants in the tumor-suppressor genes *TP53*, *CDKN2A*, and *SMAD4* have been frequently identified. Recently, published whole-exome and whole-genome sequencing data revealed additional somatic and germline variants in *ARID1A*, *ROBO2*, *BRCA1*, *BRCA2*, and *PALB1*, some of which can direct the optimal choice of adjuvant therapy. Moreover, focal gene amplifications of actionable oncogenes have been identified, including *ERBB2*, *MET*, *FGFR1*, *CDK6*, *PIK3R3*, and *PIK3CA*.(7, 8)

As part of an ongoing study, NGS analysis is performed in preoperative FNA-derived DNA samples obtained from patients with a suspicion of PDAC at our center. Here, we describe a case of one such patient in which NGS analysis revealed the presence of a second primary PDAC drastically changing the treatment plan.

CASE REPORT

A 54-year-old male patient underwent a pancreaticoduodenectomy with en bloc right hemicolectomy seven years ago, followed by adjuvant gemcitabine therapy. Pathological evaluation revealed a 5-cm PDAC with negative surgical resection margins and 6 out of 21 positive peri-pancreatic lymph nodes. After five years without recurrence of the disease, the patient was discharged from follow-up. Recently, the patient presented with vague abdominal pain. A computed tomography scan revealed a poorly defined mass in the pancreatic remnant close to the pancreatic-jejunal anastomosis suggestive of a local recurrence (Figure 1A). An endoscopic ultrasound-guided FNA was performed. Cytological evaluation was not conclusive for carcinoma and was interpreted as "reactive changes" with a low number of atypical ductal cells (Figure 1B). Given the clinical suspicion of recurrent malignancy, palliative che-

motherapy was considered as the first therapeutic option during the multidisciplinary team meeting. However, in light of the long interval between the current lesion and the original primary tumor, and despite the limited number of morphologically atypical cells in the FNA sample (estimated at <10% of the cells), we opted to analyze the FNA-derived DNA using targeted NGS with the AmpliSeqCancer Hotspot Panel v2 (Thermo Fisher Scientific Inc., Cambridge, MA). The patient provided informed consent for molecular testing.

We also analyzed the primary PDAC using NGS. Our analysis revealed that the mutational profiles differed between the original lesion and the new lesion. Furthermore, we found a germline pathogenic *CDKN2A*/*P16* gene variant that predisposed the patient for developing PDAC. The patient had no documented personal history of atypical moles or melanoma. No family history of breast-ovarian carcinoma syndrome or atypical multiple mole melanoma syndrome was reported. Only after consulting the clinical genetics in a later phase, the patient turned out to have an aunt and nephew who died of melanoma and PDAC respectively at relatively young ages. At the molecular level, a second primary tumor was considered to be plausible. Based on the NGS data, the treatment plan changed drastically from providing palliative chemotherapy to curative-intended surgical resection of the residual pancreas.

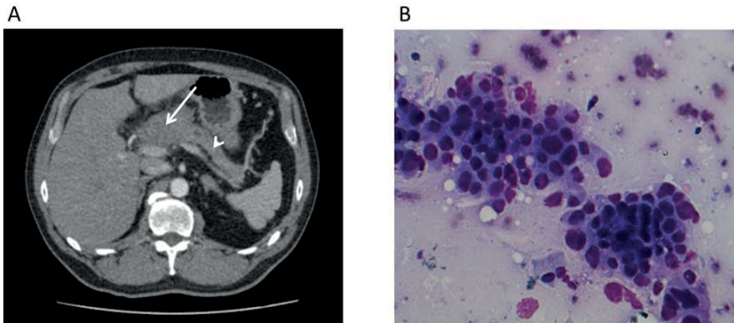

Figure 1. CT scan and cytological findings in a patient with a suspicion of recurrent PDAC. (A) Axial CT scan of the abdomen showed the suspect recurrent tumor (arrow) in the duodenal anastomosis with the remnant pancreatic tail (arrowhead). (B) Giemsa stain of FNA-derived cells obtained from the pancreatic lesion. A low number of atypical ductular cells were visible in the complete slide; based on their morphology, these cells were not judged to be unequivocally dysplastic.

METHODS

Selection of tumor cells, DNA isolation and Targeted Next-Generation Sequencing

FNA slides were generated using methanol fixation and Giemsa staining. In general, there are two approaches for molecular analysis of cytology smears, either with or without tumor cell enrichment. The enrichment step is chosen if tumor cells can clearly be distinguished

from non-tumor cells. In the case described here no enrichment step for the FNA sample could be performed. A single FNA slide was used, which was photographed and attached to the patient files. Subsequently, the cover slip was removed by incubation in xylene at room temperature in a separate 50-ml tube to avoid contamination. The incubation period was till the moment the cover slip got loose. Next, the slide was washed in alcohol three times for rehydration of the tissue, once in 100%, once in 70% and once in 50%. The FNA material was scraped from the slide and collected in a micro tube for DNA isolation. Because there was no enrichment step, which resulted in a low percentage of atypical cells, bioinformatics thresholds were adopted accordingly. The PDAC resection specimens were examined for regions with the highest tumor percentages. After examination, five 10μm additional sections were prepared for microdissection and stained with hematoxylin (eosin staining was omitted to preserve the integrity of the DNA). Slides were visualized with an inverted microscope and manually microdissected with a sharp, pointed knife.

After scraping, DNA was isolated from FNA-derived material and formalin-fixed, paraffin-embedded PDAC tissue using a fully automated DNA extraction procedure.(9) The concentration of DNA was measured using a fluorometer (Qubit dsDNA HS, Life Technologies, Carlsbad, CA). The AmpliSeq Cancer Hotspot Panel v2 consists of a single primer pool and is designed to detect somatic cancer hotspot mutations in 200 amplicons covering 50 genes, including genes that are often altered in PDAC (e.g., *KRAS*, *TP53*, *SMAD4*, and *CDNK2A*). Libraries were prepared with 10 ng of genomic DNA, and each sample was uniquely barcoded using IonXpress barcodes (Life Technologies). Ion PGM 318 or Proton P1 chips were prepared using the Ion Chef system and sequenced using the Personal Genome Machine or Proton system, respectively (all from Life Technologies). Variants were analyzed using the Geneticist Assistant NGS Interpretative Workbench (version 1.1.8, SoftGenetics, State College, PA). The identified variants were classified into five classes, and only class 4 (likely pathogenic) and class 5 (pathogenic) variants were reported.(10)

Evaluation of genetic variants in the context of morphology

Genetic variations in the *KRAS* or *GNAS* gene can occur in precursor lesions of PDAC, including low- or high-grade pancreatic intraepithelial neoplasia, intraductal papillary mucinous neoplasm, and mucinous cystic neoplasms.(6) Because a stepwise increase in genetic variations occurs during the development of PDAC, we developed a clinical decision scheme in which confirmed genetic variants are placed in the context of the observed morphology and tumor percentage. The sole finding of a pathogenic *KRAS* variant is molecularly scored as a "proliferative lesion, at least low-grade dysplasia", keeping in mind that *KRAS* variants are also present in a low percentage of cases with pancreatitis.(11) A combination of two or more pathogenic variants (e.g., a *KRAS* variant in combination with *TP53, SMAD4*, *CDKN2A*, and/or other variants) is scored as "at least high-grade dysplasia". If genetic variants are absent, it is scored as "no molecular support of a proliferative lesion". In the

multidisciplinary team meeting, the molecular findings are discussed in the context of the clinical and radiological findings.

RESULTS

NGS of FNA-derived DNA

The obtained FNA sample of the suspected recurrent PDAC was morphologically scored as atypia with no clear dysplasia or malignancy present. However, NGS analysis revealed the presence of a class 5 *KRAS*:c.35G>A p.Gly12Asp pathogenic variant and a class 4 *TP53* (intron, splice-site) c.376-1G>T variant in 3.2% and 3.8% of all reads, respectively. The variant calling in our analysis pipeline was confirmed by manual inspection and revealed that the variants were present in both directions. The finding of these gene variants prompted us to change our initial morphological evaluation of atypia to a molecular evaluation of at least high-grade dysplasia. Surprisingly, we also identified a 19-bp deletion in the *CDKN2A* gene (exon 2; c.225_243del19, p.Ala76fs*64) in 47% of all DNA reads. The difference in frequency between this *CDKN2A* variant and the *KRAS* and *TP53* variants suggested that the *CDKN2A* deletion was germline in origin. This particular *CDKN2A* deletion variant is a known germline variant present in Dutch familial atypical multiple mole melanoma families and is known as the p16-Leiden variant.

A similar NGS analysis of the primary PDAC revealed the same *KRAS:*c.35G>A pathogenic variant, but not the *TP53* variant with an on target depth of coverage of 2,000 DNA reads. Furthermore, a class 5 *SMAD4* c.1242_1245del4bp (p.Asp415fs) pathogenic variant was found in 30% of all DNA reads in the original PDAC sample, but not in the recent FNA sample with a depth of coverage of 303 DNA reads. Lastly, the presumed *CDKN2A* germline deletion variant was also found in the original PDAC sample (Figure 2). The patient was referred to the department of clinical genetics for analysis of leucocyte DNA, which confirmed the germ line origin of the *CDKN2A* deletion.

Although a second primary tumor is a possibility, clonal heterogeneity of the first tumor is an important alternative. The *KRAS* c.35G>A variant, which was identified in both lesions would support this option, although it is the most commonly found *KRAS* variant in PDAC. However, due to the long interval between the two lesions (7 years) the patient's genetic predisposition, and the different mutation patterns between the two lesions, we concluded that a second primary PDAC was more likely than recurrence of the original primary PDAC with molecular clonal divergence.

As a result of our analysis, the patient underwent surgical resection instead of palliative chemotherapy. Postoperative examination of the lesion revealed a 2 cm sized PDAC without lymph node metastases, extensive inflammation of the residual pancreas, and focally a tumor-positive resection margin at the pancreatic-jejunal anastomosis. The presence of all

gene variants in *KRAS*, *TP53* and *CDKN2A* identified in the FNA sample was later confirmed in the resected material. Again, the class 5 *SMAD4* c.1242_1245del4bp (p.Asp415fs) pathogenic variant that was identified in the primary PDAC was not present in this sample (on target depth of coverage of 534 DNA reads).

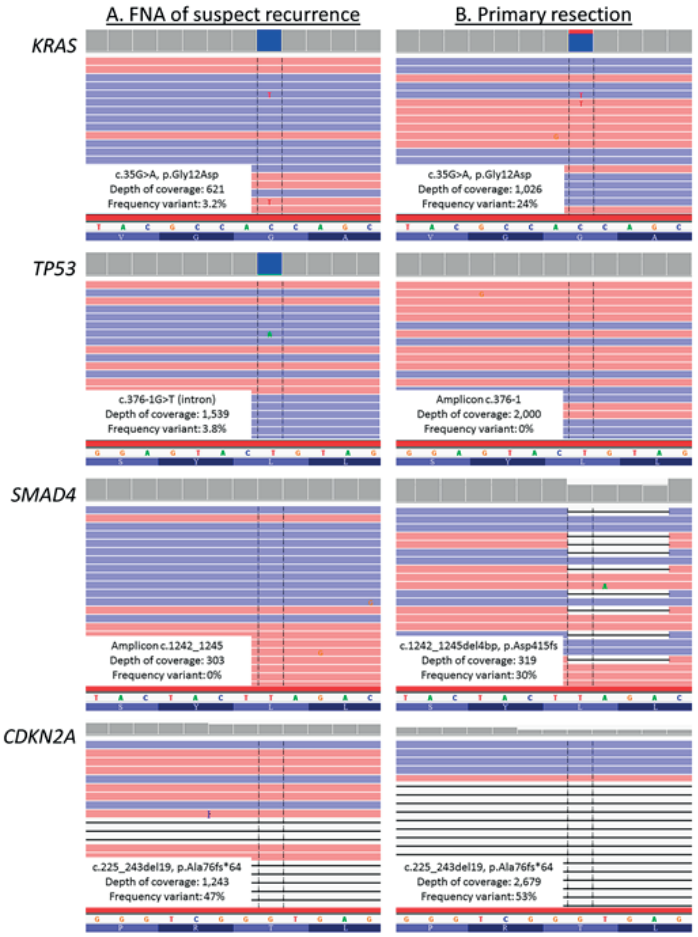

Figure 2. Overview of the NGS results.

NGS analysis of DNA obtained from the endoscopic ultrasound-guided FNA of the suspect pancreatic cancer recurrence (A) and the primary lesion obtained seven years ago (B). The analysis revealed the following variants in the suspect recurrent cancer: a class 5 *KRAS*: c.35G>A p.Gly12Asp pathogenic variation was present in 3.2% of DNA reads; a class 4 *TP53* (intron, splice-site) c.376-1G>T mutation was present in 3.8% of DNA reads; and a 19-bp deletion (c.225_243del19, p.Ala76fs*64) in *CDKN2A* (also known as the p16-Leiden mutation) was present in 47% of DNA reads. The following variants were identified in the primary lesion: the *KRAS* c.35G>A variant was present in 24% of the DNA reads; a class 5 *SMAD4* c.1242_1245del4bp p.Asp415fs pathogenic variant was present in 30% of DNA reads; and the 19-bp *CDKN2A* deletion was present in 53% of DNA reads.

DISCUSSION

This report illustrates that the application of an NGS panel designed for use in somatic tumor variant analysis also can identify unexpected germline variants. In the described case, a germline *CDKN2A* deletion variant (the p16-Leiden mutation) was detected by our NGS analysis. *CDKN2A* encoding for p16 is completely inactivated in PDAC by a variety of mechanisms.(12) Carriers of a germline variant in *CDKN2A* (i.e., p16-Leiden) have an increased risk of developing multiple tumor types at a young age, and a cumulative lifetime risk of developing pancreatic cancer of 15–20%.(13) Therefore, carriers of the p16-Leiden mutation are offered the opportunity to participate in a screening program that includes annual magnetic resonance imaging.(14) An increased prevalence of second primary tumors has been described among patients with a genetic predisposition for PDAC.(15) Therefore, total pancreatectomy should be considered in PDAC patients with a known germline variant in the *BRCA2*, *PALB2*, *CDKN2A*, *STK11*, *ATM*, or *PRSS1* gene, given the significantly increased risk of developing PDAC.(15)

It has to be discussed whether and how patients should be informed about potential results of tumor NGS, because some of these findings can be beneficial for families of these patients, e.g. by enrolling in effective surveillance programs. On the other hand, identification and reporting of germline defects, such as *TP53* pathogenic variants associated with the Li-Fraumeni syndrome, is not always considered to be beneficial for patients and families involved. Molecular tumor boards and independent institutional expert review panels are currently installed in institutions worldwide to discuss such medical ethical and legal dilemmas.(16)

In an ongoing study at our institution, NGS analysis is performed successfully in all consecutive suspect PDAC patients. Similar to the described case, this analysis can lead to a change in the treatment plan in some patients. In other patients clinicians choose to wait for the NGS results due to inconclusive cytology and/or imaging results. In a large majority of patients, the NGS results supports the cytology and imaging results (data not shown). We perform NGS analysis using a focused gene panel targeting the mutation hotspot regions of 50 genes. For other diagnostic or therapeutic purposes, this panel could be expanded to include additional informative gene targets. However, the ability of such an expanded panel to identify low frequency gene variants in limited amounts of material is questionable. Therefore, the use of tumor cell enrichment techniques, such as microfluidic cell sorting, may increase the ability to identify gene variants and to stratify focal gene amplifications and/or deletions.(17)

Multiple preanalytical factors may influence the success of NGS analysis of FNA derived DNA.(18) In our institute, the use of automated nucleic acid extraction decreased the failure rate extensively.(9)

Despite its clear advantages, current NGS methods are time-consuming and delay the diagnostic process by at least five days. However, future advances in the technology will likely decrease this delay considerably. Moreover NGS-based diagnostics are currently not covered by health insurance in many countries, making the approach potentially impractical from a strictly financial perspective.

In conclusion, we believe that FNA NGS shows great potential to detect germline pathogenic variants in addition to somatic variants in solid tumors. Furthermore, this case shows that the genomic profile of abnormalities might help in distinguishing "de novo" tumors from metastases or recurrences. Future studies should include large patient series and additional testing of other gene panels.

REFERENCES

1. Kipp BR, Fritcher EG, Clayton AC, Gores GJ, Roberts LR, Zhang J, et al. Comparison of KRAS mutation analysis and FISH for detecting pancreatobiliary tract cancer in cytology specimens collected during endoscopic retrograde cholangiopancreatography. J Mol Diagn. 2010;12(6):780-6.
2. van Eijk R, Licht J, Schrumpf M, Talebian Yazdi M, Ruano D, Forte GI, et al. Rapid KRAS, EGFR, BRAF and PIK3CA mutation analysis of fine needle aspirates from non-small-cell lung cancer using allele-specific qPCR. PLoS One. 2011;6(3):e17791.
3. Luthra R, Chen H, Roy-Chowdhuri S, Singh RR. Next-Generation Sequencing in Clinical Molecular Diagnostics of Cancer: Advantages and Challenges. Cancers (Basel). 2015;7(4):2023-36.
4. Young G, Wang K, He J, Otto G, Hawryluk M, Zwirco Z, et al. Clinical next-generation sequencing successfully applied to fine-needle aspirations of pulmonary and pancreatic neoplasms. Cancer Cytopathol. 2013;121(12):688-94.
5. Gleeson FC, Kerr SE, Kipp BR, Voss JS, Minot DM, Tu ZJ, et al. Targeted next generation sequencing of endoscopic ultrasound acquired cytology from ampullary and pancreatic adenocarcinoma has the potential to aid patient stratification for optimal therapy selection. Oncotarget. 2016.
6. Amato E, Molin MD, Mafficini A, Yu J, Malleo G, Rusev B, et al. Targeted Next-Generation Sequencing of cancer genes dissects the molecular profiles of intraductal papillary neoplasms of the pancreas. J Pathol. 2014;233(3):217-27.
7. Waddell N, Pajic M, Patch AM, Chang DK, Kassahn KS, Bailey P, et al. Whole genomes redefine the mutational landscape of pancreatic cancer. Nature. 2015;518(7540):495-501.
8. Bailey P, Chang DK, Nones K, Johns AL, Patch AM, Gingras MC, et al. Genomic analyses identify molecular subtypes of pancreatic cancer. Nature. 2016;531(7592):47-52.
9. van Eijk R, Stevens L, Morreau H, van Wezel T. Assessment of a fully automated high-throughput DNA extraction method from formalin-fixed, paraffin-embedded tissue for KRAS, and BRAF somatic mutation analysis. Exp Mol Pathol. 2013;94(1):121-5.
10. Plon SE, Eccles DM, Easton D, Foulkes WD, Genuardi M, Greenblatt MS, et al. Sequence variant classification and reporting: recommendations for improving the interpretation of cancer susceptibility genetic test results. Hum Mutat. 2008;29(11):1282-91.
11. Kamisawa T, Tsuruta K, Okamoto A, Horiguchi S, Hayashi Y, Yun X, et al. Frequent and significant K-ras mutation in the pancreas, the bile duct, and the gallbladder in autoimmune pancreatitis. Pancreas. 2009;38(8):890-5.
12. de vos tot Nederveen Cappel WH, Offerhaus GJ, van Puijenbroek M, Caspers E, Gruis NA, De Snoo FA, et al. Pancreatic carcinoma in carriers of a specific 19 base pair deletion of CDKN2A/p16 (p16-leiden). Clin Cancer Res. 2003;9(10 Pt 1):3598-605.
13. Vasen HF, Gruis NA, Frants RR, van Der Velden PA, Hille ET, Bergman W. Risk of developing pancreatic cancer in families with familial atypical multiple mole melanoma associated with a specific 19 deletion of p16 (p16-Leiden). Int J Cancer. 2000;87(6):809-11.
14. Vasen H, Ibrahim I, Ponce CG, Slater EP, Matthai E, Carrato A, et al. Benefit of Surveillance for Pancreatic Cancer in

High-Risk Individuals: Outcome of Long-Term Prospective Follow-Up Studies From Three European Expert Centers. J Clin Oncol. 2016.

15. Potjer TP, Bartsch DK, Slater EP, Matthai E, Bonsing BA, Vasen HF. Limited resection of pancreatic cancer in high-risk patients can result in a second primary. Gut. 2015;64(8):1342-4.
16. Erdmann J. All aboard: Will molecular tumor boards help cancer patients? Nat Med. 2015;21(7):655-6.
17. Bolognesi C, Forcato C, Buson G, Fontana F, Mangano C, Doffini A, et al. Digital Sorting of Pure Cell Populations Enables Unambiguous Genetic Analysis of Heterogeneous Formalin-Fixed Paraffin-Embedded Tumors by Next Generation Sequencing. Sci Rep. 2016;6:20944.
18. Roy-Chowdhuri S, Goswami RS, Chen H, Patel KP, Routbort MJ, Singh RR, et al. Factors affecting the success of next-generation sequencing in cytology specimens. Cancer Cytopathol. 2015;123(11):659-68.

3

Diagnostic value of targeted Next-Generation Sequencing in patients with suspected pancreatic or periampullary cancer

B.G. Sibinga Mulder, J.S.D. Mieog, A. Farina Sarasqueta, H.J.M. Handgraaf, H. Vasen, R.J. Swijnenburg, S.A.C. Luelmo, S. Feshtali, A. Inderson, A.L. Vahrmeijer, B.A. Bonsing, T. van Wezel, H. Morreau

Journal of Clinical Pathology, 2018 March. Supplementary data available online.

ABSTRACT

Radiologic imaging and morphological assessment of cytology material have limitations for preoperative classification of pancreatic or periampullary lesions, often resulting in surgical resection without definitive diagnosis. Our prospective study aims to define the diagnostic value of Targeted Next-Generation Sequencing (NGS) of DNA from cytology material.

Patients with a suspect pancreatic or periampullary lesion underwent standard diagnostic evaluation including preoperative morphological cytology assessment. Treatment options for suspect lesions were surgical exploration with possible resection, follow-up, or palliation. The cytology samples were analysed with NGS, in which 50 genes were sequenced for the presence of pathogenic variants. The NGS results were integrated with the clinical information during multidisciplinary team meetings and changes in the treatment plan were scored. Diagnostic accuracy of NGS analysis (malignancy vs benign disease) was calculated.

NGS results of the cytology samples were confirmed in the resection specimens of the first ten included patients. The integration of the NGS results led to a change in treatment plan in seven out of 70 patients (from exploration to follow-up, n=4; from follow-up to exploration and resection, n=2; from palliation to resection, n=1). In four patients the NGS results were contradictory, but did not affect the treatment plan. In the remaining 59 patients NGS analysis supported the initial treatment plan. The diagnostic accuracy of NGS analysis was 94% (sensitivity=93%; specificity=100%).

NGS can change the treatment plan in a significant portion of patients with suspect pancreatic or periampullary lesions. Application of NGS can optimize treatment selection and diminish unnecessary surgeries.

INTRODUCTION

For patients with pancreatic ductal adenocarcinoma (PDAC) surgery is currently the only option to achieve long-term survival. In 5-11% of pancreatic resections for a clinically presumed malignancy, a benign lesion is found, resulting in unnecessary morbidity and mortality for these patients.(1, 2) Autoimmune pancreatitis, for example, can mimic the clinical signs of PDAC.(3) Therefore, an accurate distinction of (pre-)neoplastic lesions from non-malignant lesions would significantly improve the identification of patients that require surgery. Currently, the treatment plan for patients with a suspicion of PDAC or other periampullary tumors, is mainly based on radiologic imaging, the morphological analysis of preoperative cytology and clinical judgment. However, current imaging techniques are significantly limited in differentiating between PDAC and inflammation, benign lesions, or preneoplastic lesions.(4-6) Endoscopic ultrasound-guided fine needle aspiration (EUS-FNA) and biliary brush can be performed to obtain a preoperative pathological diagnosis. However, discriminating between reactive atypia due to inflammation and (pre)neoplastic dysplasia remains challenging, and classifying the grade of dysplasia and the presence of invasion is often not possible.(7-9) Therefore, false or inconclusive results occur in 12-33% of the cases and are mainly caused by sampling error, suboptimal sample quality, low cellular yield and the presence of an intense desmoplastic stromal reaction.(10-14) Additional immunohistochemistry testing of blocked FNA material can aid in further characterizing suspicious lesions.(15) However, FNA is in many cases not sufficiently diagnostic. Altogether, the accuracy of diagnostic procedures for suspect PDAC should be improved.

Targeted Next-Generation Sequencing (NGS) of FNA-derived DNA samples might be useful in distinguishing benign from malignant lesions.(16) The advantage of NGS is that only a limited quantity of material is required for ultra-deep DNA sequencing with NGS panels targeting hotspot gene variants. Even analysis of samples containing as little as 100 cancer cells or DNA obtained from formalin-fixed paraffin-embedded (FFPE) tissue can be done.(9, 17) The mutational landscape of PDAC was previously described and updated by Waddell et al.(18) Gene variants identified in PDAC mainly include *KRAS*, *TP53*, *CDKN2A* and *SMAD4*, but also variants in *ARID1A, ROBO2, BRCA1, BRCA2*, and *PALB1* and focal gene amplifications in *ERBB2, MET, FGFR1, CDK6, PIK3R3*, and *PIK3CA*.

The aim of this prospective cohort study was to determine the diagnostic value of targeted NGS DNA analysis of preoperative cytology material of patients with a suspect malignancy of the pancreas or periampullary region.

METHODS

Patients

Consecutive patients with a suspicious lesion in the pancreas or periampullary region and with diagnostic material (EUS FNA or brushes) were included in this study between January and August 2016. Because of the indication for diagnostic material the a priori chance of pancreatic or periampullary cancer was increased in these patients. All the patients were discussed during the multidisciplinary pancreatic cancer team (MDT) meeting at the Leiden University Medical Center (LUMC). The preoperative samples were assessed for routine pathological work-up and analysed using targeted NGS. NGS analysis for primary diagnostic and companion diagnostic stratification of human cancer is fully implemented in the department of Pathology of the LUMC. Therefore, the prospective analysis of cytology and biopsy samples was performed within the framework of routine clinical care. All patient samples and clinical data were handled in accordance with the medical ethics guidelines described in the Code of Conduct for the Proper Secondary Use of Human Tissue of the Dutch Federation of Biomedical Scientific Societies.(19) For this manuscript patient data were anonymized.

First, the feasibility and reproducibility of the NGS analysis were tested. The NGS results of the FNA or brush were compared with the NGS results of the resected specimen. For this purpose, the first ten patients who underwent a resection, were included in the 'initial cohort'. Subsequently, 60 patients were included in the 'additional cohort' to investigate the diagnostic value of NGS of FNA or brush material.

Conventional EUS-FNA analysis

An experienced gastroenterologist performed the FNA during EUS or brush during endoscopic retrograde cholangiopancreatography. In challenging cases, a pathologist was present during the procedure, checking the quality and representativeness of the sample. The cytology samples acquired with either FNA or brush were morphologically assessed by an experienced pathologist (HM, AFS) and reported in four categories: (1) no conclusion, (2) atypia / inflammation, (3) low grade dysplasia (LGD) and (4) at least high grade dysplasia (HGD).

Selection of tumor cells, DNA isolation and Targeted Next-Generation Sequencing

The method of selection of tumor cells, DNA isolation and the NGS analysis was previously described.(20) In short, a fully automated DNA extraction procedure was used to isolate DNA from FNA-derived material and FFPE (possible) malignant tissue.(21) The AmpliSeq™ Cancer Hotspot Panel v2 (ThermoFisher Scientific, USA) consists of a single primer pool and is designed to detect somatic cancer hotspot mutations in 200 amplicons covering 50 genes.

The minimum coverage threshold is 100 reads target, although in real practice the coverage is way higher. Minimum variant allele frequencies in molecular diagnostics is automatically set at 10% of all reads. All variants under 10% are visually inspected in the programme Integrated Genomics Viewer (IGV, http://software.broadinstitute.org/software/igv/) and assessed for validity in the context of tumor cell percentages. Variants appearing in both read directions have more chance to be considered as valid. Especially in the current study low tumor cell percentages is an issue. The identification of false positivity of low frequent C>T transitions in FFPE material can be a challenge. However, due to fixation of the cytologic material in methanol and not in formalin, false positivity of low level and aberrant C>T transitions is not (often) seen. The reliability of low frequent individual variants increases once additional pathogenic variants are seen in other genes with similar read on target frequencies.

Bioinformatic analysis of amplifications of *ERBB2, MET, FGFR1* and *PIK3CA* is also standardly performed on the cytological material, but the results are not reliably due to low tumor cell percentages. Variants were analysed using the Geneticist Assistant NGS Interpretative Workbench (version 1.1.8, SoftGenetics, State College, PA). The identified variants were classified into five classes, and only class 4 (likely pathogenic) and class 5 (pathogenic) variants were reported, using a three tiered molecular evaluation.(22) All identified pathogenic variants were included in the classification as follows: if no gene variant(s) were identified, it was reported as "no molecular support for dysplasia"; the sole finding of a *KRAS* or *GNAS* class 4 or 5 gene variant as "molecularly at least low grade dysplasia (LGD)"; more than one class 4 or 5 gene variant, for example a combination of *KRAS*, *PTEN*, *ATM*, *CDKN2A* or *APC*, or a single *TP53* or *SMAD4* variant as "molecularly at least high grade dysplasia (HGD)".(23)

Treatment plan

The MDT proposed an individual treatment plan based on the clinical presentation (including blood results for tumor markers), radiologic assessment and morphological assessment of cytology. Subsequently, the NGS results were integrated during the consecutive meeting and the treatment plan could be changed, confirmed or not altered.

The following treatment plans were considered in case of a malignancy: exploration, potentially followed by resection of the tumor, or palliation (chemotherapy, bypass surgery, stent placement or a combination) in case of a metastatic or irresectable disease. The treatment plan was follow-up, including clinical and radiological evaluation every three months, in case of pancreatitis or another benign lesion. All patients were monitored for a follow-up period longer than six months. The decision scheme is shown in Figure 1.

Final Diagnosis

Final diagnosis was defined as malignant or benign disease based on definitive pathological assessment of resected specimen or on the MDT opinion after six months follow-up (based on the course of disease or, if available, repeated imaging). Malignant was defined as a carcinoma of the pancreas, ampulla of Vater, distal choledochus or duodenum, and also in case of a malignant IPMN. Diagnostic accuracy was calculated, as were sensitivity and specificity for morphological assessment of cytology and NGS, using final diagnosis as a reference.

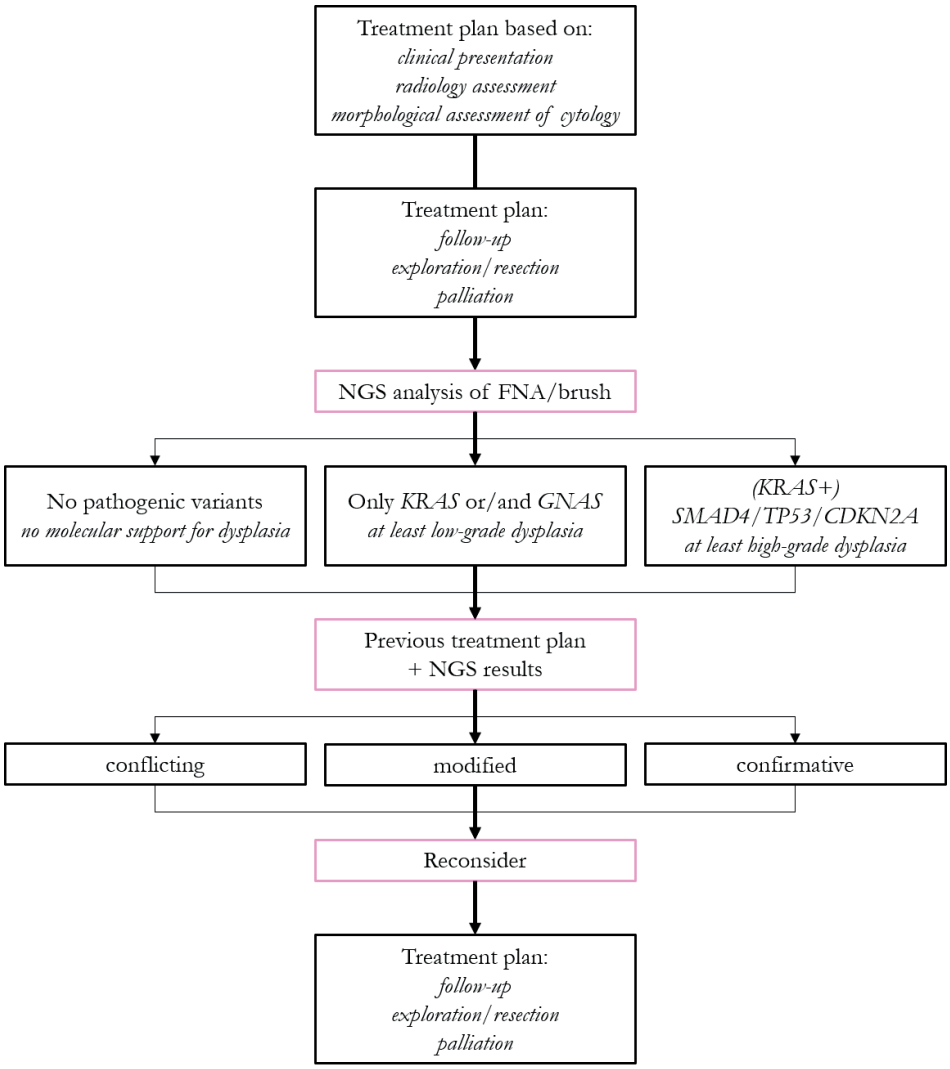

Figure 1. Decision scheme of the study.

RESULTS

Patient cohorts

DNA of 70 patients with preoperative samples, either FNA (N = 50) or cytological brushes (N = 20), were analysed with targeted NGS of isolated DNA (Table 1).

The NGS results of the FNA or brush of the ten patients of the 'initial cohort' were completely identical with the NGS results of the matching resection material (Supplementary Table 1, patients 1-10). In all cases of the 'initial cohort', NGS identified a pathogenic *KRAS* variant in all the cases and in nine out of the ten cases additional pathogenic variants were identified, mostly *TP53*. NGS was additionally performed on the preoperative cytological material of another 60 patients with pancreatic lesions (the 'additional cohort'). The results of both cohorts were combined for further evaluation.

Table 1. Characteristics at baseline and the actual treatment and final diagnosis of the included patients.

	Initial cohort (n=10)		Additional cohort (n=60)		Total (n=70)	
Gender [n; %]						
Male	5	50%	37	62%	42	60%
Female	5	50%	23	38%	28	40%
Age [median; range]	62	53-84	67	24-83	66	24-84
Sort material [n; %]						
Brush	2	20%	18	30%	20	29%
FNA	8	80%	42	70%	50	71%
Referral from other hospital [n; %]						
Yes	4	40%	28	47%	32	46%
No	6	60%	32	53%	38	54%
Cytology [n; %]						
No conclusion	0	0%	1	2%	1	1%
Normal/atypia	2	20%	16	27%	18	26%
LGD	2	20%	12	20%	14	20%
HGD	6	60%	31	52%	37	53%
Imaging performed [n; %]						
CT	10	100%	59	98%	69	99%
MRI	2	20%	22	37%	24	34%
PET	0	0%	3	5%	3	4%
Location [n; %]						
Head	7	70%	32	53%	39	56%
Body	1	10%	8	13%	9	13%
Tail	2	20%	2	3%	4	6%
Other	0	0	18	31%	18	25%

Table 1. Characteristics at baseline and the actual treatment and final diagnosis of the included patients. (*continued*)

	Initial cohort (n=10)		Additional cohort (n=60)		Total (n=70)	
Stent [n; %]						
Yes	4	40%	24	40%	28	40%
No	6	60%	36	60%	42	60%
CEA [median; range]	4.8	3.8-8.0	4.0	0.9-24.7	4.4	0.9-24.7
CA19.9 [median; range]	287.5	29.4-1025.0	238.2	0.6-6437.0	251.90	0.6-6437.0
Actual treatment [n; %]						
Follow-up	0	0%	12	20%	12	17%
Exploration	2	20%	3	5%	5	4%
Resection	8	80%	25	42%	33	50%
Palliation	0	0%	20	33%	20	29%
Final diagnosis [n; %]						
Pancreatitis	0	0%	6	10%	6	9%
AIP	0	0%	3	5%	3	4%
IgG4 mediated disease	0	0%	2	3%	2	3%
SPEN	0	0%	1	2%	1	2%
IPMN	1	10%	2	3%	3	4%
PDAC	9	90%	33	55%	42	60%
Peri-ampullair carc.	0	0%	3	5%	3	4%
Duodenum carc.	0	0%	3	5%	3	4%
Distal cholangio carc.	0	0%	7	12%	7	10%

FNA: fine needle aspiration; LGD: low grade dysplasia; HGD: high grade dysplasia; AIP: auto-immune pancreatitis; SPEN: solid pseudopapillary tumor; IPMN: intraductal papillary mucinous neoplasm; PDAC: pancreatic ductal adenocarcinoma.

Morphological and NGS assessment of cytological material

NGS analysis was successfully performed in all patients. In 56 patients (80%), 118 pathogenic variants were identified (Figure 2). As expected, *KRAS* was the most prevalent gene variant, and was seen in the cytological DNA of 50 patients. *TP53* and *SMAD4* class 4 and 5 pathogenic variants were seen in 34 and 12 patients, respectively. Other identified pathogenic variants were *CDKN2A*, *GNAS*, *ATM*, *APC*, *BRAF*, *PTEN*, *CTNNB1* and *PTPN11*. No pathogenic variants were identified in the cytological material of 14 patients.

The morphological assessment of the cytological material was compared with the molecular NGS data (Table 2), which showed that 33 cases (47%) were scored differently.

In nine cases the results were completely different: FNA of one patient could not be assessed morphologically (due to an insufficient amount of material) and showed at least HGD with NGS, in six patients morphological assessment was atypia, whilst NGS showed at least HGD. In two patients morphological assessment was HGD/malignancy whilst no

pathogenic variants were identified with NGS. In the other discordant 24 cases, the assessments were one category different from each other.

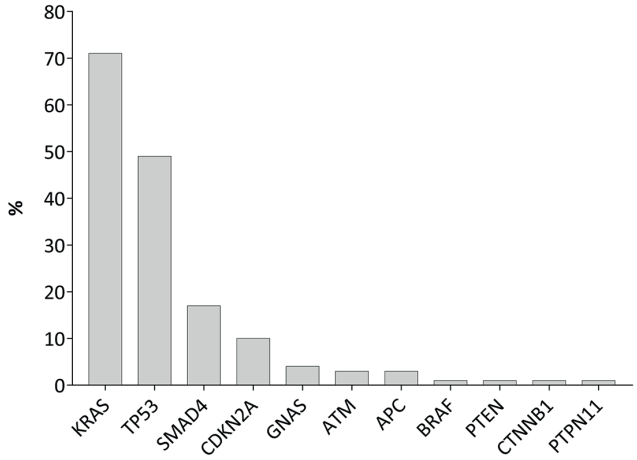

Figure 2. All gene variants detected in the 70 included patients.

Table 2. Comparison of morphological assessment and NGS results of cytological material.

		NGS results				
		no conclusion	**no molecular support for dysplasia**	**at least LGD**	**at least HGD**	**total**
morphological results	**no conclusion**				**1**	1
	atypia		9	3	**6**	18
	low grade dysplasia		3	3	9	14
	high grade dysplasia/ malignancy		**2**	9	25	37
	total		14	15	41	70

LGD: low grade dysplasia; HGD: high grade dysplasia. Severe discordance in assessment is highlighted.

Changes in treatment plan

Due to the integration of the NGS results, the initial treatment plan was changed in seven patients of the 70 patients (10%; Table 3; Suppl Table 1 patients 1, 11-16).

Four of these seven patients (Supplementary Table 1, patients 11-14) were evaluated for suspected PDAC and planned for exploration with possible resection. NGS analysis revealed no class 4 or 5 gene variants in the cytological DNAs. Due to the absence of unequivocal PDAC on basis of clinical and radiological evaluation, the initial surgical plan was waived and stringent follow-up was instigated. During the follow-up period, two of the four patients (patients 11 and 12) were finally diagnosed with IgG4 mediated disease,

one with an auto-immune pancreatitis (patient 13) and one with a non-specific pancreatitis (patient 14). Conversely, the initial treatment plan was follow-up for two of the seven patients (patients 15, 16), which was changed to exploration with possible resection due to multiple pathogenic variants identified with NGS. NGS results revealed two pathogenic KRAS variants and one pathogenic GNAS variant (patient 15) and a pathogenic KRAS and a pathogenic TP53 variant in the second patient (patient 16). Patient 15 underwent exploration followed by resection, pathological assessment of the resected specimen revealed PDAC. Patient 16 rapidly presented with liver metastases after the first diagnosis and could only receive palliative treatment. The final patient (patient 1) for whom the treatment plan was changed due to the NGS results is previously described (20). This patient was thought to have a local recurrence after a previous pylorus preserving pancreatectomy for PDAC. By comparing the NGS results of the FNA of the suspected recurrence with the NGS results of the resected specimen, this patient turned out to have a second primary tumor on basis of a genetic predisposition for PDAC. Instead of palliation, the remnant of the pancreas was resected. For the 63 remaining patients, the treatment plan was not altered due to the NGS results. The NGS results were supportive in 60 of the 63 patients. In three patients the NGS results were conflicting, but did not change the initial treatment plan. These patients are discussed below.

Table 3. Comparison of the treatment plan proposed based on the standard MDT meeting and the treatment plan proposed after integration of the NGS results.

		treatment plan with addition of NGS results			
		follow-up	**resection/ exploration**	**palliation**	**total**
treatment plan based on standard MDT meeting	**follow-up**	8	**2**		10
	resection/exploration	**4**	44		49
	palliation		**1**	11	11
	total	12	47	11	70

MDT: multidisciplinary team. Changes in treatment plan are highlighted.

Final treatment and final diagnosis

NGS results were in line with the final diagnosis in 66 of the 70 patients (Table 1). No pathogenic variants were identified in four patients with discordant NGS results, although these patients were finally diagnosed with a malignancy. In three out of four patients with negative NGS results the treatment plan was not influenced (patients 17-19) because the clinical and radiological evaluation were too suspect to refrain from surgery. In patient 17, the FNA was morphologically assessed as LGD. The cause of the negative NGS result was probably sampling error as the resected specimen revealed a PDAC with a diameter of only 5 mm. Additional NGS analysis on the resected specimen revealed a *KRAS* and a *TP53*

pathogenic variant. For patient 18, the MDT decision was challenging due to conflicting results (imaging suggestive for pancreatitis, a CA19.9 level of 855 and FNA morphological assessed as LGD, NGS identified no pathogenic variants). After three months of follow-up, it was decided to operate the patient because of a significant rise of CA19.9 level. During surgery, biopsies were taken from the omentum, suspect lymph nodes and the mesenterium of the colon, all were positive for malignancy and subsequently NGS analysis revealed *KRAS* and *TP53* pathogenic variants. For patient 19, the ductus choledochus was morphologically assessed as normal and no pathogenic variants were detected with NGS. However, the initial treatment plan of exploration was maintained because of high suspicion of malignancy and a likely sample error. Eventually, the patient was unfit for surgery and a subsequent scan suggested development of an irresectable distal cholangiocarcinoma. Patient 20 was initially diagnosed with auto-immune pancreatitis based on clinical presentation, radiological evaluation and a morphological assessment of the FNA suggestive for pancreatitis and atypia due to inflammation. Additionally, with NGS no pathogenic variants were identified. Morphological assessment of a subsequent brush of the ductus choledochus showed acute inflammation, atypia and normal ductal epithelia. Moreover, at first the patient demonstrated a decline of CA19.9 level but after three months a significant rise of CA19.9 level was observed. The CT scan that was made three months later was suspicious for liver metastases, which were biopsied and pathologically confirmed. NGS analysis of the liver metastasis biopsy revealed *KRAS, SMAD4* and *TP53* pathogenic variants.

Altogether, in this study, the diagnostic accuracy of NGS analysis was 94%. Sensitivity and specificity of NGS analysis were 93% and 100%, respectively. (Supplementary Table 2). When the NGS results are combined with the radiological, cytological and clinical evaluation, the sensitivity was 98%. Depending on whether the LGD category is deemed as true malignant or true benign, the sensitivity and specificity of the morphological assessment of the cytology were between 58-81% and 73-82%, respectively (Supplementary Table 3). The cytology material of 34% of the patients was first assessed in a referring hospital. There was a difference in morphological assessments between the referring hospitals and the LUMC in 47%.

The number of identified pathogenic variants per patient in relation to the final diagnosis is shown in Figure 3. A higher number of pathogenic variants was associated to a more advanced disease.

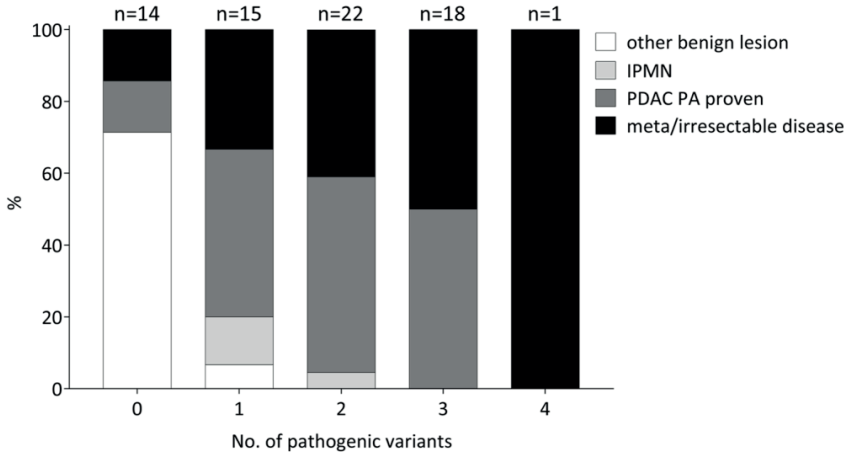

Figure 3. Number of pathogenic variants identified in the patients in relation to the final diagnosis. In four cases the results were false negative. One patient had a *KRAS* pathogenic variant (frequency of 3%) and was diagnosed with a pancreatitis. Two patients with an IPMN had a *KRAS* variant; one patient with an IPMN had a *KRAS* and a *GNAS* variant, these IPMNs did not progress towards malignancy.

DISCUSSION

This study underlines the added value of NGS analysis of DNA of patients with suspect pancreatic and periampullary tumors during the multidisciplinary diagnostic decision making of these patients. Although hopeful, NGS results should be carefully weighed in the MDT discussions as sampling errors during FNA or brush procedures can occur, potentially leading to false negative results.

Our results are consistent with other reports using diagnostic applications of in-depth molecular analyses. For example, recent studies showed that molecular genetic analysis of cystic fluid could aid the preoperative classification of cystic neoplasm of the pancreas and that the discrimination of serous from mucinous cystic pancreatic lesions could be improved.(24, 25) NGS analysis of DNA was used to increase the accuracy of classifying pancreatic cystic neoplasm as either benign or premalignant lesions. In addition, NGS analysis of DNA has also been used to identify actionable molecular targets for on- or off-label targeted systemic therapies in patients with advanced PDAC.(26, 27) A recent study of Gleeson *et al.*(28) in which EUS derived FNA samples of patients with PDAC were analysed with NGS suggests that NGS analysis could be useful for the development of future biomarker driven therapeutic innovations.

In our study a focused gene panel was used that targets the mutation hotspot regions of 50 genes. This is a commercial available panel, therefore, not all genes that are sequenced are of value for this cohort. This panel can be expanded for other diagnostic or therapeutic

purposes. In the previously mentioned study of Gleeson *et al*. a comprehensive cancer panel of 160 genes was used, therefore, an overview of the multigene mutational landscape of PDAC was acquired. This panel can also be used for other diagnostic and therapeutic purposes, because additional informative gene targets are included. However, by using large gene panels, cytology slides with a low percentage of tumor cells in a background of benign cells might have to be excluded from analysis. In our 50 genes panel, we could reliably include cytology slides with only 2-5% dispersedly positioned tumor cells, as previously described. Additional methods to increase the ability to identify gene variants and to stratify for structural variants such as focal gene amplifications and/or deletions might be the use of enrichment techniques such as microfluidic cell sorting.(29)

In theory, FNA samples with low numbers of lesional cells can lead to false positive results due to amplification of PCR artefacts. For that reason molecular barcoding is advocated in which individual DNA molecules are flagged prior to amplification, thereby helping to recognize PCR artefacts.(30) However a disadvantage of molecular barcoding is that relatively higher input DNA is required. Furthermore, due to a prior fixation step with only methanol preoperative FNA derived DNA is of far better quality than DNA isolated from FFPE tissue. In the latter, C>T transitions can be potentially seen leading to false positive variant calling results. Our results now suggest that false positivity might not be an issue in FNA derived DNA when looking at hotspot gene regions for pathogenic variants.

NGS is able to provide valuable molecular information about suspect lesions, also if radiology, cytology, and clinical results are inconclusive. In our evaluation, the NGS results changed the treatment plan in 10% of patients. NGS had a sensitivity of 93% and a specificity of 100%, significantly higher than morphological assessment. Off course the correctness of morphological assessment is dependent on the pathologist, specialized pancreatic cancer pathologist are required. Over time, NGS is increasingly performed during the diagnostic process of patients with suspect pancreatic lesions at our centre and clinicians increasingly rely on the results to confirm their working diagnosis. NGS analysis can support the latter resulting in more certainty and confidence for both patients and clinicians. Therefore, NGS analysis might be of even more value than expressed by numbers and percentages in this study.

The unique key point of this study is the implementation of NGS analysis during MDT meetings. To make sure the MDT could rely on the results, the accuracy of NGS analysis had to be determined. Therefore, the cytology material of 70 consecutive patients, representing a real patient population with different types of benign and malignant lesions and with both brushes and FNA derived cytology material, was analysed. Potentially, NGS analysis should only be used in selected cases, for example when clinical, radiological and cytological results are contradictory. In such a case a supportive diagnosis by NGS can be of paramount importance, since neoadjuvant therapy followed by surgery is increasingly performed.

In conclusion, the present study demonstrates that performing NGS on DNA obtained from suspect pancreatic or periampullary lesions can improve patient care and possibly patient outcome.

REFERENCES

1. Abraham SC, Wilentz RE, Yeo CJ, Sohn TA, Cameron JL, Boitnott JK, et al. Pancreaticoduodenectomy (Whipple resections) in patients without malignancy: are they all 'chronic pancreatitis'? Am J Surg Pathol. 2003;27(1):110-20.
2. Kennedy T, Preczewski L, Stocker SJ, Rao SM, Parsons WG, Wayne JD, et al. Incidence of benign inflammatory disease in patients undergoing Whipple procedure for clinically suspected carcinoma: a single-institution experience. Am J Surg. 2006;191(3):437-41.
3. Lee-Felker SA, Felker ER, Kadell B, Farrell J, Raman SS, Sayre J, et al. Use of MDCT to Differentiate Autoimmune Pancreatitis From Ductal Adenocarcinoma and Interstitial Pancreatitis. AJR Am J Roentgenol. 2015;205(1):2-9.
4. Zhang TT, Wang L, Liu HH, Zhang CY, Li XM, Lu JP, et al. Differentiation of pancreatic carcinoma and mass-forming focal pancreatitis: qualitative and quantitative assessment by dynamic contrast-enhanced MRI combined with diffusion-weighted imaging. Oncotarget. 2016.
5. Shrikhande SV, Barreto SG, Goel M, Arya S. Multimodality imaging of pancreatic ductal adenocarcinoma: a review of the literature. HPB (Oxford). 2012;14(10):658-68.
6. Hur BY, Lee JM, Lee JE, Park JY, Kim SJ, Joo I, et al. Magnetic resonance imaging findings of the mass-forming type of autoimmune pancreatitis: comparison with pancreatic adenocarcinoma. J Magn Reson Imaging. 2012;36(1):188-97.
7. Saftoiu A, Vilmann P. Role of endoscopic ultrasound in the diagnosis and staging of pancreatic cancer. J Clin Ultrasound. 2009;37(1):1-17.
8. Iqbal S, Friedel D, Gupta M, Ogden L, Stavropoulos SN. Endoscopic-ultrasound-guided fine-needle aspiration and the role of the cytopathologist in solid pancreatic lesion diagnosis. Patholog Res Int. 2012;2012:317167.
9. Amato E, Molin MD, Mafficini A, Yu J, Malleo G, Rusev B, et al. Targeted Next-Generation Sequencing of cancer genes dissects the molecular profiles of intraductal papillary neoplasms of the pancreas. J Pathol. 2014;233(3):217-27.
10. Afify AM, al-Khafaji BM, Kim B, Scheiman JM. Endoscopic ultrasound-guided fine needle aspiration of the pancreas. Diagnostic utility and accuracy. Acta Cytol. 2003;47(3):341-8.
11. Woolf KM, Liang H, Sletten ZJ, Russell DK, Bonfiglio TA, Zhou Z. False-negative rate of endoscopic ultrasound-guided fine-needle aspiration for pancreatic solid and cystic lesions with matched surgical resections as the gold standard: one institution's experience. Cancer Cytopathol. 2013;121(8):449-58.
12. Brand B, Pfaff T, Binmoeller KF, Sriram PV, Fritscher-Ravens A, Knofel WT, et al. Endoscopic ultrasound for differential diagnosis of focal pancreatic lesions, confirmed by surgery. Scand J Gastroenterol. 2000;35(11):1221-8.
13. Fritscher-Ravens A, Brand L, Knofel WT, Bobrowski C, Topalidis T, Thonke F, et al. Comparison of endoscopic ultrasound-guided fine needle aspiration for focal pancreatic lesions in patients with normal parenchyma and chronic pancreatitis. Am J Gastroenterol. 2002;97(11):2768-75.
14. Varadarajulu S, Tamhane A, Eloubeidi MA. Yield of EUS-guided FNA of pancreatic masses in the presence or the absence of chronic pancreatitis. Gastrointest Endosc. 2005;62(5):728-36; quiz 51, 53.
15. Chu PG, Schwarz RE, Lau SK, Yen Y, Weiss LM. Immunohistochemical staining in the diagnosis of pancreatobiliary and ampulla of Vater adenocarcinoma:

application of CDX2, CK17, MUC1, and MUC2. Am J Surg Pathol. 2005;29(3):359-67.
16. Kinde I, Wu J, Papadopoulos N, Kinzler KW, Vogelstein B. Detection and quantification of rare mutations with massively parallel sequencing. Proc Natl Acad Sci U S A. 2011;108(23):9530-5.
17. Scarpa A, Sikora K, Fassan M, Rachiglio AM, Cappellesso R, Antonello D, et al. Molecular typing of lung adenocarcinoma on cytological samples using a multigene next generation sequencing panel. PLoS One. 2013;8(11):e80478.
18. Waddell N, Pajic M, Patch AM, Chang DK, Kassahn KS, Bailey P, et al. Whole genomes redefine the mutational landscape of pancreatic cancer. Nature. 2015;518(7540):495-501.
19. Federa. The code of conduct for the use of data in health research [Available from: https://www.federa.org/codes-conduct.
20. Sibinga Mulder BG, Mieog JS, Handgraaf HJ, Farina Sarasqueta A, Vasen HF, Potjer TP, et al. Targeted Next-Generation Sequencing of FNA-derived DNA in pancreatic cancer. J Clin Pathol. 2017;70(2):174-8.
21. van Eijk R, Stevens L, Morreau H, van Wezel T. Assessment of a fully automated high-throughput DNA extraction method from formalin-fixed, paraffin-embedded tissue for KRAS, and BRAF somatic mutation analysis. Exp Mol Pathol. 2013;94(1):121-5.
22. Plon SE, Eccles DM, Easton D, Foulkes WD, Genuardi M, Greenblatt MS, et al. Sequence variant classification and reporting: recommendations for improving the interpretation of cancer susceptibility genetic test results. Hum Mutat. 2008;29(11):1282-91.
23. Bosman FTC, F.; Hruban, R.H.; Theise, N.D. WHO Classification of Tumors of the Digestive System, Fourth Edition2010.
24. Springer S, Wang Y, Dal Molin M, Masica DL, Jiao Y, Kinde I, et al. A combination of molecular markers and clinical features improve the classification of pancreatic cysts. Gastroenterology. 2015;149(6):1501-10.
25. Jones M, Zheng Z, Wang J, Dudley J, Albanese E, Kadayifci A, et al. Impact of next-generation sequencing on the clinical diagnosis of pancreatic cysts. Gastrointest Endosc. 2016;83(1):140-8.
26. Wright GP, Chesla DW, Chung MH. Using next-generation sequencing to determine potential molecularly guided therapy options for patients with resectable pancreatic adenocarcinoma. Am J Surg. 2016;211(3):506-11.
27. Valero V, 3rd, Saunders TJ, He J, Weiss MJ, Cameron JL, Dholakia A, et al. Reliable Detection of Somatic Mutations in Fine Needle Aspirates of Pancreatic Cancer With Next-generation Sequencing: Implications for Surgical Management. Ann Surg. 2016;263(1):153-61.
28. Gleeson FC, Kerr SE, Kipp BR, Voss JS, Minot DM, Tu ZJ, et al. Targeted next generation sequencing of endoscopic ultrasound acquired cytology from ampullary and pancreatic adenocarcinoma has the potential to aid patient stratification for optimal therapy selection. Oncotarget. 2016;7(34):54526-36.
29. Bolognesi C, Forcato C, Buson G, Fontana F, Mangano C, Doffini A, et al. Digital Sorting of Pure Cell Populations Enables Unambiguous Genetic Analysis of Heterogeneous Formalin-Fixed Paraffin-Embedded Tumors by Next Generation Sequencing. Sci Rep. 2016;6:20944.
30. Eijkelenboom A, Kamping EJ, Kastner-van Raaij AW, Hendriks-Cornelissen SJ, Neveling K, Kuiper RP, et al. Reliable Next-Generation Sequencing of Formalin-Fixed, Paraffin-Embedded Tissue Using Single Molecule Tags. J Mol Diagn. 2016;18(6):851-63.

4

Accuracy of targeted Next-Generation Sequencing in the diagnostic process for pancreatic cancer: A multi-center prospective cohort study

B.G. Sibinga Mulder, Q. Janssen, B. Groot Koerkamp, L. Hol, R. Quispel,
B. Bonsing, A.L. Vahrmeijer, C.H.J. van Eijck, D. Roos, L. Perk,
E. van der Harst, M. Doukas, R.R. de Krijger, M. Kliffen,
M.F. van Velthuysen, V. Terpstra, A. Farina Sarasqueta, H. Morreau, J.S.D. Mieog

Submitted: HPB Journal.

ABSTRACT

Targeted Next-Generation Sequencing (NGS) on cytological material obtained with fine needle aspiration (FNA) or biliary brushing can aid in establishing a diagnosis for patients with suspect pancreatic lesions. In this prospective multicenter study the value of NGS was determined for establishing the correct diagnosis, and subsequent treatment plan, of patients with suspect pancreatic lesions and inconclusive cytology.

NGS was performed with AmpliSeq Cancer Hotspot Panel v2 and v4b in patients with inconclusive cytology results or uncertain diagnosis. All diagnostic results were evaluated by the oncology pancreatic multidisciplinary team. Influence of the additional yield of NGS was determined by comparing the diagnosis (malignancy, cystic lesion or benign condition) and the proposed treatment plan (exploration/resection, preoperative chemotherapy, follow-up, palliation or repeated EUS) before and after integration of NGS results.

In 50 of the 53 included patients cytology material (40 FNA, 13 brushes) was sufficient for NGS analysis. Diagnosis before and after integration of NGS results differed in 32% of the patients. The treatment plan was changed in 18% of the patients and made definitive in 44%. The repetition of endoscopic ultrasound with FNA was prevented in 14% of the patients. In the remaining 24%, NGS had no additional value. Based on the final diagnosis, all changes in treatment plan were correctly made after integration of NGS.

This study demonstrates the additional value of NGS in patients with an initial inconclusive diagnosis. Integration of NGS results can not only prevent repeated EUS/FNA, but can also rigorously change the final diagnosis and treatment plan.

INTRODUCTION

Analyzing patients with a suspect lesion in the pancreas can be difficult, leading to frequent inconclusive diagnoses. Current imaging techniques are limited in differentiating between pancreatic cancer and inflammation, benign lesions, or preneoplastic lesions.(1) Moreover, preoperative pathological confirmation of malignancies is increasingly required in the context of upcoming neoadjuvant treatments. Endoscopic ultrasound-guided fine needle aspiration (EUS-FNA) and biliary duct brushing can be performed to obtain a cytopathological diagnosis. However, a significant drawback of this technique is the frequent false positive/negative or inconclusive results, which have been reported in 12-33% of the cases. These are mainly caused by sampling error, suboptimal sample quality, low cellular yield and the presence of an intense desmoplastic stromal reaction.(2) Due to these shortcomings in the diagnostic process of patients with a suspect pancreatic lesion, misdiagnosis occurs frequently leading to an inappropriate treatment or requirement of additional repetition of EUS-FNA, which can delay treatment.(3)

NGS has proven to be useful in distinguishing benign from malignant pancreatic lesions.(4) Targeted Next-Generation Sequencing (NGS) on FNA-derived DNA can identify pathogenic variants in known driver genes of malignancy and can therefore be used to confirm neoplasia.(5) For ultra-deep sequencing using NGS panels that target hotspot gene variants such as *KRAS, TP53, BRAF, PTEN etc.* only a limited quantity of material is required, up to 100 cells.(6)

In a previous study, we evaluated 70 consecutive patients with a suspect pancreatic lesion and reported a diagnostic accuracy, sensitivity and specificity of NGS of 94%, 93% and 100%, respectively.(4) Since NGS might be superfluous in all patients with a suspect pancreatic lesion, the focus of the current study was on the value of NGS in patients with inconclusive cytology material. Therefore, the aim of this study was to determine the additional diagnostic yield of NGS in the diagnostic process and treatment plan proposition in patients with a suspect pancreatic lesion with an inconclusive cytopathologic diagnosis.

METHODS

Study design

This multicenter study between Leiden University Medical Center (LUMC), Erasmus Medical Center, Maasstad hospital and Reinier de Graaf hospital was approved by the medical ethical reviews board of the LUMC (Dutch trial register: NTR7006). The primary aim of the study was to determine the value of NGS in the diagnostic process and treatment plan proposition in a patient population with inconclusive cytopathology diagnoses.

During the oncology pancreatic multidisciplinary team (MDT) meetings (including a gastrointestinal (GE) surgeon, gastroenterologist, GE-radiologist, GE-pathologist and an oncologist), all patients without a definitive diagnosis, or without a conclusive cytopathologic diagnosis were included. Further inclusion criteria were: patients with a suspect solid or cystic pancreatic or periampullary lesion (papilla or distal bile duct) on recent multi-phase abdominal CT or MRI scans. An available cytology sample for pathological assessment either obtained by common bile duct brushing or by EUS-FNA. All cytology samples were reviewed at the department of Pathology in the LUMC and classified by specialized pancreatic pathologists (A.F.S., H.M.) based on morphological assessment as: 1) normal/atypia, 2) dysplasia or, 3) inconclusive (in case of too few cells or bloody material).

Based on all available diagnostic information, a probability diagnosis was proposed by the MDT, either: 1) malignancy, including pancreatic ductal adenocarcinoma, distal cholangiocarcinoma, ampullary carcinoma, cystic lesion with malignant degeneration, 2) benign condition, including (autoimmune) pancreatitis, pseudocyst, or, 3) cystic lesion, including mucinous cystic neoplasm and/or, low grade IPMN (not malignant degenerated). Furthermore, the most suitable treatment for the probable diagnosed condition was determined as either: 1) surgical exploration with possible resection(resection was refrained in case of a metastatic of locally advanced disease), 2) neoadjuvant therapy for study purpose or in case of locally advanced disease, 3) palliation in case of locally advanced disease, metastatic disease or patient unfit for surgery, 4) follow-up for benign conditions or 5) repetition of diagnostic FNA. For patients diagnosed with low grade IPMN/MCN, both surveillance or resection are widely accepted treatment options. The ultimate decision differs per patient and also depends on the expertise of the MDT members.

Subsequently, the cytology sample was analyzed with NGS, using the AmpliSeq Cancer Hotspot Panel v2 and v4b, as previously described.(4) The results were reported as: 1) "no molecular support for dysplasia" if no pathogenic variants were identified, 2) "a proliferative lesion with molecularly at least low grade dysplasia (LGD)" in case of *KRAS* or *GNAS* class 4 or 5 DNA variants with sufficient coverage and high frequent variant reads on target, or the sole finding of *ATM, CDKN2A, PTEN or APC DNA variants*. The sole finding of a *KRAS* pathogenic variant with low frequency could also be suggestive for pancreatitis. 3) "molecularly at least high grade dysplasia (HGD)" if at least a *TP53* or *SMAD4* DNA variant was identified or 4) "inconclusive" if NGS was not possible or reliable on the presented material.(7)

After integration of the NGS results during the following MDT meeting, the diagnosis and treatment plan could be changed or confirmed. Furthermore, the MDT could ignore the NGS results in case of too contradictive or inconclusive results or if the clinical suspicion of a malignancy was too high (i.e. false-negative NGS results).

The final diagnosis was determined, either based on histological assessment of the resected specimen or by evaluation during follow-up after at least six months. NGS analysis of

the resected specimen was not repeated since correlation was already validated in an earlier study.(4)

Figure 1 gives an overview of the study design.

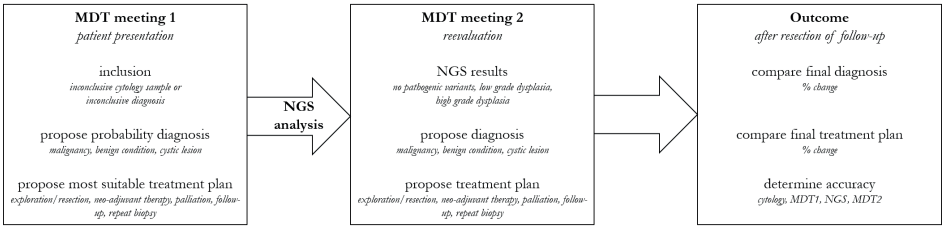

Figure 1. Flowchart of study method.

Outcomes

For analysis of the contribution of NGS to the diagnostic process only the patients with technically feasible NGS analysis were included. Diagnosis based on the information before and after integration of the NGS results was correlated to the final diagnosis. Differences were analyzed with a McNemar test. Proposed treatment plans before and after integration of NGS results were compared and classified as 'changes in treatment plan', 'confirmation of treatment plan' or 'no value of NGS results'.

All patients were included (including technical unsuccessful NGS) for determination of accuracy of 1) morphological assessment of the cytology samples on itself independent of quality, quantity or representatively, 2) suggested diagnosis during first MDT meeting, 3) NGS results on itself and, 4) suggested diagnosis during second MDT meeting were determined by comparing to the final diagnosis. Since LGD can be interpreted in several ways and does not provide a definitive diagnosis on itself, the accuracy is reported two-fold: all LGD incorrect, or all LGD correct.

Power calculation

Assuming that NGS analysis has an additional diagnostic yield of 20%, a total of 57 patients were required in the study (80% power and 2-sided significance level α=0.05).

RESULTS

In total, 57 patients were included. Four patients were excluded from further analysis due to incorrect inclusion: lymph node biopsy (n=2), suspect GIST tumor (n=1) and biopsy of suspect pancreatic liver metastasis (n=1). Table 1 provides an overview of the patient characteristics.

Table 1. Patient Characteristics.

		N	%
Total		**53**	
Sex	**Female**	23	43
	Male	30	57
Age	Mean, SD	63.1	13.7
CA 19.9	Median, range	39	0-5126
Type of cytology material	**FNA**	40	76
	Brush	13	24
Cytology result	**Dysplasia**	10	19
	Atypia	32	60
	Inconclusive	11	21
Reason NGS	**Cytology**	22	41
	PA required	9	18
	MDT unsure	22	41
NGS result	**HGD**	11	21
	LGD	17	32
	No pathogenic variants	22	41
	Inconclusive	3	6
Final diagnosis	**Malignancy**	32	60
	Benign condition	15	28
	Cystic lesion	6	12

PA: pathology; MDT: multidisciplinary team; HGD: high grade dysplasia; LGD: low grade dysplasia

NGS was technically feasible in 50 of the 53 patients. Figure 2 gives an overview of the pathogenic DNA variants identified in 50 patients.

Table 2 gives an overview of the probability diagnoses before and after integration of the NGS results, related to the final diagnosis. Integration of the NGS results significantly improved the probability diagnosis: from 16 incorrect diagnoses (32%) to three incorrect diagnoses (6%) (p-value < 0.001).

Table 2. Diagnosis with and without NGS results correlated to final diagnosis

		Final diagnosis		
		Malignancy	**Benign condition**	**Cystic lesion**
MDT 1: without NGS results	**Malignancy**	**27**	10	2
	Benign condition	1	**5**	1
	Cystic lesion	2		**2**
MDT 2: with NGS results	**Malignancy**	**30**	1	2
	Benign condition		**13**	
	Cystic lesion			**4**

MDT: multidisciplinary team meeting; Bold: concordant results

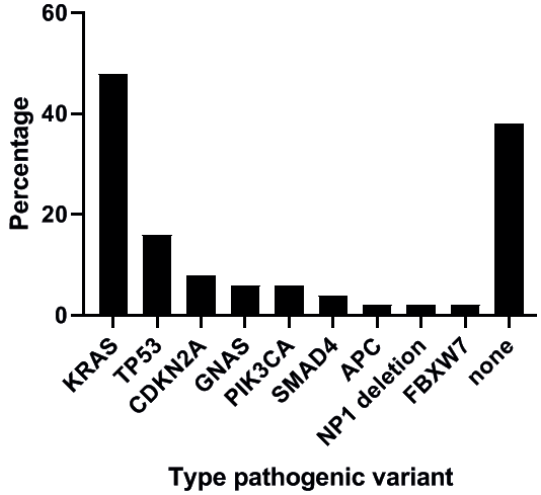

Figure 2. Pathogenic variants identified in 50 patients.

The treatment plan proposition changed in 16 cases (32%) after integration of the NGS results (Table 3). After integration of the NGS results surgical exploration with possible resection (n=6) and palliation (n=2) was prevented as NGS did not show proliferative lesions (with absent DNA variants) suggesting benign diseases which were confirmed during follow-up. Conversely, in one patient only the NGS results pointed at least HGD and therefore the treatment plan was changed to surgical exploration. In seven patients repeated EUS was prevented by integrating the NGS results, resulting in surgery (n=1), palliation (n=4) or follow-up (n=2). Table 4 gives an overview of the treatment plan proposition determined during the second MDT meeting compared to the final diagnosis. In one patient NGS showed no pathogenic variants but the other diagnostic information was suspect for a malignancy, therefore, the patient was scheduled for resection of the lesion. However, the patient was not fit enough for surgery or systemic treatment, and during follow-up he turned out

Table 3. Changes in treatment plan after integration of NGS results

		With NGS results				
		Exploration	**Neoadjuvant**	**Palliation**	**Follow-up**	**Repeat biopsy**
Without NGS results	**Exploration**	**16**			6	
	Neoadjuvant		**5**			
	Palliation			**6**	2	
	Follow-up	1			**5**	
	Repeat biopsy	1		4	2	2

Bold: concordant

to have a pancreatitis instead of the presumed malignancy. In two patients the lesion was diagnosed as low grade IPMN/MCN during the second MDT meeting and exploration/resection was chosen as the most suitable treatment plan, in two patients the lesions were clinically diagnosed as malignancies but turned out to be low grade IPMNs.

Table 4. Treatment plan after NGS integration compared to final diagnosis.

		Final diagnosis		
		Malignancy	**Benign condition**	**Cystic lesion**
With NGS results	**Exploration**	**13**	1*	*4***
	Neoadjuvant	**5**		
	Palliation	**10**		
	FU		**13**	**2**
	Repeat biopsy	2		

**Pancreatitis; **low grade IPMN, 2 were diagnosed as cystic lesion during the MDT meeting and too suspect, therefore, exploration/resection was chosen. The other two lesions were diagnosed as malignancies but turned out to be low grade IPMNs. Bold: concordant*

During the second MDT meetings the NGS results were ignored in 12 patients (24%) (no value), because no pathogenic variants were identified but there was a strong clinical suspicion of malignancy. In nine patients NGS results were correctly ignored because all had a malignancy. In three patients, no pathogenic variants were identified, however, the lesions were clinically diagnosed as malignant, but final histologic assessment showed a pancreatitis (n=1) and a low grade IPMN (n=2). In the remaining 22 patients (44%), the NGS results provided enough support to confirm the initial clinical diagnosis, which was correct in all patients.

Of all 53 patients, the accuracy of cytology (on itself), MDT 1 without NGS results, NGS (on itself) and MDT 2 with NGS results was 17%, 70-81%, 43-79% and 94-98%, respectively (Table 5).

Of the 17 patients with a proliferative lesion at least LGD at NGS analysis, 11 patients had a sole finding of *KRAS* pathogenic variant and no strong conclusion could be drawn for malignancy or a cystic lesion, or in case of a low frequency for pancreatitis. Furthermore, two patients also had a *GNAS* and *PIK3CA* pathogenic variant besides a *KRAS* variant, both were clinically diagnosed with a malignant degenerated IPMN and received oncologic treatment. One patient had a lesional *GNAS* and *KRAS* pathogenic variant and was clinically diagnosed with low grade IPMN with follow-up. One patient only showed a lesional *PIK3CA* pathogenic variant, was diagnosed with a malignancy and underwent surgical resection. One patient only had a *CDKN2A* pathogenic variant in exon 2, with a coverage of 1864 reads and a frequency of 0.50, which is the reason for surveillance of the patient (genetic predisposition

for the development of pancreatic cancer). One patient only had a *APC* pathogenic variant, was clinically diagnosed with a malignancy and underwent surgical resection.

Table 5. Accuracy per diagnostic tool.

	Definitely correct	Definitely incorrect	No strong conclusion	Accuracy
Morphology assessment (on itself)	9	11	33*	17%
First MDT meeting (without NGS)	37	10	6**	70-81%
NGS (on itself)	23	11	19***	43-79%
Second MDT meeting (with NGS)	50	1	2**	94-98%

MDT: multidisciplinary team
**: assessed as atypia, definitely insufficient for determining an adequate diagnosis*
***: cystic lesions*
****: combination of 1) LGD (n=17), and 2) no pathogenic variants identified with as final diagnosis cystic lesion (n=2)*

DISCUSSION

In this study, the additional value of NGS in case of inconclusive cytology of a suspicious pancreatic lesion was assessed. Integrating the NGS results in the diagnostic process increased the accuracy with 18-24% to a final, overall accuracy of 98%. The treatment plan was correctly changed in 30% (no incorrect changes occurred) of the patients and confirmed the probability diagnosis in 44% of the patients.

NGS has already gained an important role in cancer research and treatment and can aid in predicting response or resistance to cancer treatments.(7) NGS is used in patients with advanced stage cancers and mostly in lung cancer, because of the multiple described pathways of oncogenic addiction. NGS aids in detection of mutations for applying the most suitable treatment.(8)

Most studies evaluating NGS determine the feasibility of NGS or provide insight in pathogenic variants for personalized systemic treatment. Studies focusing on the diagnostic yield of NGS in suspicious pancreatic lesions are limited. Larson *et al.* evaluated types of biopsy for success rate of NGS analysis of suspect pancreatic lesions or metastases.(9) Percutaneous biopsies of potential metastases were more adequate than FNA or fine needle biopsies from the suspect primary tumor. They performed NGS with the commercially available set FoundationOne (Foundation Medicine, Inc, Cambridge, Massachuttes).

In our previous study, NGS showed to be of value in consecutive patients with a suspect lesion in the pancreas.(4) The previous study concluded that unselective use of NGS is not necessary in clear-cut cases of malignancy. Therefore, the current study focused on the value of NGS in a patient population with inconclusive cytology results regardless of the

reason and patients with an uncertain diagnosis. Corresponding diagnostic accuracies were reported: 94% for integration of NGS in the diagnostic process in an unselective patient population and 98% in the current study.

NGS can often be performed in casemorphological assessment is not possible due to low cellular yield since only a limited quantity of material is necessary for NGS analysis. In this study this repeated EUS-FNA was spared in seven out of nine patients. Although the costs of NGS are relatively high, approximately €600 per sample, repetition of EUS-FNA in patients with inconclusive samples is more costly than performing NGS analysis. Suggesting cost-effectiveness of NGS in this patient population.

In our study, NGS was inconclusive in 3/53 samples (6%), which was significantly lower than the reported 29% (of the 76 samples) in Larson' study.(9)

The results of NGS analysis have to be integrated into the diagnostic process and are an addition to the clinical and radiological data. Only in case of a HGD as NGS result (in this study in 21%), meaning the identification of class 4 or 5 *TP53* or *SMAD4* pathogenic variants, a malignancy is proven. In case of molecular LGD, or if no pathogenic variants are identified, the diagnosis and treatment plan are still unsure. Firstly, in case of no pathogenic variants, this can be due to a truly benign condition, but this can also be the result of tumors without mutations or of sampling error, e.g. in case of not on target FNA, a very small tumor or an extensive inflammatory component. Secondly, in case of LGD, the identification of a sole *KRAS* pathogenic variant can indicate a pancreatitis, IPMN or malignancy. In our study, no significant difference was identified in the frequency of the pathogenic variant between benign conditions or malignancies. However, this study was not adequately powered to test this association.

Although not used in this study, NGS can also be applied on cystic fluid. Rosenbaum *et al.* analyzed fluid from 113 cysts, where 67 cysts showed pathogenic variants.(10) A significant difference in identification of *KRAS* pathogenic variants was present between non-mucinous cysts (12.5% of samples) and mucinous cysts/IPMN (100% of samples). Furthermore, in 33% of the IPMN samples a *GNAS* pathogenic variant was also identified. In the IPMNs with a malignant component additional pathogenic variants in the following genes were identified: *TP53, CDKN2A, SMAD4, NOTCH1.* Singi *et al.* analyzed fluid from 308 cysts and also identified *KRAS* and *GNAS* pathogenic variants in IPMNs and MCNs and showed *TP53, PIK3CA* and *PTEN* in neoplasia.(11) Volckmar *et al.* published the first results of the ZYSTEUS study that investigates whether detection of driver mutations in IPMN patients by liquid biopsy (cystic fluid) is technically feasible.(12) Comparable results were obtained, in 12 IPMNs *KRAS* (n=12) and *GNAS* (n=4) pathogenic variants were identified. In three pseudocysts no pathogenic variants were identified. Lastly, Suenaga *et al.* studied whether patients under surveillance for IPMNs would benefit from pancreatic juice punction for NGS analysis.(13) In case a *TP53* or *SMAD4* pathogenic variant was identified the lesion was resected. The results of all these studies are in line with ours, the identification

of a *SMAD4* or *TP53* is suspect for a malignancy, identification of a *CDKN2A, NOTCH1, PIK3CA* or *PTEN* is also suggestive for a malignancy. Based on our results and the above mentioned studies the NGS results of patients with a pathogenic variant in *PIK3CA* could also be classified as HGD. A pathogenic variation in *GNAS* is suggestive for an IPMN and the interpretation of a pathogenic variant in *KRAS* remains somewhat challenging since this can be seen in in IPMNs, malignancies but also in pancreatitis. Future studies should focus more on differentiation between, frequencies or the mutated exon of *KRAS* to be able to better distinguish between these conditions.

In conclusion, NGS can aid in determining the suitable treatment for patients with a suspect pancreatic lesions without convincing pathology or imaging assessment. By integrating NGS in the diagnostic process, an accuracy of 98% for correct diagnosing was reached. NGS is of value by either providing molecular confirmation of neoplasia for preoperative chemotherapy or surgery, thereby preventing repeated EUS-FNA/brushing or surgery in patients with benign conditions.

REFERENCES

1. Shrikhande SV, Barreto SG, Goel M, Arya S. Multimodality imaging of pancreatic ductal adenocarcinoma: a review of the literature. HPB (Oxford). 2012;14(10):658-68.
2. Iqbal S, Friedel D, Gupta M, Ogden L, Stavropoulos SN. Endoscopic-ultrasound-guided fine-needle aspiration and the role of the cytopathologist in solid pancreatic lesion diagnosis. Patholog Res Int. 2012;2012:317167.
3. Gerritsen A, Molenaar IQ, Bollen TL, Nio CY, Dijkgraaf MG, van Santvoort HC, et al. Preoperative characteristics of patients with presumed pancreatic cancer but ultimately benign disease: a multicenter series of 344 pancreatoduodenectomies. Ann Surg Oncol. 2014;21(12):3999-4006.
4. Sibinga Mulder B. Diagnostic Value of Targeted Next-Generation Sequencing in Patients with Suspected Pancreatic of Periampullary Cancer. 2017.
5. Kinde I, Wu J, Papadopoulos N, Kinzler KW, Vogelstein B. Detection and quantification of rare mutations with massively parallel sequencing. Proc Natl Acad Sci U S A. 2011;108(23):9530-5.
6. Amato E, Molin MD, Mafficini A, Yu J, Malleo G, Rusev B, et al. Targeted Next-Generation Sequencing of cancer genes dissects the molecular profiles of intraductal papillary neoplasms of the pancreas. J Pathol. 2014;233(3):217-27.
7. Morganti S, Tarantino P, Ferraro E, D'Amico P, Viale G, Trapani D, et al. Complexity of genome sequencing and reporting: Next generation sequencing (NGS) technologies and implementation of precision medicine in real life. Crit Rev Oncol Hematol. 2019;133:171-82.
8. Volckmar AL, Leichsenring J, Kirchner M, Christopoulos P, Neumann O, Budczies J, et al. Combined targeted DNA and RNA sequencing of advanced NSCLC in routine molecular diagnostics: Analysis of the first 3,000 Heidelberg cases. Int J Cancer. 2019.
9. Larson BK, Tuli R, Jamil LH, Lo SK, Deng N, Hendifar AE. Utility of Endoscopic Ultrasound-Guided Biopsy for Next-Generation Sequencing of Pancreatic Exocrine Malignancies. Pancreas. 2018;47(8):990-5.
10. Rosenbaum MW, Jones M, Dudley JC, Le LP, Iafrate AJ, Pitman MB. Next-generation sequencing adds value to the preoperative diagnosis of pancreatic cysts. Cancer Cytopathol. 2017;125(1):41-7.
11. Singhi AD, McGrath K, Brand RE, Khalid A, Zeh HJ, Chennat JS, et al. Preoperative next-generation sequencing of pancreatic cyst fluid is highly accurate in cyst classification and detection of advanced neoplasia. Gut. 2018;67(12):2131-41.
12. Volckmar AL, Endris V, Gaida MM, Leichsenring J, Stogbauer F, Allgauer M, et al. Next generation sequencing of the cellular and liquid fraction of pancreatic cyst fluid supports discrimination of IPMN from pseudocysts and reveals cases with multiple mutated driver clones: First findings from the prospective ZYSTEUS biomarker study. Genes Chromosomes Cancer. 2019;58(1):3-11.
13. Suenaga M, Yu J, Shindo K, Tamura K, Almario JA, Zaykoski C, et al. Pancreatic Juice Mutation Concentrations Can Help Predict the Grade of Dysplasia in Patients Undergoing Pancreatic Surveillance. Clin Cancer Res. 2018;24(12):2963-74.

II

Preoperative imaging techniques

5

Gadoxetic acid-enhanced magnetic resonance imaging significantly influences the clinical course in patients with colorectal liver metastases

B.G. Sibinga Mulder, K. Visser, A.L. Vahrmeijer, R.J. Swijnenburg,
H.H. Hartgrink, S. Feshtali, R. van den Boom, M.C. Burgmans, J.S.D. Mieog

BMC Medical Imaging, 2018 Nov. Supplementary data available online.

ABSTRACT

Gadoxetic acid (Primovist™)-enhanced magnetic resonance imaging (P-MRI) scans have higher accuracy and increased detection of small colorectal liver metastases (CRLM) compared to CT scans or conventional MRI scans. But, P-MRI scans are still inconsistently acquired in the diagnostic work up of patients with CRLM. The aim of this study was to determine the influence of P-MRI scans on treatment plan proposition and subsequently the clinical course of the patient.

Eighty-three consecutive patients with potentially resectable CRLM based on a conventional CT scan underwent P-MRI scanning prior to treatment. Treatment plans proposed by the multidisciplinary team were compared before and after P-MRI scanning and related to the final treatment and diagnosis, the accuracy for the CT scan and P-MRI scan was calculated.

P-MRI scans led to a change of treatment in 15 patients (18%) and alteration of extensiveness of local therapy in another 17 patients (20%). All changes were justified leading to an accuracy of 93% for treatment proposition based on P-MRI scan, compared to an accuracy of 75% for the CT scan.

P-MRI scans provide additional information that can aid in proposing the most suitable treatment for patients with CRLM and might prevent short-term reintervention.

INTRODUCTION

Liver metastases arise in 50-65% of patients with colorectal cancer.(1, 2) Long-term survival can be achieved with surgical resection or local ablation therapy in patients with resectable colorectal liver metastases (CRLM).

Imaging plays a principal role in staging of CRLM. Nowadays, the most used imaging modalities are contrast-enhanced computed tomography (CT) or multi-detector row CT (MDCT). Both are limited in the detection of nodal involvement and characterization of small liver lesions compared to magnetic resonance imaging (MRI) scans.(3) A CT scan has a sensitivity and specificity of 68% and 94%, respectively, and a gadolinium contrast-enhanced MRI scan of 90% and 87%, respectively.(4) Different contrast agents can be administered for contrast-enhanced hepatic MRI scans, like gadoxetic acid, also called Primovist™ (P-MRI) (Bayer AG, Germany).(5, 6) The reported sensitivity of P-MRI for the detection of CRLM is 87-100% and the specificity is approximately 95%.(7-9) However, a CT scan is still the most frequently used to assess liver involvement and plan surgical resection (Dutch Oncoline guidelines: CRC). A P-MRI scan is not routinely acquired prior to liver resection in most centers.(8, 10). In addition, literature is lacking about the direct effect on treatment strategy in a clinical setting, including local therapy, systemic therapy or conservative treatment in a larger patient cohort. Therefore, there is still no convincing evidence whether P-MRI scans should play a more prominent role in the diagnostic process of patients with potential treatable CRLM and should be standardly acquired. The aim of this study was to determine the impact of P-MRI scans on treatment plan proposition and subsequently the clinical course of patients with potentially treatable CRLM, based on preoperative CT scans.

METHODS

The study was designed as a retrospective cohort study in which consecutive patients were included. The study was approved by the scientific review board of the Department of Radiology of the Leiden University Medical Center (LUMC) in 2017. Patient confidentiality was guaranteed using anonymized data and radiologic images, and all data was entered into an encrypted and secured database.

Patients

All patients with potential CRLM were discussed by a multidisciplinary team (MDT) of hepatobiliary surgeons, medical oncologists and (interventional) radiologists. In Figure 1 a flowchart is presented illustrating the standard operation procedure concerning the loco-regional treatment of CRLM in the LUMC. Patients presented at the MDT meeting

between July 2014 and August 2017 with primary resectable or primary irresectable (but potentially resectable after conversion therapy) CRLM based on the contrast enhanced (CE)-CT scan, of whom a P-MRI scan was obtained, were included in this study. Patients with permanent irresectable CRLM were not included. Patients who were previously treated for their CRLM with local therapy or systemic chemotherapy were also included. Patients in whom the time interval between acquirement of the CT scan and P-MRI scan or P-MRI scan and treatment was more than 2 months were excluded. Age, sex, localization of CRC, number of comorbidities, previous surgery and/or systemic therapy for CRC, and previous local therapy and/or systemic therapy for CRLM were noted.

CT scan

All CT scans included an arterial phase scan and a portal venous phase scan, using slices of 5 mm or less for reconstructive images. Contrast-enhance CT scans obtained in the LUMC were performed on a 16-slice spiral CT (Aquillion-16, Toshiba, Tokyo, Japan) using the following scanning parameters: 16x1 mm scanning, 120 KV, rotation 0.5 s, contrast Ultravist 370 (dose weight depended: for a standard patient (75 kg) 120ml was injected. Based on weight categories 46-60 kg, 60-80 kg, 80-100 kg, 100+ kg 20% more or less of the dose was administered) with a delay of 75 s for portal venous phase. Further parameters of CT scanning: the current modulation for the tube varying is from 10 to 500 mA. The pitch factor is 0.8125. Noise index with standard deviation of 10 is used. An Adaptive Iterative Dose Reduction (AIDR) 3D is used as reconstruction algorithm. The reconstruction kernel is FC 18 (soft tissue filter). The CT scans were scored for the presence, the number, location and size of all liver metastases. All scans were evaluated by one of four radiologists from the LUMC, all with at least five years of experience in liver imaging.

P-MRI scan

All P-MRI scans were performed in the LUMC on a Philips Ingenia 1.5 or 3.0 tesla. Gadoxetic acid was the intravenously administered contrast medium (10ml Primovist). MRI sequences included transveral and coronal T2 TSE (TE 80 and 250), transversal T1FFE mDIXON, diffusion weighted imaging at b0-10-500-1000, dynamic multiphase contrast-enhanced T1FFE images, including 20 minutes post-contrast images. See Supplementary Information table S1 for additional information about the used sequences. P-MRIs were read by one of four dedicated abdominal radiologist, each with at least five years of experience after board certification in radiology. Readers were not blinded for clinical information or prior medical imaging.

Study design

All patients were discussed by the MDT, which is a weekly meeting during which all patients who are potentially operable are discussed. As stated before, Figure 1 gives an overview of all possible treatment options in the LUMC. During the first MDT meeting a treatment plan was proposed based on the CT scan and classified as: (1) local therapy, consisting of either resection, percutaneous ablation or resection + ablation by radiofrequency ablation or microwave ablation, (2) conversion therapy with intent of local therapy or (3) follow-up in case of suspicion of benign lesion(s). Of note, patient with irresectable disease were excluded. Subsequently, an P-MRI scan was made and a treatment plan was proposed during the second MDT meeting, potentially changing the previously proposed treatment plan: (1) local therapy, (2) adjustment of the local therapy, in case the extensiveness of the local therapy was altered, (3) conversion therapy, (4) palliation, in case of diffuse disseminated disease resulting in less than 20% of healthy liver parenchyma, or extrahepatic disease (EHD) or (5) follow-up.

Finally, the proposed treatment plan based on the P-MRI scan was compared to the actual performed treatment.

For clarification, 'conversion therapy' is administered with the purpose of reverting the disease from irresectable to resectable. Conversion therapy was mostly a combination of capecitabine with oxaliplatin (CAPOX) usually given in three week cycles with a maximum of eight cycles total. 'Palliation' is applied if resection is not considered a (future) option.

In case the patients underwent surgery, the liver was assessed with intraoperative ultrasound by a radiologist. Additionally, in some patients near-infrared fluorescence (NIRF) imaging, using indocyanine green, was performed for the detection of occult (sub)capsular liver metastases.(11)

Follow-up

In case the liver lesions were resected, standard pathological assessment of the lesions was performed. The pathological assessment was used as reference. Follow-up of the liver occurred every four months with CE-CT scan and CEA serum level measurements. In case new intrahepatic lesions were identified during the first follow-up visit, these lesions were probably already present during the procedure and were therefore missed on the P-MRI scan. During the follow-up process of the patients whose lesions were defined as benign, it became clear if these lesions were indeed not CRLM. A minority of patients were referred back to the external hospital for follow-up.

Statistical analysis

Data were analyzed using a statistical software program (SPSS, version 23.0). The change in treatment proposition between MDT meeting 1 and 2 was evaluated using an independent samples *t*-test with standard error and 95% confidence interval. Furthermore, an indepen-

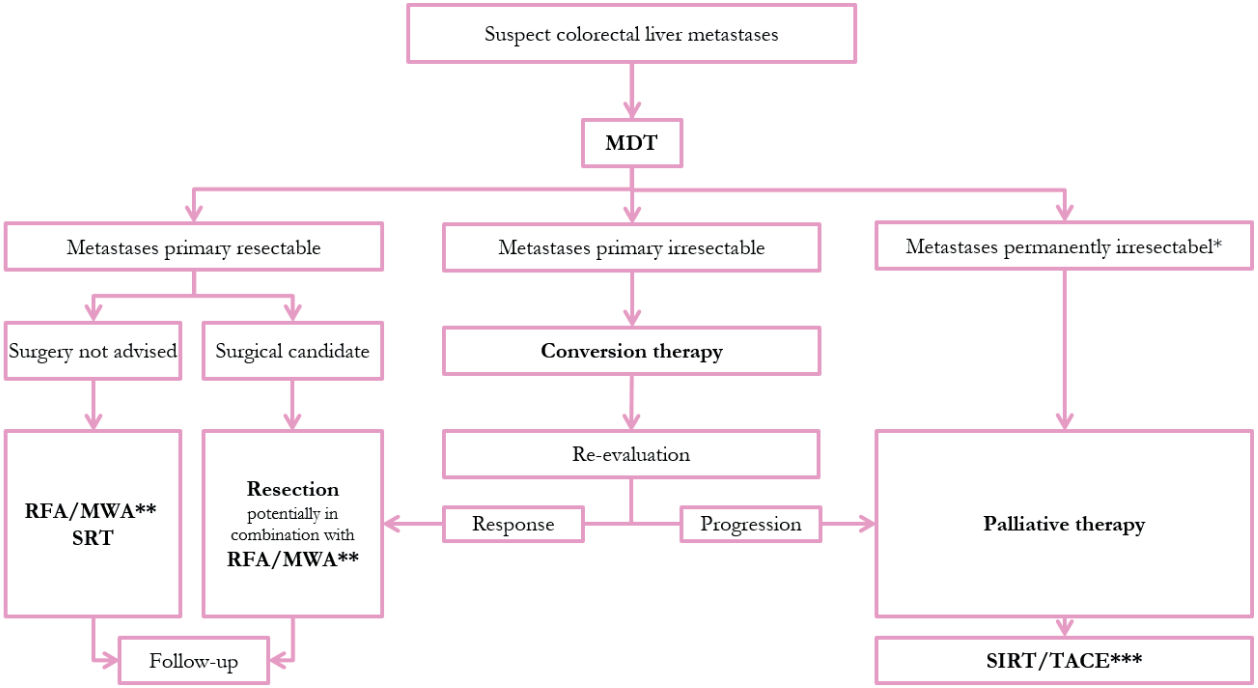

Figure 1. Standard operation procedure concerning the loco regional treatment of CRLM in the Leiden University Medical Center.

* Permanently irresectable: <20% healthy liver parenchyma, extrahepatic disease (not curable)

** For a small (<3cm) centrally located solitaire metastasis in a surgical candidate, percutaneous ablation can be preferred over surgery in the context of parenchyma sparing treatment

*** Dutch guideline only advises TACE in study context

MDT: multidisciplinary team; RFA: radiofrequency ablation; MWA: microwave ablation; SRT: stereotactic radiotherapy; SIRT: selective internal radiation therapy ; TACE: trans arterial chemoembolization

dent samples *t*-test was performed for 1) comparison of the interval between the date of P-MRI scan and date of actual treatment between the patients who underwent local therapy without adjustment of the local therapy and with adjustment, and 2) for the change in treatment proposition between the group with CT-scan acquired in an external hospital and in the LUMC. The statistical results were considered to indicate significance if the P-value was less than 0.05.

RESULTS

Patients

In total, 83 patients were included in the study cohort. Patient and treatment characteristics are summed in Table 1.

Table 1. Patient and treatment characteristics.

Characteristics	
	N=83
Age at time of CT scan; mean ± SD	64.8 ± 10.7
Sex, male; n (%)	56 (68)
Synchronous CRLM; n (%)	44 (53)
Comorbidities; n (%)	
0	36 (43)
1	28 (34)
≥2	19 (23)
Previous CRLM surgery, n (%)	18 (22)
CT scan made in LUMC, n (%)	32 (39)
Days between; mean ± SD	
CT and P-MRI	29.0 ± 17.1
Days between P-MRI and treatment	28.0 ± 15.8
Actual treatment; n (%)	
Local	50 (60)
Neo-adjuvant chemotherapy	15 (18)
Palliation	10 (12)
Follow-up	8 (10)

CRLM: colorectal liver metastases; P-MRI: primovist MRI scan

Treatment proposition

The type of treatment was changed in 15 patients (18%) due to the P-MRI scans, all these changes were in concordance with the actual treatment performed.

The intended extensiveness of the local therapy was altered in another 17 patients (20%) due to the P-MRI scan: in 11 patients more malignant lesions were identified with P-MRI (mean number additional lesions: 1.6 range; 1-3) (mean size additional lesions: 6.7 mm; range 2-16 mm), the additional identified lesions were located peripheral, superficial and central in the liver. In six patients less lesions were defined as malignant (mean number: 2.0 range; 1-6). These lesions were either considered as cysts (n=3), haemangiomas (n=5), steatosis (n=2) or could not be retrieved (n=2) on the P-MRI scan.

Together the treatment plan proposition was altered in 32 patients (38%; standard error of the mean: 5%; 95% confidence interval: 28-49%). The treatment plan of the remaining 51 patients (61%) was not altered. Table 2 gives an overview of the changes in treatment plan.

Table 2. Comparison of treatment plans proposed during MDT 1 and MDT 2.

		MDT 2					
		Local	**Local therapy adjustment**	**Neoadjuvant**	**Palliation**	**Follow-up**	**Total**
MDT 1	**Local**	39	*17*	**5**	**3**	**4**	68
	Neoadjuvant			9	**1**	**1**	11
	Follow-up	**1**				3	4
	Total	40	17	14	4	8	83

Changes in treatment plan are shown in bold. Extensiveness adjustment of local therapy in italic.

Actual treatment

In 56 patients the intended treatment based on the P-MRI scan was local therapy and the extensiveness of the local therapy was altered during the treatment in 10 patients, either more lesions (in six patients) or less lesions (in 4 four patients) were detected and resected during surgery. For detection of lesions intra-operative ultrasound and NIRF imaging could be used. The additional lesions were biopsied for histological confirmation. The patients with lesions that could not be retrieved did not develop CRLM during the follow-up period, so these lesions were considered false-positive.

In five patients, who were deemed resectable on both CT scan and P-MRI scan, no resection or ablation was performed because a too diffuse disease (n=3) or too extensive tumor burden (n=2) was encountered during surgical exploration. They were palliated instead.

In one patient the proposed treatment based on the CT scan and P-MRI scan was local therapy, but eventually this patient was not fit for surgery, therefore, he was palliated.

The extensiveness of local therapy of the other 40 patients was not altered, they were treated within a mean of 29.0 days (SD 12.6 days) after the P-MRI scan was obtained, which

was not significantly different from the 15 patients with adjusted local therapy (28.3 days (SD 20.7 days)) (P-value = 0.904).

In addition, there was no significant difference in change of treatment plan between patients whose CT scans were from external hospitals (31% change of treatment) and patients whose CT scans were from the LUMC (41% change of treatment) (p-value = 0.48).

An overview of the changes in treatment plan proposition during MDT meeting 1 and 2, and the actual treatment performed is given in Figure 2.

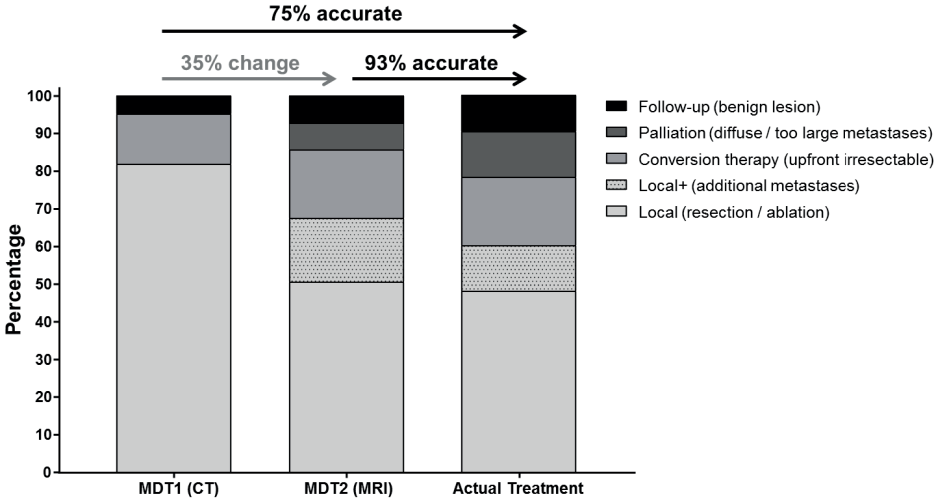

Figure 2. Changes in treatment plan and actual treatment in percentages.

Follow-up

All patients had a follow-up period of at least three months, median follow-up period was 14.4 months (1.38-41.7). Fifteen (18%) patients developed new intrahepatic CRLM within a median time of 5.3 months (0.8-14.0) after local treatment, in three of these patients the new intrahepatic CRLM occurred within 4 months after local therapy. Of the eight patients with lesions deemed as benign, the median follow-up period was 22.0 months (4.1-41.2). One patient developed diffuse CRLM within six months. This patient presented with one lesion that couldn't be characterized on the CT scan and was assessed as a hemorrhagic-cyst on the P-MRI scan, but eventually turned out to be a metastasis.

Accuracy

The treatment plan proposition based on the P-MRI scan was accurate in 77 patients (93%). In five patients an too extensive disease was encountered during surgery and in one patient a CRLM was characterized as a hemorrhagic-cyst on the P-MRI scan. The treatment plan proposition based on the CT scan of these six patients was the same as the one based on the

P-MRI scan. The 15 changes of treatment type due to findings on the P-MRI scans were all correct, so the accuracy of the CT scan for treatment plan proposition was accurate in 62 patients (75%).

DISCUSSION

Our study focusses on the effect of the P-MRI scans on the treatment plan proposition and clinical course in patient with potential resectable CRLM based on CT scans. The initial treatment plan proposal based on the CT scan was changed in 38% of the patients due to the findings on P-MRI scans. Compared to the final treatment, the proposition based on the P-MRI scan was accurate in 93% of the patients, compared to 75% of the propositions based on CT scans.

The diagnostic accuracy of the P-MRI scans in patients with CRLM and also the impact on surgical strategy has been previously described: in a study of Sofue *et al.*, the surgical strategy changed in 33% of the patients due to the P-MRI scans.(12) The recent study of Jhaveri *et al.* describes changes in surgical strategy due to P-MRI scans in 45% of the patients receiving neoadjuvant therapy.(13) In contrast, Kang *et al*. also investigated the changes in surgical strategy, but only changed the surgery in 3% of the patients.(14) Only Vreugdenburg *et al*. also determined the impact of P-MRI scans on patient management, but only four of the 13 included studies investigated patient outcome, mainly focusing on surgical strategy instead of treatment strategy.(9)

Our single center study emphasizes not only the impact of P-MRI scans on surgical strategy but on the entire treatment plan proposition. The implementation of obtaining a P-MRI scan in the diagnostic work-up of patients has several positive effects on the clinical course of the patients. The most important consequence is the prevention of unnecessary surgeries due to better differentiation between malignancies and benign lesions on P-MRI scans. A second advantage, which is also nicely demonstrated by the study of Knowles *et al.* is the more accurate staging based on P-MRI scans prior to conversion chemotherapy, thereby reducing intra-hepatic recurrence and avoid repeated hepatectomy.(15) In our study more patients were treated with conversion therapy prior to surgery due to new findings on the P-MRI scan. Furthermore, in other patients the intended local therapy was extended due to the additional identification of small lesions with P-MRI scans, resulting in the prevention of short-term reinterventions for new intrahepatic lesion development after treatment. P-MRI scanning aids in surgical planning, surgeons and/or interventional radiologist are preoperatively better prepared in comparison to CT scan alone, which might result in more curative resections and less new intrahepatic CRLM formation quickly after surgery. However, these lesions might be detected during local treatment anyway with intraoperative ultrasound or other additional techniques as NIRF-guided surgery, which has the potential

to detect additional small superficial lesion in approximately 15% of the patients.(11, 16) All current studies still advocate repeated therapy or resection to treat all CRLM, including recurrent CRLM, to improve survival rate.(17, 18) In addition, liver parenchyma sparing therapy improves 5-year survival rates, because repeated therapy can be applied if desired. (19) Therefore, accurate imaging can aid in proposing the most suitable treatment strategy, prevent reinterventions and treat as liver parenchyma sparing as possible. In combination with supplementary techniques, like NIRF guided surgery and intra-operative ultrasound, not only detection of CRLM will increase, also radical resection rates will improve and reinterventions can be prevented, all resulting in improved patient outcome. Therefore, future studies should also focus on the bundling of all pre- and intraoperative techniques.

Our study has several limitations. Due to the retrospective study design, decision making was retrospectively collected, however, consecutive patients were included and image and treatment plan evaluation during the MDT meetings was performed in real time and well-documented in the electronic patient charts. This resulted also a non-standardized assessment of the scans by four different radiologists. Differences between CT scans and P-MRI scans could be explained due to the differences between readers. Furthermore, readers were not blinded for the CT scans during P-MRI scan assessment. However, this resulted in a realistic representation of the "everyday practice". Additionally, the follow-up scans were CT scans and not P-MRI scans because follow-up is performed according to the current national guidelines. Time-interval between obtaining the P-MRI scan and the actual treatment might be of influence. But, we found no significant differences for both the origin of acquirement of CT scans or for the time-interval. Sensitivity and specificity could not be calculated based on our study results without introducing bias. Moreover, sensitivity and specificity have been examined extensively in multiple studies, and will be of no additional value. Finally, we can interpret our results only by looking at the patient's clinical course, based on which the treatment plan proposition using P-MRI scan had an accuracy of 93%. However, we have no proof that these treatment propositions were superior to the treatment propositions based on the CT scans, especially, those in whom the patients were administered conversion therapy instead of upfront local therapy, as described above.

To conclude and most importantly, our study is a display of the clinical decision making in a Dutch academic center, underlining the added value of a P-MRI scan in the entire treatment process of CRLM, improving cancer care and clinical outcome for these patients. In which we showed that P-MRI scans provide additional information that can aid in proposing the most suitable treatment and might prevent short-term reintervention of patients with CRLM. Incorporating an P-MRI scan in the work-up of CRLM patients can improve treatment proposition and clinical outcome compared to CT scanning alone.

REFERENCES

1. Haddad AJ, Bani Hani M, Pawlik TM, Cunningham SC. Colorectal liver metastases. Int J Surg Oncol. 2011;2011:285840.
2. Alberts SR, Poston GJ. Treatment advances in liver-limited metastatic colorectal cancer. Clin Colorectal Cancer. 2011;10(4):258-65.
3. Koh FHX, Tan KK, Teo LLS, Ang BWL, Thian YL. Prospective comparison between magnetic resonance imaging and computed tomography in colorectal cancer staging. ANZ J Surg. 2018;88(6):E498-E502.
4. Schulz A, Viktil E, Godt JC, Johansen CK, Dormagen JB, Holtedahl JE, et al. Diagnostic performance of CT, MRI and PET/CT in patients with suspected colorectal liver metastases: the superiority of MRI. Acta Radiol. 2016;57(9):1040-8.
5. Weinmann HJ, Schuhmann-Giampieri G, Schmitt-Willich H, Vogler H, Frenzel T, Gries H. A new lipophilic gadolinium chelate as a tissue-specific contrast medium for MRI. Magn Reson Med. 1991;22(2):233-7; discussion 42.
6. Ba-Ssalamah A, Bastati N, Wibmer A, Fragner R, Hodge JC, Trauner M, et al. Hepatic gadoxetic acid uptake as a measure of diffuse liver disease: Where are we? J Magn Reson Imaging. 2017;45(3):646-59.
7. Colagrande S, Castellani A, Nardi C, Lorini C, Calistri L, Filippone A. The role of diffusion-weighted imaging in the detection of hepatic metastases from colorectal cancer: A comparison with unenhanced and Gd-EOB-DTPA enhanced MRI. Eur J Radiol. 2016;85(5):1027-34.
8. Kim HJ, Lee SS, Byun JH, Kim JC, Yu CS, Park SH, et al. Incremental value of liver MR imaging in patients with potentially curable colorectal hepatic metastasis detected at CT: a prospective comparison of diffusion-weighted imaging, gadoxetic acid-enhanced MR imaging, and a combination of both MR techniques. Radiology. 2015;274(3):712-22.
9. Vreugdenburg TD, Ma N, Duncan JK, Riitano D, Cameron AL, Maddern GJ. Comparative diagnostic accuracy of hepatocyte-specific gadoxetic acid (Gd-EOB-DTPA) enhanced MR imaging and contrast enhanced CT for the detection of liver metastases: a systematic review and meta-analysis. Int J Colorectal Dis. 2016;31(11):1739-49.
10. Cho JY, Lee YJ, Han HS, Yoon YS, Kim J, Choi Y, et al. Role of gadoxetic acid-enhanced magnetic resonance imaging in the preoperative evaluation of small hepatic lesions in patients with colorectal cancer. World J Surg. 2015;39(5):1161-6.
11. van der Vorst JR, Schaafsma BE, Hutteman M, Verbeek FP, Liefers GJ, Hartgrink HH, et al. Near-infrared fluorescence-guided resection of colorectal liver metastases. Cancer. 2013;119(18):3411-8.
12. Sofue K, Tsurusaki M, Murakami T, Onoe S, Tokue H, Shibamoto K, et al. Does Gadoxetic acid-enhanced 3.0T MRI in addition to 64-detector-row contrast-enhanced CT provide better diagnostic performance and change the therapeutic strategy for the preoperative evaluation of colorectal liver metastases? Eur Radiol. 2014;24(10):2532-9.
13. Jhaveri KS, Fischer SE, Hosseini-Nik H, Sreeharsha B, Menezes RJ, Gallinger S, et al. Prospective comparison of gadoxetic acid-enhanced liver MRI and contrast-enhanced CT with histopathological correlation for preoperative detection of colorectal liver metastases following chemotherapy and potential impact on surgical plan. HPB (Oxford). 2017;19(11):992-1000.

14. Kang SI, Kim DW, Cho JY, Park J, Lee KH, Son IT, et al. Is MRI of the Liver Needed During Routine Preoperative Workup for Colorectal Cancer? Dis Colon Rectum. 2017;60(9):936-44.
15. Knowles B, Welsh FK, Chandrakumaran K, John TG, Rees M. Detailed liver-specific imaging prior to pre-operative chemotherapy for colorectal liver metastases reduces intra-hepatic recurrence and the need for a repeat hepatectomy. HPB (Oxford). 2012;14(5):298-309.
16. Handgraaf HJM, Boogerd LSF, Hoppener DJ, Peloso A, Sibinga Mulder BG, Hoogstins CES, et al. Long-term follow-up after near-infrared fluorescence-guided resection of colorectal liver metastases: A retrospective multicenter analysis. Eur J Surg Oncol. 2017;43(8):1463-71.
17. Kishi Y, Nara S, Esaki M, Shimada K. Feasibility of "Watch-and-Wait" Management before Repeat Hepatectomy for Colorectal Liver Metastases. Dig Surg. 2018.
18. Neal CP, Nana GR, Jones M, Cairns V, Ngu W, Isherwood J, et al. Repeat hepatectomy is independently associated with favorable long-term outcome in patients with colorectal liver metastases. Cancer Med. 2017;6(2):331-8.
19. Mise Y, Aloia TA, Brudvik KW, Schwarz L, Vauthey JN, Conrad C. Parenchymal-sparing Hepatectomy in Colorectal Liver Metastasis Improves Salvageability and Survival. Ann Surg. 2016;263(1):146-52.

6

A dual-labeled cRGD-based PET/optical tracer for preoperative staging and intraoperative treatment of colorectal cancer

B.G. Sibinga Mulder, H.J.M. Handgraaf, D.J. Vugts,
C. Sewing, M.A. Stammes, M.W. Bordo, A.D. Windhorst,
C.J.H. van de Velde, J.S.D. Mieog, J.V. Frangioni, A.L. Vahrmeijer

American Journal of Nuclear Medicine and Molecular Imaging, 2018 Oct. Supplementary data available online.

ABSTRACT

cRGD peptides target integrins associated with angiogenesis (e.g., αvβ3) and cancer, and have been used as binding ligands for both positron emission tomography (PET) and near-infrared fluorescence (NIRF) optical imaging. This study introduces the hybrid tracer cRGD-ZW800-1-Forte-[^{89}Zr]Zr-DFO, which is based on a novel zwitterionic fluorophore structure that reduces non-specific background uptake during molecular imaging of tumors.

An *in vitro* binding assay was used to validate tracer performance. 10 nmol ZW800F-cRGD-Zr-DFO was injected in mice (n=7) bearing orthotopic human colorectal tumors (HT29-luc2) for tumor detection with NIRF imaging. Subsequently, ZW800F-cRGD-Zr-DFO was loaded with ^{89}Zr and 10 nmol cRGD-ZW800-1-Forte-[^{89}Zr]Zr-DFO (3 MBq) was injected in mice (n=8) for PET/CT imaging. Imaging and biodistribution was performed at 4 and 24 h. NIRF imaging was performed up to 168 h after administration.

Sufficient fluorescent signals were measured in the tumors of mice injected with ZW800F-cRGD-Zr-DFO (emission peak ~800nm) compared to the background. The signal remained stable for up to 7 days. The fluorescence signal of cRGD-ZW800-1-Forte-[^{89}Zr]Zr-DFO remained intact after labeling with ^{89}Zr. PET/CT permitted clear visualization of the colorectal tumors at 4 and 24 h. Biodistribution at 4 h showed the highest uptake of the tracer in kidneys and sufficient uptake in the tumor, remaining stable for up to 24 h.

A single molecular imaging agent, ZW800F-cRGD-[^{89}Zr]Zr-DFO, permits serial PET and NIRF imaging of colorectal tumors, with the latter permiting image-guided treatment intraoperatively. Due to its unique zwitterionic structure, the tracer is rapidly renally cleared and fluorescent background signals are low.

INTRODUCTION

Up to 50% of patients diagnosed with colorectal cancer have either obvious or occult metastases. Initially the liver tends to harbor metastases, but peritoneal and pulmonary metastases arise as well, either synchronously or metachronously.(1) Patients with metastases require a different form of therapy (e.g. liver metastasectomy, HIPEC, palliative treatment) compared to those without. Therefore, selection of truly non-metastatic patients who will benefit from curative-intended surgery is of paramount importance. For those receiving surgery, complete resection of the primary tumor with minimal morbidity is the goal. Although resection of primary tumors in the upper colon is straightforward, lower rectal resections are extremely difficult when preservation of rectal function is intended.(2)

Currently, distinguishing fibrosis, inflammation, and viable tumor tissue remains difficult both preoperatively and intraoperatively, especially in patients who received neoadjuvant chemoradiotherapy. As a consequence, even patients with a pathological complete response need to undergo resection, with potentially major complications, or an ostomy, as a result. During surgery, differentiation between malignant and benign tissue is mostly performed by visual inspection and palpation, being subjective and inaccurate. Near-infrared fluorescence (NIRF) imaging is an optical technique that permits real-time visualization of tumors during surgery using targeted fluorescent tracers.(3) Several clinical studies have demonstrated successful intraoperative identification of various tumor types.(4-6) However, NIRF imaging has an important drawback; it has a limited depth penetration of approximately 5-8 mm.(7, 8) Therefore, small metastatic tumor deposits located deeper or outside the surgeon's field of view cannot be directly identified.

To improve the management of patients diagnosed with colorectal cancer, biomedical imaging needs to meet two main requirements: 1) accurate identification of metastatic disease to preoperatively select those patients who will ultimately benefit from surgery, and, 2) real-time visualization of tumor margins in order to minimize surgical morbidity. Furthermore, obtaining market approval for even a single drug typically costs hundreds of millions of dollars and over seven years of time. There is therefore great need to develop single contrast agents (drugs) that have more than one indication.(9)

Several prior reports have combined radioscintigraphy and optical imaging to perform these tasks. The first *ex vivo* study with dual-labeled girentuximab, an antibody targeting carbonic anhydrase IX (CAIX), demonstrated that the combination of radionuclide (SPECT) and fluorescence imaging is feasible.(10) Full-length antibodies have long serum half-lives, though, resulting in non-specific background fluorescence after injection, and imaging possible only four to seven days later. In addition, they have the potential for adverse immunological reactions, and are costly to produce.

This paper focuses on a small molecule imaging agent that can be used to improve the care of colorectal cancer patients. This agent is based on the tripeptide Arg-Gly-Asp (RGD),

which targets various integrins (αvβ1, αVβ3, αvβ5, αvβ6, αvβ8, α5β1, α8β1 and αIIbβ3), some of which are overexpressed on tumor cells and tumor-associated vascular endothelium, correlating with neoangiogenesis.(11) Indeed, multiple tumor types have successfully been identified in several phase I and II clinical trials with RGD-based PET tracers.(12-14) In our previous preclinical study (15), cyclic RGD (cRGD) was conjugated to the near-infrared (NIR) fluorophore ZW800-1. Intravenous administration of cRGD-ZW800-1 permitted *in vivo* fluorescence imaging of multiple tumor types in mice. A clinical study investigating cRGD-ZW800-1 in patients is currently ongoing (NL6250805817).

ZW800-1 Forte is a novel zwitterionic NIR fluorophore that has the potential to further improve the tumor-to-background ratio because of its unusually high stability *in vivo.*(16) A disadvantage of the previously described cRGD-ZW800-1 agent for use with long half-life tracers, such as ^{89}Zr, is its short-lived stability in serum. We therefore focus in this paper on a hybrid tracer with a more stable NIR fluorophore variant ZW800-1 Forte (ZW800F), which retains the zwitterionic motif known to reduce non-specific background in non-tumor tissues.(17) We aim to assess the feasibility to perform PET and NIR fluorescence imaging of tumors with a single injection of ZW800F-cRGD-Zr-DFO.

METHODS

Figure 1 gives an overview of the study design and study purposes.

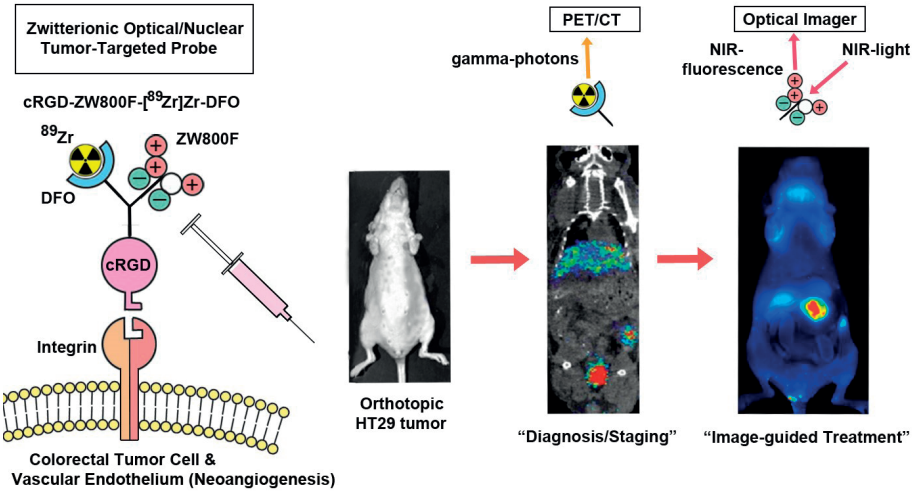

Figure 1: Study design and purposes.

Tracer synthesis and labeling procedures

Synthesis of tracer cRGD-ZW800-1-Forte-[^{89}Zr]Zr-DFO (cRGD-ZW800F-[^{89}Zr]Zr-DFO), and labeling procedures are extensively described in the supplementary data file. In short, commercially available deferoxamine (DFO) was pre-loaded and coupled to an activated boc-L-glutamic acid 1 tert-butyl ester (NHS-ester) to produce Boc-Glu(OtBu)-DFO[Fe]. The near-infrared contrast agent ZW800F was conjugated to the L-GLU-DFO[Fe] compound using a pre-activated NHS-ester. The remaining carboxyl group on the glutamic acid was converted into a TFP-ester using EDC/TFP in a MES buffer. The TFP-ester was reacted with commercially available cRGDyK to produce ZW800F-Glu(cRGDyK)-DFO[Fe]. Hereafter, 0.49 mL 0.5 M HEPES and 20 µL 2 mM cRGD-DFO-ZW800F were added to 100 µL 1 M oxalic acid containing 56.3 MBq of zirconium (mixed and reacted with 37 µL 0.9% NaCl and 45 µL 2M Na_2CO_3) and applied to a tC18 Sep-Pak, which was preconditioned with 10 mL ethanol and 10 mL water. After washing and collection of the product it was formulated to achieve a dose of 10 nmol/3 MBq ZW800F-cRGD-[^{89}Zr]Zr-DFO per mouse, and was immediately injected. For preparation of ZW800F-cRGD-Zr-DFO 100 µL 1 M oxalic acid containing 400 nmol (2 equivalents) of zirconium was used (mixed and reacted with 345 µL 0.9% NaCl and 45 µL 2M Na_2CO_3). Stability results are presented in Figure 2A.

The absorbance peak of the previously described cRGD-ZW800-1 is 773 nm.(15) The hybrid tracer ZW800-1 Forte variant has two absorbance peaks, a dominant one at 754 nm and a minor one at 680 nm. DFO was used to enable radiolabeling with the isotope zirconium-89. Because of its long half-life, ^{89}Zr has the major advantage of permitting imaging long after injection, when most background has cleared from the body. To match the long radioisotope half-life, the ZW800-1 Forte variant was used instead of ZW800-1. Chemical structures are displayed in Figure 2B.

In vitro binding assay

To evaluate the binding capacity of ZW800F-cRGD-Zr-DFO *in vitro*, the human colorectal cell line HT29-luc2 was used. Experiments were performed in triplicate. The cells were plated in a 96-well plate at a density of ~40,000 cells per well. At 90-100% confluence, cells were washed and incubated with various concentrations of ZW800F-cRGD-DFO at 37º C for 1 h. The cells were then washed. Subsequently, the cells were imaged using the Odyssey NIR scanner (LI-COR Biosciences, Lincoln, Nebraska; 800 nm channel) to quantify the fluorescence intensity. Next, cells were permeabilized with a 40/60 mixture of acetone and methanol followed by a washing step and 5 minutes incubation with ToPro3 (1/2000, Invitrogen), a far-red fluorescent dye. The wells were then washed again and imaged with the Odyssey scanner (700 nm channel) to quantify the number of cells in each well. No negative cell line could be used, because none of the cells are negative for cRGD-binding integrins. For example, the αvβ3 negative cell line HT-29 shows high expression of integrin avb5.(15)

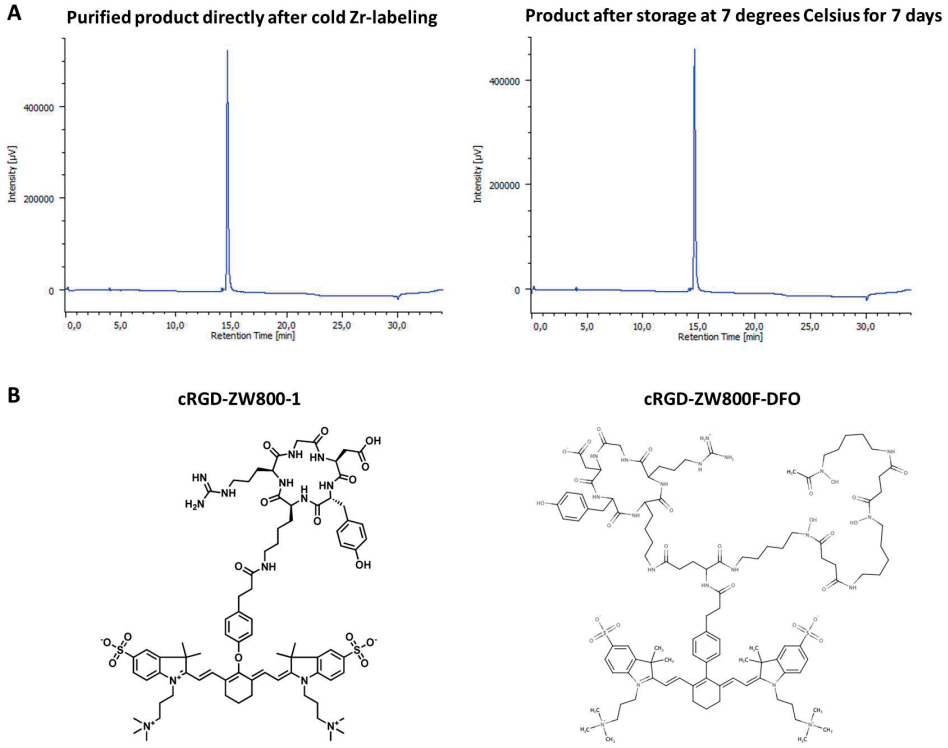

Figure 2: Stability results and chemical structures.
A: Stability results over 7 days**.** B: Chemical structures

In vivo tumor model

For *in vivo* PET and fluorescence imaging, the previously described orthotopic colorectal tumor model with HT29-luc2 cells was used.(15, 18) In short: six week-old athymic female mice (CD1-Foxn1nu, Charles River Laboratories, Wilmington, MA, U.S.A.) were housed in ventilated cages. To induce subcutaneous tumors, colorectal cancer cells (HT-29) were injected at 4 sites on the back (500,000 cells per spot). Subsequently, these colorectal tumor cells were transplanted to the colons of fresh mice, as described by Tseng *et al.*(19) Tumor growth and potential metastases were checked regularly using luciferin and *in vivo* bioluminescence imaging with the IVIS Spectrum (In Vivo Imaging System, PerkinElmer, Waltham, MA, U.S.A.). The Animal Welfare Committee of Leiden University Medical Center approved all animal experiments for animal health, ethics, and research. All animals received humane care and maintenance in compliance with the "Code of Practice Use of Laboratory Animals in Cancer Research" (Inspectie WandV, July 1999).

Fluorescence imaging

Evaluation of fluorescence imaging with ZW800F-cRGD-Zr-DFO was performed with zirconium-90, a non-radioactive isotope, this was done to meet the radiation hygiene requirements for the optical imaging facility. Animals were imaged using the Pearl® imager (LICOR, Lincoln, NE, U.S.A.). The Pearl® imager uses an excitation laser of 785 nm and detects all fluorescence above 800 nm. Based on previously achieved results with cRGD-ZW800-1, all mice were imaged at 4 h and 24 h post injection.(15) Tumor-to-background ratios (TBRs) were calculated by dividing the tumor signal by the background signal (colon without tumor). After sacrificing the mice, all organs were collected and imaged using the Pearl® to evaluate the biodistribution based on fluorescence signals.

In vivo comparison of cRGD-ZW800-1 and ZW800F-cRGD-Zr-DFO

For evaluation of the stability and tumor-specificity of ZW800F-cRGD-Zr-DFO, the TBRs and fluorescence signal in the tumor obtained with the hybrid tracer were compared with the previously reported results with ZW800-cRGD-1.(15) In that study, mice bearing orthotopic HT29-luc2 tumors were injected with the optimal dose of 10 nmol cRGD-ZW800-1 and imaged at 4 h and 24 h post injection. Therefore, seven mice bearing orthotopic HT29-luc2 tumors were injected with 10 nmol ZW800F-cRGD-Zr-DFO. Bioluminescence imaging was performed with luciferin and the IVIS Spectrum to compare the size of each orthotopic HT29-luc2 tumor. The percentage decrease in fluorescence intensity (arbitrary units; AU) at 24 h compared to 4 h and TBRs were calculated. To assess the stability of the fluorescence signals *in vivo*, mice bearing subcutaneous HT29-luc2 tumors were injected with 10 nmol ZW800F-cRGD-Zr-DFO. The signals in the tumors and background were measured up to 168 h post injection with the Pearl® imager. Furthermore, a complete biodistribution was performed and assessed with the Pearl® imager at 24 h (n=3). The fluorescence signals of the organs compared to the tumor (organ-to-tumor ratio; OTR) of both tracers were evaluated. Because of the differences in excitation wavelengths of ZW800-1 and ZW800F and the fixed excitation wavelength of the Pearl® imager, the TBRs and the OTRs were compared instead of the fluorescence intensity of the tracers.

PET/CT

Animals were imaged with a dedicated small animal NanoPET/CT scanner (Mediso Ltd., Hungary) at VU University Medical Center. Eight mice bearing orthotopic HT29-luc2 tumors were each injected with 10 nmol cRGD-ZW800F-[^{89}Zr]Zr-DFO(3 MBq). Mice were anesthetized by inhalation of 2% isoflurane and scanned at 1, 4 and 24 h post injection. A CT scan was acquired prior to the PET scan and was used for morphological correlation and for attenuation and scatter correction purposes. Reconstruction was performed with a fully 3-dimensional (3-D) reconstruction (Tera-Tomo; Mediso Ltd., Hungary) with four iterations and six subsets, resulting in an isotropic 0.4 mm voxel dimension. The scanner was

cross-calibrated with the dose calibrator and well counter, enabling the derivation of accurate standard uptake value (SUV) measures. Biodistribution was performed at 4 h (n=4) and 24 h (n=4) post-injection. After sacrificing the mice, all organs and several tissues were excised to determine the percentage of the injected dose per gram (%ID/g) with the gamma counter to evaluate biodistribution. Tumor visualization and biodistribution with NIRF imaging using ZW800F-cRGD-Zr-DFO were compared with PET/CT using cRGD-ZW800F-[^{89}Zr]Zr-DFO.

Statistical analysis

GraphPad Prism software (version 7.0, GraphPad Software Inc., La Jolla, California, U.S.A.) was used for statistical analyses. All values were reported using mean and standard deviation, unless otherwise described. For all *in vivo* studies at least three mice per group were included in order to be able to perform statistical power. Statistical significance for comparison of TBRs of the Pearl®, and comparison of fluorescence intensity of tumors, was determined using an independent *t*-test. Differences in the biodistribution were calculated by two-way analysis of variance (ANOVA). Group means were calculated for continuous data and medians were calculated for discrete data (scores). Test statistics were calculated on the basis of exact values for means and pooled variances. All tests were two-sided and in all an alpha of 5.0% was used.

RESULTS

Stability of cRGD-ZW800F-[^{89}Zr]Zr-DFO

HPLC at 780 nm of ZW800F-cRGD-Zr-DFO demonstrated a stable product up to 7 days after labeling with ^{89}Zr (Supplementary Information S1).

In vitro binding assay

A binding assay with ZW800F-cRGD-Zr-DFO on HT29-luc2 cells showed an almost linear increase in fluorescence intensity with increasing concentrations (Figure 3A).

Comparison of cRGD-ZW800-1 and ZW800F-cRGD-Zr-DFO

Clear tumor demarcation was possible in the mice that were injected with ZW800F-cRGD-Zr-DFO. Figure 3B shows the concordance between the bioluminescent signal of the tumor measured with the IVIS and the fluorescent signal measured with the Pearl. In one mouse, bioluminescence showed a metastasis, which was also detected by NIR fluorescence imaging.

TBRs obtained in mice injected with ZW800F-cRGD-Zr-DFO were significantly higher (p=0.03) than those injected with cRGD-ZW800-1 at 24 h (Figure 4A). The fluorescence intensity of the tumor remained more stable using ZW800F-cRGD-Zr-DFO: only

a decrease in intensity of 37% was observed between 4 and 24 h, compared to a 56% decrease in mice injected with cRGD-ZW800-1. In the subcutaneous HT29-luc2 tumor model, ZW800F-cRGD-Zr-DFO demonstrated a similar decrease of 33% ± 5.1% at 24 h (Figure 4B). Approximately 50% of the fluorescence signal in tumors remained at 48 h post injection and approximately 20% of the signal remained at 7 days post injection (Figure 3).

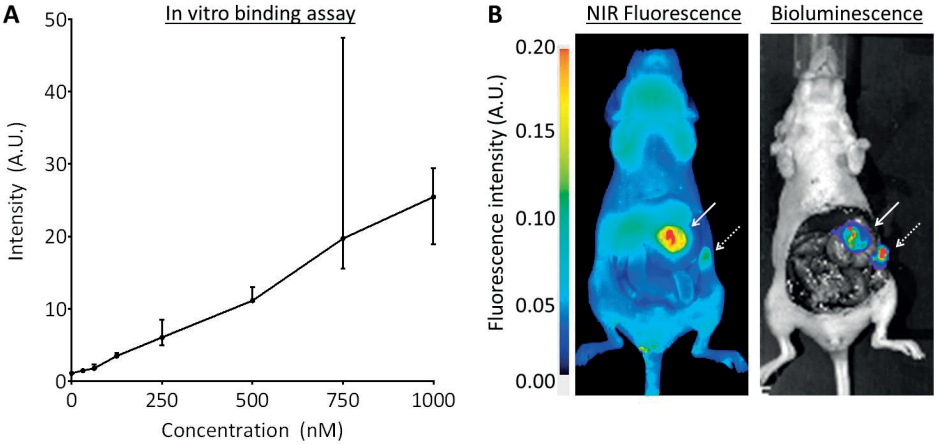

Figure 3: Binding of ZW800F-cRGD-DFO to HT-29 colorectal tumor cells.
A: *In vitro* binding assay (median and range). B: *In vivo* binding of ZW800F-cRGD-Zr-DFO to the tumor (white arrow) and a peritoneal metastasis (dashed arrow) at 4 h after injection. NIRF imaging (Pearl) is in concordance with bioluminescence signals (IVIS).

The organ-to-tumor ratio (OTR) measured at 24 h (Figure 4C) demonstrated that conjugation of DFO did not significantly change distribution. In fact, even better results were obtained, with background in the liver, skin, intestines and all other organs at least half as fluorescent as the tumor. The only exception was the kidney, which is expected since the tracer predominantly shows renal clearance. The biodistribution of ZW800F-cRGD-Zr-DFO at 4 and 24 h, expressed in fluorescent intensity (AU) is shown in Figure 5A-B. As expected, the fluorescence signal in urine and blood decreased rapidly, as well as the signal in the kidneys.

PET imaging and biodistribution of cRGD-ZW800F-[^{89}Zr]Zr-DFO

PET/CT imaging at 4 h permitted visualization of colorectal tumors of mice injected with cRGD-ZW800F-[^{89}Zr]Zr-DFO (Figure 6). Based on the gamma counter, biodistribution at 4 h after injection showed the highest uptake of the tracer in kidneys (16.8±8.6 %ID/g) followed by urine, liver, colon content and tumor (0.9±0.1 %ID/g). Biodistribution at 24 h showed the highest uptake of the tracer in kidneys (8.6±1.0 %ID/g) followed by liver and tumor (0.8±0.2 %ID/g). Figure 3 demonstrates the biodistribution of cRGD-ZW800F-

[^{89}Zr]Zr-DFO in all organs at 4 and 24 h post injection; the %ID/g strongly decreased in urine (-93%), colon content (-82%), blood (-70%), and kidneys (-48%), while it only mildly decreased in liver (-20%) and tumor (-14%).

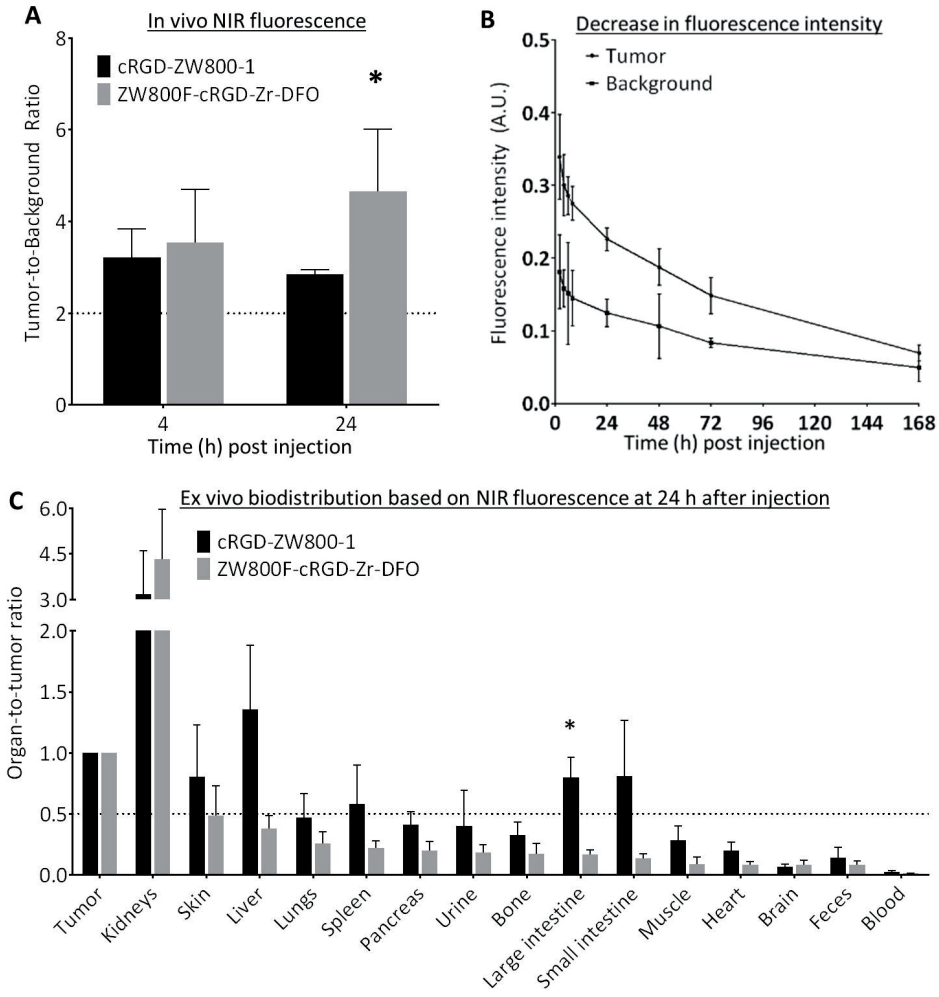

Figure 4: Comparison of cRGD-ZW800-1 and ZW800F-cRGD-DFO.
A: The TBRs obtained with the ZW800F-cRGD-Zr-DFO were significantly higher at 24 h post injection (p=0.03). B: Tumor-specific signals of ZW800F-cRGD-DFO remained above 50% for up to 2 days after injection and detectable up to 7 days after injection. C: Organ-to-tumor ratios of cRGD-ZW800-1 compared to ZW800F-cRGD-Zr-DFO at 24 h after injection. The ratios are lower and more favorable for ZW800F-cRGD-Zr-DFO. *: significant differences

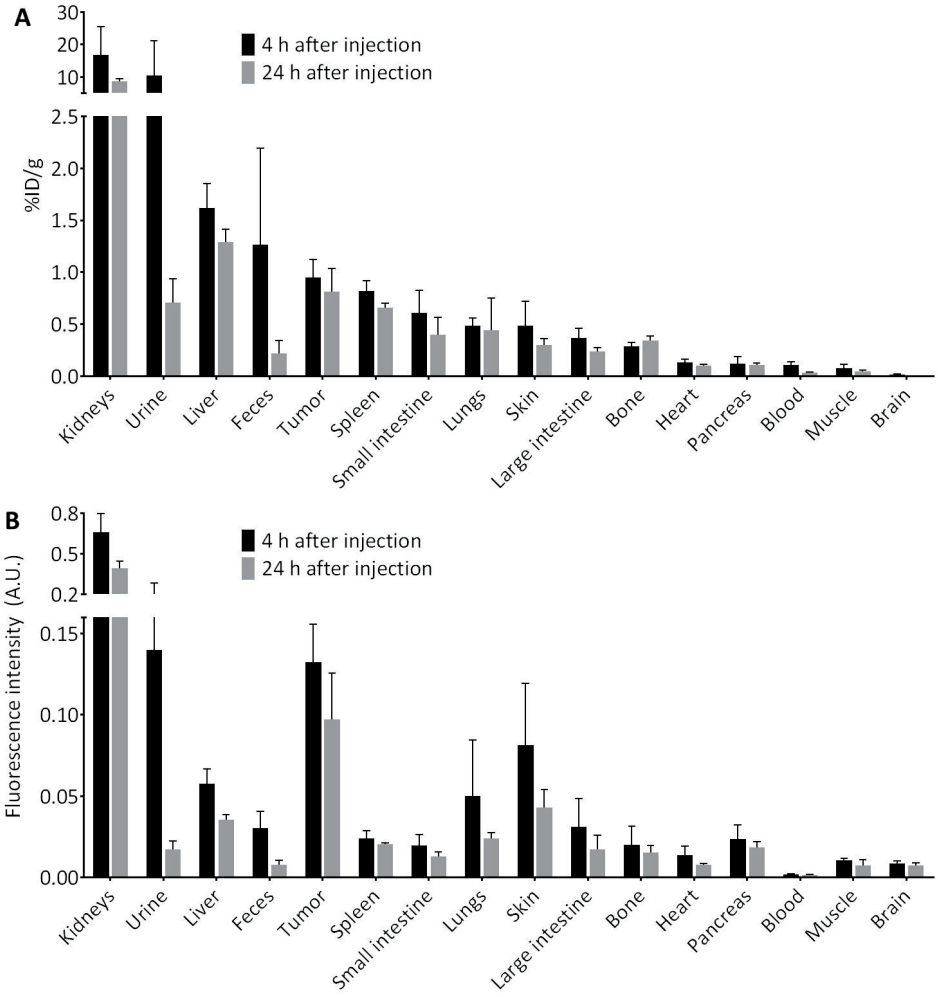

Figure 5: Biodistribution studies.

A: Biodistribution of cRGD-DFO[^{89}Zr]-ZW800F measured with the gamma counter. B: Biodistribution of ZW800F-cRGD-Zr-DFO measured with fluorescence imaging (Pearl).

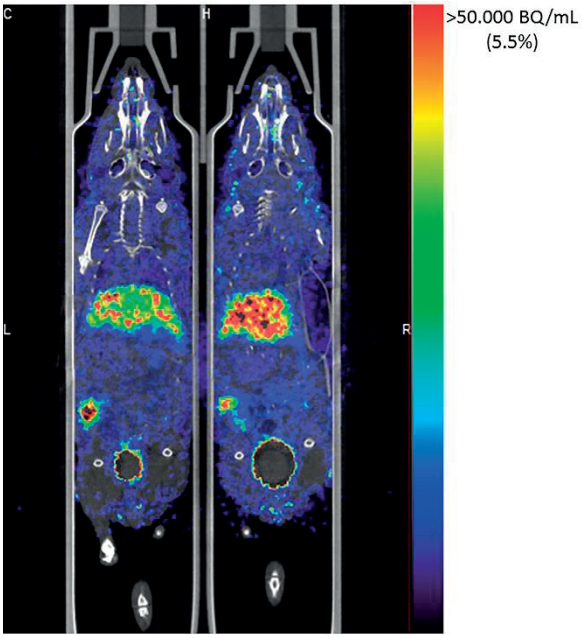

Figure 6: PET/CT of mice.
Tumor specific signal of HT29 colorectal tumors (with arrow) at 4 h after injection of ZW800F-cRGD-[^{89}Zr]Zr-DFO. Also visible are the liver and bladder (dashed arrow).

DISCUSSION

This study demonstrates the feasibility of identifying tumors preoperatively and intra-operatively using a single ^{89}Zr-labeled or unlabeled molecule. Our hybrid tracer, cRGD-ZW800F-[^{89}Zr]Zr-DFO, permits both nuclear as well as NIRF imaging, with optimal results for each obtained at 24 h post-injection. Due to the use of the more stable variant of the zwitterionic fluorophore ZW800-1 Forte, superior results were obtained in comparison to cRGD-ZW800-1, thus enabling NIRF imaging for a longer time interval, up to seven days, and with lower background.

PET imaging using RGD-based tracers has proven to be successful in several clinical studies including multiple solid tumor types, such as breast, colorectal, pancreatic, and head and neck cancer.(12, 20, 21) For example, in a multicenter study, fluorine-18 labeled fluciclatide showed reproducibility in patients with several tumor types (e.g. renal cell carcinoma, breast cancer, rectal cancer) and no side effects were reported. Consistent with its zwitterionic chemical structure, the biodistribution of cRGD-Zr^{89}Z was satisfying due to the relatively low background activity, especially when compared to previously reported RGD results. For example, Zhai *et al.*, performed experiments with an RGD tracer, also radiolabeled with ^{89}Zr, conjugated to fusarine C (FSC).(22) FSC is comparable to DFO

but [^{89}Zr]FSC was found to be even more stable than [^{89}Zr]DFO in blood due to its cyclic structure. Nonetheless, in comparison with our tracer, their biodistribution obtained with [^{89}Zr]FSC-RGD at 4 h was less favorable: for all organs, except kidneys, a significant higher uptake (%ID/g) was present. For spleen, intestines, heart, lung, muscle and bone, the tracer uptake of [^{89}Zr]FSC-RGD was at least 3 times higher than the uptake of cRGD-ZW800F-[^{89}Zr]Zr-DFO, for liver and pancreas the tracer uptake was at least twice as high for [^{89}Zr]FSC-RGD compared to cRGD-Zr^{89}Z. Despite the use of a more stable radiometal chelator, FSC, our biodistribution was, therefore, more favorable, even with an extra structure conjugated, the fluorophore ZW800F. Another study of Li *et al.*, evaluating a dual-labeled RGD agent, 111In-DTPA-Lys(IRDye800)-c(KRGDf), allowing single photon emission computed tomography (SPECT) and fluorescence imaging of human melanoma xenografts. (23) The tracer distribution at both 4 and 24 h after injection was also less favorable than presented in the current study: higher uptake (%ID/g) was present in all organs, including the kidneys.

With regards to ^{89}Zr, in the feasibility study of Heuveling *et al.,* ^{89}Zr-nanocolloidal albumin was locally injected in the oral cavity or neck of patients, 24 hours prior to surgery for the detection of the sentinel lymph node in oral cavity cancer.(24) Peroperatively, surgeons used a gamma probe to detect the radioactive lymph node(s).

Our vision for the use of ^{89}Zr-labeled PET/optical tracers, such as ZW800F-cRGD-Zr-DFO, though, is to avoid radiation exposure to surgical caregivers, while also optimizing imaging results. A single injection of cRGD-ZW800F-[^{89}Zr]Zr-DFO for both PET and optical imaging is inappropriate because the dose required for optical imaging is over 1,000-times higher than the dose required for PET imaging, which would result in an abnormally low specific activity (i.e., blocking) during PET. We avoid this problem by injecting the agent serially. All patients would receive tracer levels, typically < 1 μg of the labeled cRGD-ZW800F-[^{89}Zr]Zr-DFO and PET would be used to select those eligible for surgery. Then, preoperatively, unlabeled ZW800F-cRGD-Zr-DFO would be injected and NIRF imaging can be used for real-time intraoperative margin detection for treatment.

Contrast agents such as DFO-cRGD-ZW800-1 minimize the overall cost and time of market approval. Using two different molecules for pre-surgical staging and intraoperative imaging would mean double the cost and time, because each chemical entity would require separate market approval. Developing a single drug with two different indications greatly decreases both the costs and time required to have both indications available to patients. The savings could be as high as $ 100M and 7 years.(9)

Finally, another advantage of our dual-labeled zwitterionic tracer is its renal clearance, which bypasses biliary excretion and renders the abdominal cavity non-fluorescent. This should improve identification of primary tumor margins from a variety of tumor, such as colorectal, liver, and pancreas, as well as identification of occult intra-abdominal metastases. Of note, despite rather rapid renal clearance of the agent, we recommend imaging at long

time points, such as at 24 h post injection, in order to reduce background signal in non-target organs, and thus increase TBR, as much as possible.

A single molecular imaging agent, ZW800F-cRGD-[^{89}Zr]Zr-DFO, permits serial PET and NIRF-guided treatment of colorectal tumors. The tracer is rapidly cleared via the kidneys and, due to the use of zwitterionic stable ZW800-1 Forte, fluorescent background signals are low. ^{89}Zr-labelled tracer may be used to select patients for surgery. Subsequently, the same non-radiolabelled tracer can be used intra-operatively for real-time tumor detection.

REFERENCES

1. Jones RP, Kokudo N, Folprecht G, Mise Y, Unno M, Malik HZ, et al. Colorectal Liver Metastases: A Critical Review of State of the Art. Liver Cancer. 2016;6(1):66-71.
2. Marr R, Birbeck K, Garvican J, Macklin CP, Tiffin NJ, Parsons WJ, et al. The modern abdominoperineal excision: the next challenge after total mesorectal excision. Ann Surg. 2005;242(1):74-82.
3. Vahrmeijer AL, Hutteman M, van der Vorst JR, van de Velde CJ, Frangioni JV. Image-guided cancer surgery using near-infrared fluorescence. Nat Rev Clin Oncol. 2013;10(9):507-18.
4. Hoogstins CE, Tummers QR, Gaarenstroom KN, de Kroon CD, Trimbos JB, Bosse T, et al. A Novel Tumor-Specific Agent for Intraoperative Near-Infrared Fluorescence Imaging: A Translational Study in Healthy Volunteers and Patients with Ovarian Cancer. Clin Cancer Res. 2016;22(12):2929-38
5. Lamberts LE, Koch M, de Jong JS, Adams ALL, Glatz J, Kranendonk MEG, et al. Tumor-Specific Uptake of Fluorescent Bevacizumab-IRDye800CW Microdosing in Patients with Primary Breast Cancer: A Phase I Feasibility Study. Clin Cancer Res. 2017;23(11):2730-41.
6. Rosenthal EL, Warram JM, de Boer E, Chung TK, Korb ML, Brandwein-Gensler M, et al. Safety and Tumor Specificity of Cetuximab-IRDye800 for Surgical Navigation in Head and Neck Cancer. Clin Cancer Res. 2015;21(16):3658-66.
7. Frangioni JV. New technologies for human cancer imaging. J Clin Oncol. 2008;26(24):4012-21.
8. Teraphongphom N, Kong CS, Warram JM, Rosenthal EL. Specimen mapping in head and neck cancer using fluorescence imaging. Laryngoscope Investig Otolaryngol. 2017;2(6):447-52.
9. Nunn AD. The cost of developing imaging agents for routine clinical use. Invest Radiol. 2006;41(3):206-12.
10. Hekman MC, Boerman OC, de Weijert M, Bos DL, Oosterwijk E, Langenhuijsen JF, et al. Targeted Dual-Modality Imaging in Renal Cell Carcinoma: An Ex Vivo Kidney Perfusion Study. Clin Cancer Res. 2016;22(18):4634-42.
11. Desgrosellier JS, Cheresh DA. Integrins in cancer: biological implications and therapeutic opportunities. Nat Rev Cancer. 2010;10(1):9-22.
12. Beer AJ, Lorenzen S, Metz S, Herrmann K, Watzlowik P, Wester HJ, et al. Comparison of integrin alphaVbeta3 expression and glucose metabolism in primary and metastatic lesions in cancer patients: a PET study using 18F-galacto-RGD and 18F-FDG. J Nucl Med. 2008;49(1):22-9.
13. Sharma R, Kallur KG, Ryu JS, Parameswaran RV, Lindman H, Avril N, et al. Multicenter Reproducibility of 18F-Fluciclatide PET Imaging in Subjects with Solid Tumors. J Nucl Med. 2015;56(12):1855-61.
14. Kang F, Wang Z, Li G, Wang S, Liu D, Zhang M, et al. Inter-heterogeneity and intra-heterogeneity of alphavbeta3 in non-small cell lung cancer and small cell lung cancer patients as revealed by 68Ga-RGD2 PET imaging. Eur J Nucl Med Mol Imaging. 2017;44(9):1520-8.
15. Handgraaf HJM, Boonstra MC, Prevoo H, Kuil J, Bordo MW, Boogerd LSF, et al. Real-time near-infrared fluorescence imaging using cRGD-ZW800-1 for intraoperative visualization of multiple cancer types. Oncotarget. 2017;8(13):21054-66.
16. Hyun H, Owens EA, Narayana L, Wada H, Gravier J, Bao K, et al. Central C-C Bonding Increases Optical and Chemical Stability of NIR Fluorophores. RSC Adv. 2014;4(102):58762-8.

17. Choi HS, Gibbs SL, Lee JH, Kim SH, Ashitate Y, Liu F, et al. Targeted zwitterionic near-infrared fluorophores for improved optical imaging. Nat Biotechnol. 2013;31(2):148-53.
18. Boonstra MC, Tolner B, Schaafsma BE, Boogerd LS, Prevoo HA, Bhavsar G, et al. Preclinical evaluation of a novel CEA-targeting near-infrared fluorescent tracer delineating colorectal and pancreatic tumors. Int J Cancer. 2015;137(8):1910-20.
19. Tseng W, Leong X, Engleman E. Orthotopic mouse model of colorectal cancer. J Vis Exp. 2007(10):484.
20. Beer AJ, Kessler H, Wester HJ, Schwaiger M. PET Imaging of Integrin alphaVbeta3 Expression. Theranostics. 2011;1:48-57.
21. Beer AJ, Schwarzenbock SM, Zantl N, Souvatzoglou M, Maurer T, Watzlowik P, et al. Non-invasive assessment of inter- and intrapatient variability of integrin expression in metastasized prostate cancer by PET. Oncotarget. 2016;7(19):28151-9.
22. Zhai C, Summer D, Rangger C, Franssen GM, Laverman P, Haas H, et al. Novel Bifunctional Cyclic Chelator for (89)Zr Labeling-Radiolabeling and Targeting Properties of RGD Conjugates. Mol Pharm. 2015;12(6):2142-50.
23. Li C, Wang W, Wu Q, Ke S, Houston J, Sevick-Muraca E, et al. Dual optical and nuclear imaging in human melanoma xenografts using a single targeted imaging probe. Nucl Med Biol. 2006;33(3):349-58.
24. Heuveling DA, Karagozoglu KH, Van Lingen A, Hoekstra OS, Van Dongen G, De Bree R. Feasibility of intraoperative detection of sentinel lymph nodes with 89-zirconium-labelled nanocolloidal albumin PET-CT and a handheld high-energy gamma probe. EJNMMI Res. 2018;8(1):15.

III

Intraoperative imaging techniques

7

Staging laparoscopy with ultrasound and near-infrared fluorescence imaging to detect occult metastases in pancreatic and periampullary cancer

H.J.M Handgraaf*, B.G. Sibinga Mulder*, S. Feshtali, L.S.F. Boogerd, M.J.M. van der Valk, A. Farina Sarasqueta, R.J. Swijnenburg, B.A. Bonsing, A.L. Vahrmeijer, J.S.D. Mieog

** Shared first author-ship*

Plos One, 2018 Nov.

ABSTRACT

Up to 38% of pancreatic and periampullary cancer patients undergoing curative intended surgery turn out to have incurable disease. Therefore, staging laparoscopy (SL) prior to laparotomy is advised to spare patients the morbidity, inconvenience and expense of futile major surgery. The aim of this study was to assess the added value of SL with laparoscopic ultrasonography (LUS) and laparoscopic near-infrared fluorescence imaging (LFI).

All patients undergoing curative intended surgery of pancreatic or periampullary cancer were included prospectively in this single arm study. Patients received an intravenous infusion of 10 mg indocyanine green (ICG) one or two days prior to surgery to allow LFI. Suspect lesions were analyzed via biopsy or resection. Follow-up visits after surgery occurred every three months.

A total of 25 patients were included. Suspect lesions were identified in 7 patients: liver metastases (n=2; identified by inspection, LUS, and LFI), peritoneal metastases (n=1; identified by inspection only), and benign lesions (n=4; identified by inspection or LUS). Quality of LFI was good in 67% (10/15) of patients dosed one day and 89% (8/9) dosed two days prior to surgery. Following SL the primary tumor was resected in 20 patients. Two patients (10%) developed metastases within 3 months after resection.

Despite preoperative imaging to identify metastatic disease, metastases are still identified during surgery. The current study sows limited added value of LUS and LFI during SL of pancreatic or periampullary cancer patients.

INTRODUCTION

Pancreatic and periampullary cancers are dreadful diseases with a poor prognosis. At time of diagnosis only 10% to 20% of pancreatic cancer patients is eligible for curative intended surgery, but during explorative laparotomy up to 38% of those patients turn out to have distant metastases or an unresectable primary tumor.(1) Yet, even after resection with curative intend, 5-year survival rates are still disappointingly low between 6.8% and 32%.(2) Up to 70% of patients with resectable pancreatic cancer suffer from distant metastases, of which the majority occurs within 6 months after surgery.(3) These metastases may have been present during surgery without being detected. Preoperative imaging modalities, including computed tomography (CT) and magnetic resonance imaging (MRI), have low sensitivity for subcentimeter peritoneal and liver metastases.(4) Especially superficial metastases are difficult to detect. In a disease with such a dismal prognosis, it is important to spare patients with incurable disease the morbidity, inconvenience and expense of futile major surgery.

The Society of American Gastrointestinal and Endoscopic Surgeons (SAGES) advocates that staging laparoscopy (SL) should be considered in selected patients.(5) Compared to explorative laparotomy, SL results in less postoperative pain, a shorter hospital stay and chemo- and/or radiotherapy can be administered more often and sooner to patients.(6) The chance of an unnecessary laparotomy in patients who appear eligible for curative resection based on preoperative imaging decreases from 40% to 17% by performing SL.(7) Moreover, metal stents make biliary anastomosis abundant and other palliative bypass surgery can be done laparoscopically.

The yield of SL may be amplified by adding laparoscopic ultrasonography (LUS) and laparoscopic near-infrared fluorescence imaging (LFI). LUS enables identification of metastases located deep in the liver and, additionally, vascular involvement of the primary tumor can be assessed.(8) Open-space fluorescence imaging or LFI using indocyanine green (ICG) is a safe and easy method to identify microscopic (sub)capsular liver metastases not yet visible by any other means.(9) Yokoyama *et al*. previously demonstrated that open space fluorescence imaging is able to identify additional micrometastases in the liver in 16% of the patients with pancreatic cancer.(10)

Although selection of patients for SL is being advised, there is no scientific support, nor a consensus on which selection criteria should be used.(11, 12) The current study combines SL with LUS and LFI and aims to determine the added value of these three modalities in all patients with pancreatic and periampullary cancer before undergoing surgery with curative intent.

METHODS

Patients

The clinical study protocol was approved by the local medical ethics review board and conducted in concordance with the Helsinki Declaration of 1975 (as amended in Tokyo, Venice, Hong Kong, Somerset West, Edinburgh, Washington, and Seoul), ICH-GCP guidelines, and the laws and regulations of the Netherlands. The study protocol has been registered at the Netherlands National Trial Register (registry number NTR6639). All subjects provided written informed consent prior to the start of any study-related procedure. All patients of 18 years or older undergoing resection of suspected pancreatic or periampullary cancer at the Leiden University Medical Center (LUMC) were eligible for inclusion. Exclusion criteria were contraindications for ICG administration: eGFR <55; hyperthyroidism; and allergy to iodine, shellfish or ICG. Included patients received standard-of-care, including pancreas-specific CT scan utilizing a thin-section, multi-phase technique with pancreatic phase and portal venous phase images. All patients received water as oral contrast. Additional imaging, for example contrast-enhanced MR with 3D-MRCP, (endoscopic) ultrasound or FDG-PET, was performed if deemed necessary by the multidisciplinary team. Patients who did not provide informed consent or those who were included in other trials still received SL, but without LUS and LFI.

Staging procedure

Patients received 4 mL 2.5 mg/mL (10 mg in total) ICG one day prior to surgery to allow intraoperative LFU of the liver surface. This dose and dosing time was based on previous experiences.(13) Before laparotomy, SL was performed via two ports of 10 mm and one port of 5 mm: a subumbilical port and two ports along the planned laparotomy line. Laparoscopic inspection of the abdomen was performed, including the parietal and visceral peritoneum, the pelvis, the liver, the porta hepatis, the gastrohepatic omentum, the duodenum, the transverse mesocolon and celiac region. Second, LUS (with or without Doppler; Toshiba Aplio 300, with a laparoscopic probe) of the liver was performed by a trained surgeon. LFI of the liver surface was performed lastly using a high-definition fluorescence imaging system (Karl Storz GmbH & Co. KG, Tuttlingen, Germany). Lesions with a fluorescent rim were considered suspect. Quality of fluorescence imaging was divided into three categories: good, meaning that healthy liver was dark and bile ducts and/or intestines were fluorescent; medium, meaning that healthy liver showed some remaining fluorescence; or bad, meaning that the liver was either totally fluorescent or totally dark and no fluorescence was seen in bile ducts nor intestines. The categories medium and bad were considered insufficient for adequate fluorescence imaging. We hypothesized that cholestasis would decrease the quality of fluorescence imaging at one day after ICG administration. If so, dosing time would be extended to two days before surgery.

Any lesions suspect for metastases based on inspection, LUS or LFI were sampled and analyzed, either by biopsy or by resection. In case of multiple lesions with similar appearance on inspection, LUS and LFI, only one biopsy was taken. Histopathological examination was considered the gold standard. The surgical procedure continued via laparotomy if the tumor appeared to be resectable and no metastases were identified.

Follow-up

Follow-up occurred according to the local standard protocol, including a visit every three months to the surgical outpatient clinic of surgery in conjunction with the department of oncology. A CT scan was performed only if loco-regional or metastatic disease was suspected.

Outcomes

Main outcome of this study was the percentage of averted futile laparotomies. Secondary outcome was the accuracy of the diagnostic modalities. Findings of SL, LUS, LFI were compared with histopathological examination of intraoperative biopsies, findings after laparotomy and finally, with follow-up results until at least the first visit to the outpatient clinic (i.e. approximately 3 months after surgery).

Statistics

Using A'Hern's single-stage phase II trial design and alpha=0.05 and power=80%, 25 patients were needed to distinguish between an averted laparotomy rate of 30% (worth exploring in a Phase III trial) and 10% or less (unacceptable outcome).(14) This required at least six averted laparotomies to reach the positive endpoint. Comparing the means of two groups was performed using a two-tailed *t*-test in SPSS (version 23.0, IBM Statistics, US).

RESULTS

Patient characteristics

Twenty-five patients were included between January 2016 and April 2017. Patient and tumor characteristics are summarized in Table 1. Three patients received neoadjuvant therapy. One patient was treated with gemcitabine and radiotherapy, two patients with FOLFIRINOX. In one patient a liver metastasis was already suspected based on preoperative imaging, but no histopathological diagnosis could be obtained. During SL a liver metastasis was confirmed by histopathological examination.

Table 1. Patient and tumor characteristics.

Patient and tumor characteristics	
Gender, % (n)	
Female	32 (8)
Male	68 (17)
Age at surgery, median (range)	67 (51-83)
Neoadjuvant therapy, % (n)	
Chemotherapy	12 (3)
Radiotherapy	4 (1)
Origin of primary tumor, % (n)	
Pancreas	78 (17)
Duodenum	12 (3)
Ampulla of Vater	12 (3)
Distal common bile duct	8 (2)
Radiological characteristics, % (n)	
≥ cT3*	28 (7)
cN1	16 (4)
Size of tumor (mm), % (n)*	
Not measurable	24 (6)
≥ 3 cm	36 (9)
< 3 cm	40 (10)
Laboratory values, median (range)	
CEA (μg/L)	3.0 (0.2-18.8)
CA19.9 (kU/L)	132 (3-3426)
Total bilirubin (μmol/L)	48 (6-376)
Alkaline phosphatase (U/L)	243 (57-684)
γ-glutamyl transpeptidase (U/L)	182 (12-2159)

** The tumor could not be measured in 6 patients.*

Averted laparotomies and accuracy of SL

In 16% (n=4) the surgeon decided to stop the procedure after completion of the SL due to the detection of apparent metastases. Two patients had liver metastases, which could be identified with inspection, LUS and LFI. One patient had developed peritoneal metastases, which were – as expected – only visible with inspection. In the fourth patient LUS showed a suspect lesion in the liver, while inspection and LFI were negative (Figure 1). Intraoperative frozen section analysis suspected an adenocarcinoma, whereupon the surgical procedure was stopped. The pathological diagnosis was revised postoperatively into a bile duct adenoma

after subsequent immunohistochemistry. The patient underwent a laparotomy and resection four days later and remained without metastases up to 4.5 months of follow-up.

Three other suspect lesions were resected in three other patients during SL, but turned out to be benign. All three were assessed as suspect based on inspection only. LFI did not result in false-positive outcomes. Altogether, accuracies were 57%, 57%, and 86% for inspection, LUS and LFI, respectively. In 8% (n=2) a laparotomy was performed, but the primary tumor appeared to be locally irresectable due to vascular involvement.

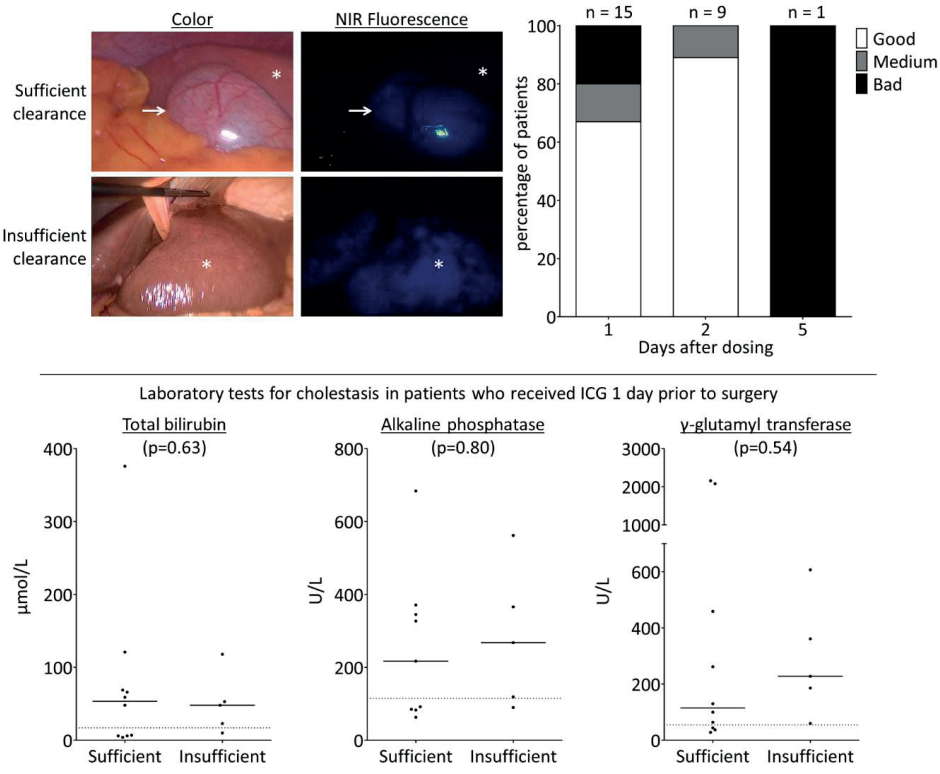

Figure 1. Quality of near-infrared fluorescence imaging.

Upper figures: In the majority of patients ICG was cleared sufficiently from healthy liver tissue (star) if administered 2 days before to surgery. The gall bladder (arrow) was used as a positive control. In 33%, the liver still showed significant background fluorescence if ICG was administered 1 day prior to surgery.

Lower figures: ICG administered 1 day showed insufficient clearance regardless of cholestatic laboratory values.

Quality of near-infrared fluorescence imaging

Results are shown in Figure 2. None of the patients experienced any adverse events related to administration of ICG. Fifteen patients received their dose of ICG one day prior to surgery. In 67% of the patients (n=10) the quality was good, resulting in sufficient visualization of potential liver lesions. Due to reduced ICG clearance in 20% of the patients (n=3), the quality was medium, while in 13% (n=2) the liver was still completely fluorescent. No significant differences were seen in laboratory tests for cholestasis between patients with sufficient or insufficient quality of LFI. ICG was cleared sufficiently by the liver in eight out of nine patients (89%) who were administered ICG two days prior to surgery. The surgical procedure of one patient was postponed after ICG administration with five days due to clinical reasons. During SL no fluorescence signal was detected at all.

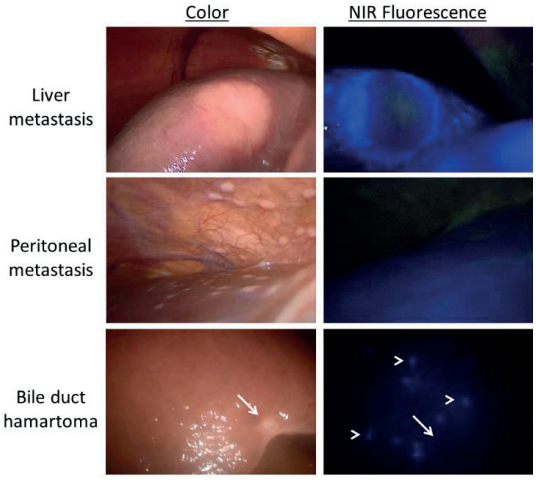

Figure 2. Laparoscopic near-infrared fluorescence imaging.
Laparoscopic near-infrared fluorescence imaging could demarcate liver metastases (note the characteristic fluorescent rim), but not peritoneal metastases. Furthermore, discrimination between malignant and benign lesions such as bile duct hamartoma was clear due to the absence of fluorescence in the latter (arrow). In two patients, abnormal fluorescent spots were visible, without a characteristic rim (arrow heads). These lesions were not biopsied, but the patients developed liver metastases within 3 months after surgery.

Follow-up

The median follow-up time of all included patients was 7.8 months (range 2.7-12.6). Liver metastases were diagnosed in 20% (n=5) of the patients in whom the primary tumor was resected. In two patients, liver metastases were diagnosed within three months after surgery. None were detected during SL or subsequent laparotomy. When including these lesions, accuracies of diagnostic modalities decreased to 44%, 44% and 67% for inspection, LUS

and LFI, respectively. In hindsight, abnormal fluorescence spots were visible in one patient who developed miliary liver metastases (Figure 3). However, since no suspect fluorescence rim pattern was observed, no biopsies were taken.

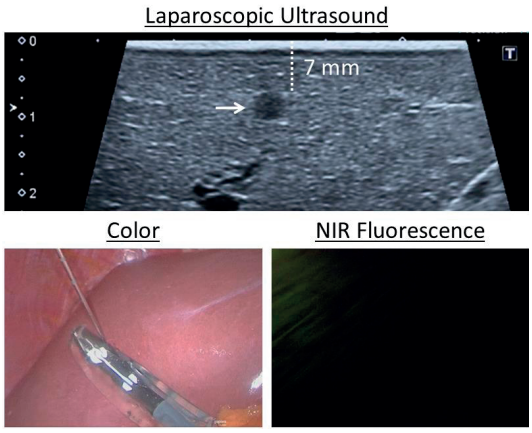

Figure 3. False-positive lesion.
A lesion suspected to be a metastasis was detected and biopsied with laparoscopic imaging (arrow). Near-infrared fluorescence imaging did not show any fluorescence signal, even though the lesion was located 7 mm below the liver capsule. The final diagnosis was a bile duct hamartoma.

DISCUSSION

Several attempts have been made to increase the yield of SL in pancreatic and periampullary cancer patients, including use of contrast-enhanced ultrasound, LUS, and selection based on preoperative imaging or blood values.(8, 15-20) This is the first study to combine SL with LUS and LFI, but not with the desired result. As mentioned, an unselected population of patients with periampullary cancer was included in this study. This may have resulted in a low *a priori* probability of metastases (12%; 3/25). In hindsight, including only patients with CA 19.9 > 150 U/L or a tumor sized > 3 cm, as suggested in a systematic review covering 24 studies (21), would increase the incidence to 21%.(3/14) However, it remains disputable if selection of patients for SL should be performed. During this study period all patients with pancreatic or periampullary cancer who were not included also received SL (without LUS or LFI) before exploratory laparotomy (data not shown). Metastases were detected in 16% (5/31) of these patients. Two of these five patients would not have received SL with the above mentioned selection criteria. Risking that patients with metastases do not undergo SL should be weighed against delaying all procedures with 10 to 15 minutes.

In surgery for colorectal liver metastases, the addition of NIRF imaging to inspection and ultrasound doubled the intraoperative detection rate of additional liver metastases from 13%

to 25%.(22) In the current study, we aimed to increase the yield of intraoperative screening for metastases of pancreatic or periampullary cancers by adding fluorescence imaging, but without success. One issue could be that, in contrast to patients with colorectal liver metastases, patients with pancreatic or periampullary cancer are more likely to have reduced ICG clearance. Reduced ICG clearance results in nonspecific background fluorescence, which can hamper detection of micrometastases. Our study suggest that within this population dosing ICG two days prior to surgery results in improved quality of fluorescence imaging than one day, regardless of cholestasis laboratory tests.

Apparently, LFI in patients with pancreatic or periampullary cancer has a certain learning curve. During open-space fluorescence imaging, Yokoyama *et al.*(10) observed abnormal fluorescence spots (larger than 1.5 mm) in 4 patients, but no malignancies could be confirmed by histopathological examination. Three of these patients developed liver metastases within six months. In the current study, only a rim pattern was considered suspect, based on previous experiences with fluorescence imaging of liver metastases.(9, 13) However, abnormal fluorescent spots were seen in two patients (Figure 3) and both developed hepatic metastases shortly after surgery. The yield of LFI may have been higher if also abnormal spots without a rim pattern were analyzed.

LUS was expected to identify intrahepatic metastases and to assess resectability before exploratory laparotomy. However, the technique failed to deliver. Instead, it even resulted in a false-positive biopsy. The added value of LUS is minimized even further when combined with pre-operative MRI scanning, which is already very sensitive for small, intrahepatic metastases.(23) However, superficial liver metastases remain difficult to distinguish on pre-operative imaging. These metastases can be detected with inspection and LFI. The current results suggest that there is no added value of LUS during SL when optimal preoperative imaging has been performed.

In conclusion, this study showed limited added value of LUS during SL in patients with pancreatic or periampullary cancers. Even though LFI had a learning curve, it had the highest accuracy compared to inspection and LUS. If ICG is administered two days prior to surgery it may have more value in a selected patient population.

REFERENCES

1. Gaujoux S, Allen PJ. Role of staging laparoscopy in peri-pancreatic and hepatobiliary malignancy. World J Gastrointest Surg. 2010;2(9):283-90.
2. Hsu CP, Hsu JT, Liao CH, Kang SC, Lin BC, Hsu YP, et al. Three-year and five-year outcomes of surgical resection for pancreatic ductal adenocarcinoma: Long-term experiences in one medical center. Asian J Surg. 2016.
3. Fujioka S, Misawa T, Okamoto T, Gocho T, Futagawa Y, Yanaga K. Predictors for postoperative liver metastasis in patients with resectable pancreatic cancer. Int Surg. 2008;93(6):324-30.
4. Holzapfel K, Reiser-Erkan C, Fingerle AA, Erkan M, Eiber MJ, Rummeny EJ, et al. Comparison of diffusion-weighted MR imaging and multidetector-row CT in the detection of liver metastases in patients operated for pancreatic cancer. Abdom Imaging. 2011;36(2):179-84.
5. Hori Y, Committee SG. Diagnostic laparoscopy guidelines : This guideline was prepared by the SAGES Guidelines Committee and reviewed and approved by the Board of Governors of the Society of American Gastrointestinal and Endoscopic Surgeons (SAGES), November 2007. Surgical endoscopy. 2008;22(5):1353-83.
6. Velanovich V, Wollner I, Ajlouni M. Staging laparoscopy promotes increased utilization of postoperative therapy for unresectable intra-abdominal malignancies. Journal of gastrointestinal surgery : official journal of the Society for Surgery of the Alimentary Tract. 2000;4(5):542-6.
7. Allen VB, Gurusamy KS, Takwoingi Y, Kalia A, Davidson BR. Diagnostic accuracy of laparoscopy following computed tomography (CT) scanning for assessing the resectability with curative intent in pancreatic and periampullary cancer. Cochrane Database Syst Rev. 2016;7:CD009323.
8. Handgraaf HJ, Boonstra MC, Van Erkel AR, Bonsing BA, Putter H, Van De Velde CJ, et al. Current and future intraoperative imaging strategies to increase radical resection rates in pancreatic cancer surgery. Biomed Res Int. 2014;2014:890230.
9. Boogerd LS, Handgraaf HJ, Lam HD, Huurman VA, Farina-Sarasqueta A, Frangioni JV, et al. Laparoscopic detection and resection of occult liver tumors of multiple cancer types using real-time near-infrared fluorescence guidance. Surgical endoscopy. 2016.
10. Yokoyama N, Otani T, Hashidate H, Maeda C, Katada T, Sudo N, et al. Real-time detection of hepatic micrometastases from pancreatic cancer by intraoperative fluorescence imaging: preliminary results of a prospective study. Cancer. 2012;118(11):2813-9.
11. Alexakis N, Gomatos IP, Sbarounis S, Toutouzas K, Katsaragakis S, Zografos G, et al. High serum CA 19-9 but not tumor size should select patients for staging laparoscopy in radiological resectable pancreas head and peri-ampullary cancer. Eur J Surg Oncol. 2015;41(2):265-9.
12. Stefanidis D, Grove KD, Schwesinger WH, Thomas CR, Jr. The current role of staging laparoscopy for adenocarcinoma of the pancreas: a review. Ann Oncol. 2006;17(2):189-99.
13. van der Vorst JR, Schaafsma BE, Hutteman M, Verbeek FP, Liefers GJ, Hartgrink HH, et al. Near-infrared fluorescence-guided resection of colorectal liver metastases. Cancer. 2013;119(18):3411-8.
14. A'Hern RP. Sample size tables for exact single-stage phase II designs. Stat Med. 2001;20(6):859-66.
15. Garcea G, Cairns V, Berry DP, Neal CP, Metcalfe MS, Dennison AR. Improving

the diagnostic yield from staging laparoscopy for periampullary malignancies: the value of preoperative inflammatory markers and radiological tumor size. Pancreas. 2012;41(2):233-7.
16. de Werra C, Quarto G, Aloia S, Perrotta S, Del Giudice R, Di Filippo G, et al. The use of intraoperative ultrasound for diagnosis and stadiation in pancreatic head neoformations. Int J Surg. 2015;21 Suppl 1:S55-8.
17. Levy J, Tahiri M, Vanounou T, Maimon G, Bergman S. Diagnostic Laparoscopy with Ultrasound Still Has a Role in the Staging of Pancreatic Cancer: A Systematic Review of the Literature. HPB Surg. 2016;2016:8092109.
18. Lin LZ, Li F, Liu Y, Xing LX, Du LF. Contrast-Enhanced Ultrasound for differential diagnosis of pancreatic mass lesions: a meta-analysis. Med Ultrason. 2016;18(2):163-9.
19. Grossjohann HS, Rappeport ED, Jensen C, Svendsen LB, Hillingso JG, Hansen CP, et al. Usefulness of contrast-enhanced transabdominal ultrasound for tumor classification and tumor staging in the pancreatic head. Scand J Gastroenterol. 2010;45(7-8):917-24.
20. Maithel SK, Maloney S, Winston C, Gonen M, D'Angelica MI, Dematteo RP, et al. Preoperative CA 19-9 and the yield of staging laparoscopy in patients with radiographically resectable pancreatic adenocarcinoma. Ann Surg Oncol. 2008;15(12):3512-20.
21. De Rosa A, Cameron IC, Gomez D. Indications for staging laparoscopy in pancreatic cancer. HPB (Oxford). 2016;18(1):13-20.
22. Handgraaf HJ, Boogerd LS, Höppener DJ, Peloso A, Sibinga Mulder BG, Hoogstins CE, et al. Long-term follow-up after near-infrared fluorescence-guided resection of colorectal liver metastases: a retrospective multicenter analysis. Eur J Surg Oncol. 2017.
23. Kim HW, Lee JC, Paik KH, Kang J, Kim YH, Yoon YS, et al. Adjunctive role of preoperative liver magnetic resonance imaging for potentially resectable pancreatic cancer. Surgery. 2017;161(6):1579-87.

8

Real-time surgical margin assessment using ICG-Fluorescence during minimally invasive resections of colorectal liver metastases

F.B. Achterberg*, B.G. Sibinga Mulder*, R.P.J. Meijer, B.A. Bonsing, H.H. Hartgrink, J.S.D. Mieog, S. Park, A. Farina Sarasqueta, A.L. Vahrmeijer, R.J. Swijnenburg
* Shared first author-ship

Submitted: Annals of Surgery.

ABSTRACT

In patients with colorectal liver metastases (CRLM) undergoing surgery, almost a third of the resections end up being tumor-margin positive. Near-infrared fluorescence (NIRF) imaging using indocyanine green (ICG) shows a characteristic fluorescent 'rim' surrounding the CRLM. By resecting a metastasis with the entire surrounding fluorescent rim, guided by NIRF imaging, the surgeon can effectively acquire margin-negative resections. Here we describe the surgical technique for using NIRF imaging to assess tumor-margins in vivo in patients with CRLM undergoing laparoscopic or robot-assisted resections.

Out of our institutional database we selected 16 CRLM based on margin-status (R0; n = 8, R1; n = 8), which were resected by minimally-invasive approach. NIRF images were acquired during surgery from both the resection specimen and the wound bed to identify potential tumor-positive margins. NIRF images were correlated to histopathological findings.

All lesions with a NIRF positive resection plane *in vivo* were reported as having a tumor-positive margin. Lesions that showcased no protruding rim in the wound bed in vivo were diagnosed as having a tumor-negative margin in 88% of cases.

Image-guided surgery using real-time ICG-fluorescence has the potential to aid surgeons in achieving a tumor-negative margin in minimally invasive liver metastasectomies.

INTRODUCTION

Laparoscopic liver resection is shown to be safe and feasible with concordant oncological outcomes compared to open surgery. Unfortunately, both procedures result in a tumor-positive resection in 28% of cases.(1) According to recent literature, achieving a tumor-negative resection with a margin of at least 1 mm is associated with improved long-term and disease-free survival in patients with metastatic disease isolated to the liver.(2, 3) Hence, in order to improve patient outcome, finding effective means to increasing tumor-negative resection rates are required.

Image-guided hepatobiliary surgery using near-infrared fluorescence (NIRF) is a technique which can improve real-time demarcation of tumors located in the liver.(4) NIRF imaging, using Indocyanine Green (ICG), has emerged as a promising method for detecting colorectal liver metastases (CRLM) in both open and minimally invasive procedures.(5) NIRF imaging studies showed an easily identifiable fluorescent rim, caused by the accumulation of ICG in the surrounding hepatocytes, which surrounds the CRLM.(6) These studies mainly focused on the identification of additional CRLM not seen on conventional imaging modalities prior to surgery. Now, we hypothesize that the surgical removal of the entire fluorescent rim, guided by NIRF imaging, can greatly improve tumor-negative resection rates during minimal invasive procedures. Improving tumor-negative resection rates could potentially lead to prolonged disease-free and overall survival.

Recent developments in fluorescent imaging systems led to a variety of laparoscopic and robotic platforms which can display fluorescence and bright field images merged and in real-time.(7) This eliminates the need to switch between imaging channels which significantly reduces any interference with the surgical procedure during fluorescent-guided resections. In addition, during NIRF guided laparoscopic liver resections, repeated introduction of the ultrasound probe to examine the progress of the resection becomes superfluous, resulting in a less interruptions of the procedure.

While the development and adaptation of these technologies in surgeries provide an immense amount of information, interpretation of these fluorescent images and mastering the technique of using fluorescence in theatre requires training and experience. In this report, we aim to share our institute's decade-long of experience with NIRF guided liver surgery. More specifically, we describe the use of NIRF image-guided CRLM resections during minimally invasive (laparoscopic or robotic) procedures. Furthermore, we highlight the advantages of this technique in properly assessing tumor margins *in vivo* using ICG as a contrast agent. The technique was explored in a patient cohort composed from our institute's database to represent a variety of possible surgical outcomes.

METHODS

For the purpose of this technical report, CRLM resected by minimally invasive approach (laparoscopic or robot-assisted) guided by ICG fluorescence imaging, were selected from the institutional database. The composed patient cohort represents a variety of common surgical outcomes to display the surgical technique and the interpretation of fluorescent signal in vivo, namely: eight lesions with tumor-negative margins in vivo matched by an equal number of lesions with tumor-positive margins, resected in the same inclusion period. This study was approved by the Institutional Ethics Review Board of the Leiden University Medical Center (The Netherlands).

Patients

CRLM were selected from patients that were above 18 years of age, were diagnosed with colorectal liver metastases and eligible for minimally invasive surgery with curative intend. According to the national protocol all patients underwent either a contrast-enhanced abdominal computed tomography (CT) scan and/or gadoxetate disodium (Primovist®) enhanced magnetic resonance imaging (MRI) scan prior to surgery. All patients were administered 10 mg (5 mg/ml) indocyanine green (Verdye, Diagnostic Green GmbH) 24 hours prior to surgery, according to the institution's standard-of-care protocol. The decision to perform a laparoscopic or robot-assisted liver resection was based on the localization of the lesion(s), patient characteristics, the availability of the robotic system and the surgeon's preferences.

Technique and signal definition

Previous data from our center consistently showed the development of a fluorescent rim which encases all CRLM.(4) Hence, the basic principle of our surgical technique relies on defining this fluorescent rim as the resection margin and to acquire a tumor-negative resection by removing the entire fluorescent rim with the metastasis included (Figure 1).

No real-time quantitative method for defining the fluorescent signal intensity during the procedure is yet available. Therefore, in vivo fluorescent signals were registered by the following classification system: 1) no fluorescent signal, 2) bright fluorescent signal; in case a very intense fluorescent signal from liver parenchyma is This signal is caused by the presence of ICG and indicates a protruding tumor rim, or, 3) intermediate fluorescent signal; in case a fluorescent light is scattered by normal liver parenchyma. A bright fluorescent signal after resection of the CRLM either produced by the resection specimen and/or the wound bed was registered as a potential tumor-positive resection (Figure 2).

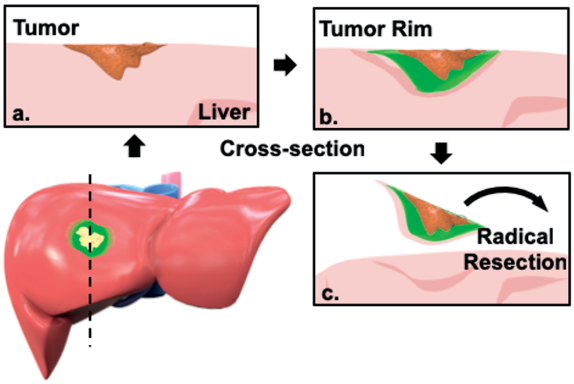

Figure 1. Computational model of the liver with a CRLM in segment V/VIII including a fluorescent rim around the lesion.
a) Cross-section through the tumor, in b) surrounded by a fluorescent rim caused by the accumulation of ICG in immature hepatocytes surrounding the tumor. c) Removing the entire rim should result in a tumor-negative resection.

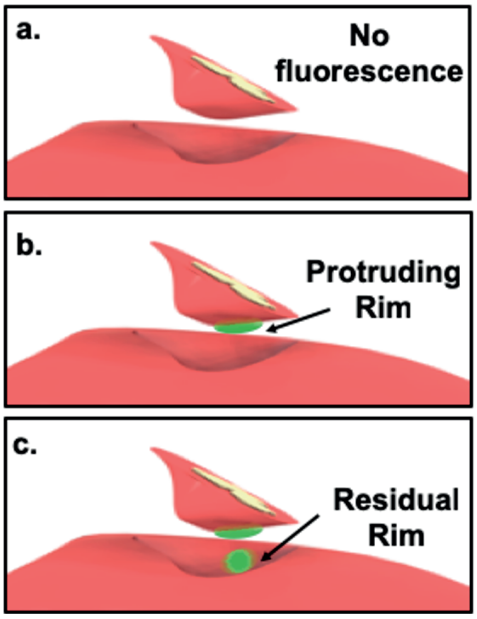

Figure 2. A computer-aided design of the liver showcasing three different scenarios.
a) No fluorescent signal produced by either the liver's wound bed or the resection specimen. b) Fluorescent rim protruding trough the liver tissue of the resection specimen indicating a potential tumor-positive resection margin and c) bright fluorescent signal in both the wound bed and protruding trough the liver tissue of the resection specimen (potential resection with tumor-positive margin).

NIRF Systems

The minimally invasive surgical procedures were performed either laparoscopically or robot-assisted. The following systems were used: 1) Viscera Elite II IR-s200 light engine (Olympus Medical Systems, Hamburg, Germany), 2) 1588 AIM platform (Stryker, Waardenburg, The Netherlands) 3) da Vinci firefly (Intuitive Surgical, Inc., Sunnyvale, California, United States). All are clinically approved and CE (Conformité Européenne) marked. All laparoscopic systems were commercially available and equipped with both NIRF imaging and regular white light imaging (WLI) modules. This allowed for a real-time coloured overlay to be produced. During the procedures a 10 mm 30-degree angled laparoscope was used.

Surgical procedure

Access to the abdominal cavity was acquired by placing a 12 mm port in the umbilicus. Peritoneal disease was excluded with laparoscopy before any additional ports were placed; pending the location of the target lesion(s) and under the surgeon's discretion. First, the liver was mobilized to facilitate visual inspection of the liver surface and in some cases to better access to the metastasis. The liver's surface is thoroughly inspected visually and the entire liver parenchyma is assessed using laparoscopic IOUS. Subsequently, NIRF imaging is used to identify the target lesion(s) (Figure 3a, b) and, if present, any additional lesions. All acquired NIRF and bright-field images were stored and documented. Fresh frozen sections were collected for histopathological confirmation of any suspected lesions. All lesions were registered on a case registration form (CRF), according to their anatomical location in the liver according to Couinaud's liver segments.(8)

The fluorescent rim was identified and correlated to the tumor's location and size using IOUS (Figure 3c, d), after which the lesion is demarcated using an electrocoagulation device. After demarcation (Figure 3e, f), the resection is performed using both a vessel sealing device (Ligasure, Medtronic, USA) and a laparoscopic compatible Cavitron Ultrasonic Surgical Aspirator (CUSA) in case of a laparoscopic procedure. In the robot-assisted procedures, the da Vinci Xi Permanent Cautery Hook was used for demarcation and the da Vinci Xi vessel sealer with endowrist in combination with bipolar cautery was used to perform the parenchymal transection. During the resection, inspection of the wound bed and resection plane using NIRF imaging was performed routinely (Figure 3g, h). Any fluorescent signal in the wound bed or resection specimen was identified and documented. All NIRF images were later analysed and correlated to histopathology. After finalizing the resection, *in vivo* white-light images (WLI) and NIRF images of the wound bed and both sides of the tissue specimen were acquired (fig 3i, j). Figure 4a - f shows the chronological documentation of the procedure where a NIRF positive resection specimen was observed.

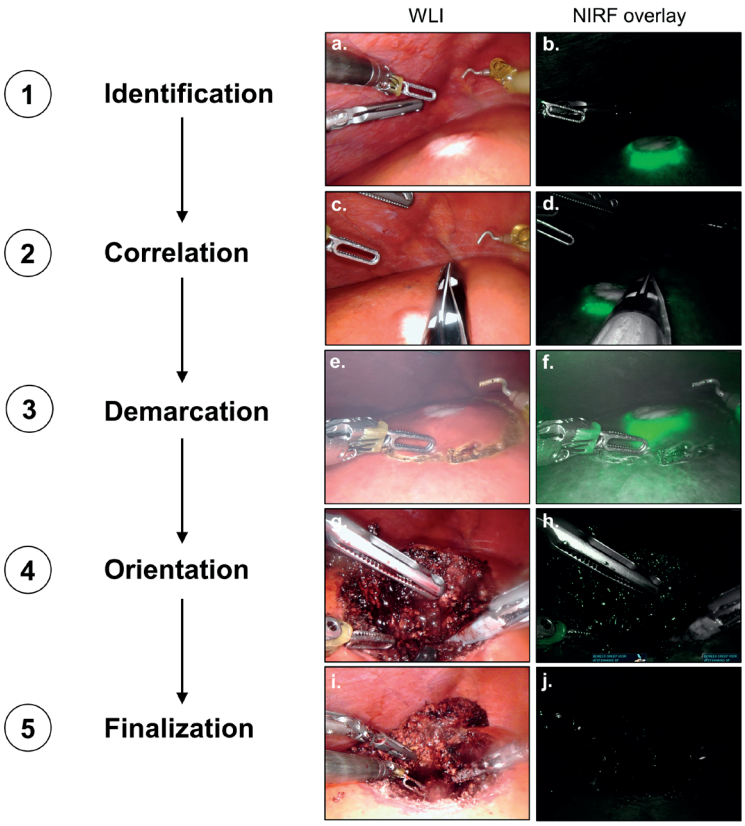

Figure 3. Identification and resection of a CRLM using IOUS and NIRF guidance.
Surgical workflow for the identification and resection of CRLM. a) Identification of the lesion in segment V using WLI and b) using NIRF. c) Correlation of the lesion's size with d) the fluorescent rim using IOUS. e) Demarcation of the lesion with the permanent cautery hook using WLI and f) using NIRF. g) Regular WLI of the resection plane and h) frequent NIRF imaging is performed to check for potential fluorescent spots (no spots on image). i) The wound bed and resection specimen in white light and j) NIRF imaging to diagnose fluorescent spots (no fluorescent spots on image). *CRLM; colorectal liver metastases, IOUS; intraoperative ultrasound, WLI; White Light Imaging, NIRF; Near-infrared Fluorescence*

Histopathology

Directly after surgery, the resected specimen is conserved on ice and transported to the pathology department. Prior to gross sectioning, white light images and NIRF images were acquired from the complete resected specimen (Figure 4g, h). Within 24 hours after surgery and after fixation with formalin, gross sectioning was performed and all bread loafs were imaged consecutively to identify the fluorescent rim. Discontinuities of fluorescent rim or the absence of overlaying liver tissue was documented as a potentially tumor-positive resec-

tion margin (Figure 4i, j). Subsequently the macroscopic resection margin is determined by the pathologist and the tissue was paraffin embedded. Any additional fluorescent spots identified during surgery are embedded separately, regardless of their macroscopic assessment. Slides with a 3 µm thickness were sectioned from FFPE tissue blocks and stained with haematoxylin and eosin (H&E) to microscopically assess the lesion and the resection margin. A resection margin with a microscopical distance of more than 1 mm from the resection plane to the tumor burden is classified as a radical or margin-negative resection (R0). While resection margins with less than 1 mm were considered as margin-positive resections (R1).(2, 3)

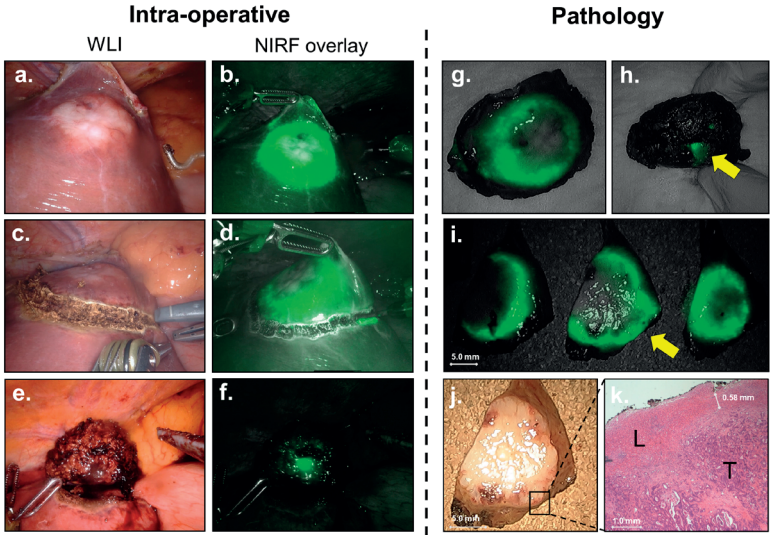

Figure 4: Correlation between *in vivo* and *ex vivo* NIRF imaging.
a) Resection of a CRLM in liver segment IVb in normal white light and, b) with NIRF imaging. c) Too close proximity of the demarcation line to the d) fluorescent rim might result in a resection with tumor-positive margin. e) Suspected resection with tumor-positive margin using WLI and f) confirmed with NIRF. Ex vivo NIRF imaging of the g) front of the lesion and h) from the back show the same protruding rim. i) Gross sectioning reveals a potential resection with tumor-positive margin, indicated by the yellow arrow. Which is confirmed by NIRF imaging. Later histopathological assessment of the suspected tumor-margin in j) is confirmed by H&E staining. *WLI; White Light Imaging, NIRF; Near-infrared Fluorescence, H&E; haematoxylin and eosin, L; normal liver tissue, T; tumor tissue*

RESULTS

Patients

A cohort was composed, in total consisting of 16 CRLM (out of 14 patients), 8 tumor-negative resections and 8 resections with tumor-positive margins. Patients were selected from the

institute's database between October 2017 and September 2018. One patient was diagnosed with more than one CRLM prior to surgery. In one case, an additional CRLM was identified during surgery. In total, 15 wedge resections were performed and one anatomical resection of liver segment 2-3. Lesion characteristics are summarized in table 1.

Table 1. Lesion characteristics.

Lesion characteristics (n=16)	
Disease, % (n)	
primary CRLM	94 (15)
recurrent CRLM	6 (1)
Occurrence, % (n)	
synchronous	19 (3)
metachronous	81 (13)
Lesion size (mm), median (range)	22.5 (8-37)
Type of surgery, % (n)	
laparoscopic	50 (8)
robotically assisted	50 (8)
Liver segments, % (n)	
I	0 (0)
II	19 (3)
III	6 (1)
II-III (anat. resection)	6 (1)
IVa-b	25 (4)
V	19 (3)
VI	6 (1)
VII	6 (1)
VIII	13 (2)
Blood loss in mL, median (range)	100 (10-500)

NIRF guided resection

All target lesions were identified using NIRF imaging and displayed a fluorescent rim in vivo. Sixteen lesions were resected and sent for histopathological examination. In one patient, diagnosed with a local recurrence after ablative therapy, a deviant fluorescent pattern was observed. ICG had accumulated around the previously ablated liver tissue causing residual fluorescent signal in both the wound bed and the resection specimen after resection of the metastasis. While in all the other cases, the fluorescent rim correlated with the tumor location and size. In total, out of the 16 lesions, seven displayed a positive fluorescent signal from the specimen's resection plane in vivo, produced by a protruding rim (Figure 4a - h).

Out of these seven cases, three also showed NIRF signal in the corresponding plane of the wound bed (fig 2c). All NIRF signals were scored as a direct fluorescent signal generated by the lesion's rim and, therefore, registered as potential tumor-positive resections. In addition, the other nine lesions showed the presence of the normal rim feature on the liver surface with no fluorescent signal at either side of the resection plane or wound bed (Table 2).

Table 2. *In vivo* tumor-margin assessment with NIRF.
In vivo tumor-margin assessed with NIRF imaging of the resection specimen, correlated to the histopathological tumor-margin. In vivo margin assessment correlated in 15/16 cases. Only one false negative lesion was observed (8.1). In two cases, an additional resection was performed based on the suspicion of a tumor-positive margin (12, 13). NIRF; near-infrared fluorescent, T-margin; tumor-margin.

	Tumor margin determined by		
Lesion No.	*In vivo* NIRF	Histopathology	T-margin (in mm)
1	Negative	Negative	6
2	Negative	Negative	16
3.1	Negative	Negative	1.2
4	Negative	Negative	8
5	Negative	Negative	4
6	Negative	Negative	1.7
7	Negative	Negative	3
8.1	Negative	Positive	<1
3.2	Positive	Positive	0
8.2	Positive	Positive	<1
9	Positive	Positive	<1
10	Positive	Positive	<1
11	Positive	Positive	<1
12	Positive	Negative*	<1†
13	Positive	Negative*	0†
14	Positive	Positive	0

*Assessment after additional resection
†Assessment of initial resection specimen

Histopathology

All lesion showed the presence of a fluorescent rim during *ex vivo* examination. The median lesion size based on histopathological examination was 22.5 mm (range 8-37). Median reported resection margin was 5.5 mm for R0 resections. All resection specimens showing a protruding rim *in vivo* and *ex vivo* were reported as a R1 resection (Figure 4i, j). An additional lesion which was identified by NIRF inspection was reported as a 15 mm CRLM

with a tumor margin smaller than 1 mm. This lesion showed no protruding fluorescent rim *in vivo* and was therefore reported as false-negative. All other *in vivo* NIRF negative lesions (n = 8) were reported as tumor-negative resections.

Discussion

In this study, we report a technique which can improve surgical margin determination *in vivo* during minimal invasive resections of CRLM, using real-time NIRF imaging with ICG. Injecting a low dose of ICG (10mg) 24 hours prior to surgery, enables the surgeon to visualize a fluorescent rim surrounding the metastasis. Current results show the concordance between the appearance of fluorescent signal *in vivo* and the histopathological resection margin, indicating that complete resection of the fluorescence rim is sufficient for obtaining a resection with tumor-negative margins. Our technical approach has the ability to differentiate between tumor margins *in vivo.* The major advancement of this technique comes from its ability to potentially increase tumor-negative resection rates in large patient cohorts. Although this cohort is not a representation of the patient population in terms of resection margins, this report does showcase the technique's ability to differentiate between tumor positive and negative margins in a realistic *in vivo* environment.

Patients with primary CRLM (synchronous and metachronous) or recurrent patients with newly developed metastases could benefit from using this technique. We were able to distinguish between tumor margins with high accuracy using our intraoperative NIRF workflow (Figure 3). If the resection plane of the specimen shows a direct fluorescent signal produced by the protruding tumor rim, a tumor-positive margin is very likely. Residual fluorescent signal in the wound bed resulted in a resection with tumor-positive margins in all cases, but is found to be less predictive than a protruding rim. In addition, in case no fluorescent signal was observed in the resection plane during the procedure, we were able to predict a tumor-negative resection in almost all cases.

This study pointed out a subset of patients who might not benefit from this surgical technique: patients with local recurrence at the site of previous resection or ablative therapy might display a deviant tumor rim. Regenerative tissue or scar tissue from the liver appears to retain ICG, therefore, we hypothesize that ICG accumulation in regenerative tissue is either caused by accumulation inside immature hepatocytes or caused by the Enhanced Permeability and Retention effect (EPR).(9)

NIRF guided resections during minimal invasive procedures provide many advantages. (5) For instance, the real-time imaging capabilities of NIRF imaging which provides an overlay of the fluorescent image on the bright field images significantly simplifies the correlation of the signal to the anatomy. Furthermore, since NIRF is directly incorporated into the laparoscopic system, it only requires one port, eliminating the need for additional ports or constant switching between instruments required for IOUS.

Previous reports by Aoki *et al.* also relied on NIRF imaging with ICG to resect tumors from patients with hepatocellular carcinoma and CRLM.(10) In this study, a high dose of ICG (0.5 mg/kg) was administered 2-14 days prior to surgery. The high doses of ICG were shown to promote passive accumulation in the tumor itself due to EPR effect. This allowed differentiation of cancerous tissue from healthy tissue through NIRF imaging. While this approach seemed very promising, we believe that highlighting the tumor itself can still provide risk of tumor-positive resection margins and potential tumor spill. Furthermore, our technique is able to better assess the resection margins by ICG accumulation around the tumor. Hence, with NIRF guided resections, the chances of tumor-negative resections are more probable.

Image interpretation and the lack of *in vivo* signal quantification is still found to be one of the major hurdles in implementing fluorescent guided surgery on a large scale and incorporating it into daily practice.(11) Although an effort is made to develop real-time fluorescent signal quantification *in vivo*, this technique is not available on current clinical systems.(12) Therefore, we feel that implementing the use of NIRF guided surgery in new clinical centers might be achieved during a study collaboration to transfer knowledge between clinicians and to train new users.

ICG has been used in many surgical interventions as a diagnostic agent.(13-15) The relatively low costs and stability in patients make it a favorable contrast agent. Nevertheless, ICG is a non-specific fluorescent dye that is either used to visualize organ perfusion (e.g. liver perfusion, biliary tract demarcation) or tumors using the EPR-effect. A variety of tumor specific fluorescent dyes are being developed to become the next generation of diagnostic fluorescent dyes. These dyes visualize the cell's molecular biology by binding to overexpressed receptors specific to one type of tumor, or in some cases specific to multiple types of cancer.(16-20) This might enable a more binary approach to discriminate between tumor and healthy tissue, since a positive *in vivo* signal resembles almost certain a resection with tumor-positive margin.

When combining a non-specific dye and a tumor-specific protein-dye conjugate that emits fluorescent light in separable wavelengths, the surgeon would be able to use the benefits of both techniques. In this 'dual-channel' approach, tumor-specific dyes allow tumor detection beyond the liver for more accurate disease staging and preventing surgery in advanced stage metastasized patients.(16) This emphasizes the need for collaboration between clinicians, probe developers and camera technicians to further expand the translatability and quantification.

However, a rim surrounding the tumor provides a dependable visual assistance for the surgeon to better delineate the safety margins and insure tumor-negative resections. Hence, the tumor rim is variable in size, but within certain limits (data not shown). This on the other hand could be overcome by accurate back table imaging in theatre. Transecting or

bread loafing of the resection specimen in theatre allows the surgeon to perform an additional resection in case of a fluorescent positive resection margin.(12)

To further study the ability of our technical approach, we started with a large multicenter prospective cohort study. In this study the techniques ability to increase tumor-negative resection margins will be investigated in a realistic patient cohort. This trial also poses the ability to transfer knowledge to other clinicians and to implement this technique into other clinics. As part of the studies endpoints, disease recurrence and patient survival will be monitored and analyzed at the 6 months and 5-year time point. In this *Minimally Invasive, ICG-guided Metastasectomy in Patients with Colorectal liver metastases* Trial (MIMIC Trial, Dutch Trial Register number NL7674) we aim to include 200 patients with the intention to improve tumor-negative resection rates. Patients will be case-matched to compare results. This multi-center nationwide trial opened for inclusion in September 2018.

Using a fluorescent rim surrounding CRLM has the potential to aid the surgeon in acquiring a tumor-negative resection in minimal invasive resections. Training and experience of the clinician performing the procedure are thought to play a pivotal role in the successful implementation of NIRF guided surgery and the accuracy of image interpretation.

REFERENCES

1. Chan AKC, Jamdar S, Sheen AJ, Siriwardena AK. The OSLO-COMET Randomized Controlled Trial of Laparoscopic Versus Open Resection for Colorectal Liver Metastases. Ann Surg. 2018;268(6):e69.
2. Margonis GA, Sergentanis TN, Ntanasis-Stathopoulos I, Andreatos N, Tzannis IG, Sasaki K, et al. Impact of Surgical Margin Width on Recurrence and Overall Survival Following R0 Hepatic Resection of Colorectal Metastases: A Systematic Review and Meta-analysis. Ann Surg. 2018;267(6):1047-55.
3. Hamady ZZ, Lodge JP, Welsh FK, Toogood GJ, White A, John T, et al. One-millimeter cancer-free margin is curative for colorectal liver metastases: a propensity score case-match approach. Ann Surg. 2014;259(3):543-8.
4. van der Vorst JR, Schaafsma BE, Hutteman M, Verbeek FP, Liefers GJ, Hartgrink HH, et al. Near-infrared fluorescence-guided resection of colorectal liver metastases. Cancer. 2013;119(18):3411-8.
5. Boogerd LS, Handgraaf HJ, Lam HD, Huurman VA, Farina-Sarasqueta A, Frangioni JV, et al. Laparoscopic detection and resection of occult liver tumors of multiple cancer types using real-time near-infrared fluorescence guidance. Surgical endoscopy. 2017;31(2):952-61.
6. Handgraaf HJM, Boogerd LSF, Hoppener DJ, Peloso A, Sibinga Mulder BG, Hoogstins CES, et al. Long-term follow-up after near-infrared fluorescence-guided resection of colorectal liver metastases: A retrospective multicenter analysis. European journal of surgical oncology : the journal of the European Society of Surgical Oncology and the British Association of Surgical Oncology. 2017;43(8):1463-71.
7. Vahrmeijer AL, Hutteman M, van der Vorst JR, van de Velde CJ, Frangioni JV. Image-guided cancer surgery using near-infrared fluorescence. Nature reviews Clinical oncology. 2013;10(9):507-18.
8. Couinaud C. Le foie, études anatomiques et chirurgicales. Paris: Masson & Cie. 1957.
9. Tummers QR, Hoogstins CE, Peters AA, de Kroon CD, Trimbos JB, van de Velde CJ, et al. The Value of Intraoperative Near-Infrared Fluorescence Imaging Based on Enhanced Permeability and Retention of Indocyanine Green: Feasibility and False-Positives in Ovarian Cancer. PloS one. 2015;10(6):e0129766.
10. Aoki T, Murakami M, Koizumi T, Matsuda K, Fujimori A, Kusano T, et al. Determination of the surgical margin in laparoscopic liver resections using infrared indocyanine green fluorescence. Langenbeck's archives of surgery. 2018;403(5):671-80.
11. Judy RP, Keating JJ, DeJesus EM, Jiang JX, Okusanya OT, Nie S, et al. Quantification of tumor fluorescence during intraoperative optical cancer imaging. Scientific reports. 2015;5:16208.
12. Koller M, Qiu SQ, Linssen MD, Jansen L, Kelder W, de Vries J, et al. Implementation and benchmarking of a novel analytical framework to clinically evaluate tumor-specific fluorescent tracers. Nature communications. 2018;9(1):3739.
13. Vlek SL, van Dam DA, Rubinstein SM, de Lange-de Klerk ESM, Schoonmade LJ, Tuynman JB, et al. Biliary tract visualization using near-infrared imaging with indocyanine green during laparoscopic cholecystectomy: results of a systematic review. Surgical endoscopy. 2017;31(7):2731-42.
14. Wada T, Kawada K, Takahashi R, Yoshitomi M, Hida K, Hasegawa S, et al. ICG fluorescence imaging for quantitative evaluation of colonic perfusion in

laparoscopic colorectal surgery. Surgical endoscopy. 2017;31(10):4184-93.

15. Knackstedt R, Couto RA, Ko J, Cakmakoglu C, Wu D, Gastman B. Indocyanine Green Fluorescence Imaging with Lymphoscintigraphy for Sentinel Node Biopsy in Melanoma: Increasing the Sentinel Lymph Node-Positive Rate. Annals of surgical oncology. 2019.
16. Gutowski M, Framery B, Boonstra MC, Garambois V, Quenet F, Dumas K, et al. SGM-101: An innovative near-infrared dye-antibody conjugate that targets CEA for fluorescence-guided surgery. Surgical oncology. 2017;26(2):153-62.
17. Miller SE, Tummers WS, Teraphongphom N, van den Berg NS, Hasan A, Ertsey RD, et al. First-in-human intraoperative near-infrared fluorescence imaging of glioblastoma using cetuximab-IRDye800. Journal of neuro-oncology. 2018;139(1):135-43.
18. Rosenthal EL, Warram JM, de Boer E, Chung TK, Korb ML, Brandwein-Gensler M, et al. Safety and Tumor Specificity of Cetuximab-IRDye800 for Surgical Navigation in Head and Neck Cancer. Clinical cancer research : an official journal of the American Association for Cancer Research. 2015;21(16):3658-66.
19. Korb ML, Hartman YE, Kovar J, Zinn KR, Bland KI, Rosenthal EL. Use of monoclonal antibody-IRDye800CW bioconjugates in the resection of breast cancer. The Journal of surgical research. 2014;188(1):119-28.
20. Day KE, Sweeny L, Kulbersh B, Zinn KR, Rosenthal EL. Preclinical comparison of near-infrared-labeled cetuximab and panitumumab for optical imaging of head and neck squamous cell carcinoma. Molecular imaging and biology : MIB : the official publication of the Academy of Molecular Imaging. 2013;15(6):722-9.

9

Intraoperative optical fluorescent detection of pancreatic cancer tissue targeting vascular endothelial growth factor (VEGF): A multicenter feasibility dose-escalation study

B.G. Sibinga Mulder, B.K. Pranger, M. Koller, E.W. Duiker, A. Farina Sarasqueta, J. Burggraaf, V.E. de Meijer, A.L. Vahrmeijer, B.A. Bonsing, J.S.D. Mieog, G. van Dam

Submitted: Journal of Nuclear Medicine. Supplementary data available online.

ABSTRACT

Tumor visualization with the use of near-infrared fluorescence (NIRF) imaging could aid during exploration and resection of pancreatic cancer in patients. Conjugation of the near-infrared fluorophore IRDye800CW to bevacizumab enables specific targeting of vascular endothelial growth factor (VEGF). The aim of this study was to determine whether intraoperative tumor-specific imaging of pancreatic cancer is feasible and safe using the fluorescent tracer bevacizumab-800CW.

In this multicenter, dose escalation trial, patients with suspicion of pancreatic ductal adenocarcinoma (PDAC) were administered bevacizumab-800CW (4.5mg, 10mg or 25mg intravenously) three days before surgery. Safety focused on occurrence of allergic or anaphylactic reactions and serious adverse events attributed to bevacizumab-800CW. Intraoperative NIRF imaging was performed immediately after laparotomy, just before and after resection of the specimen. Post-operatively, fluorescent signals on the axial slices and formalin fixed paraffine embedded tissue blocks from the resected specimens were correlated to histologic results. Subsequent, tumor-to-background ratios (TBR) were calculated.

Ten patients with clinically suspected PDAC were enrolled in the study. Four of the resected specimens were confirmed PDACs, other malignancies were distal cholangiocarcinoma, ampullary carcinoma and neuroendocrine tumors. No serious adverse events were related to bevacuzimab-800CW. *In vivo* tumor visualization with NIRF imaging differed per tumor type and was non-conclusive. *Ex vivo* TBRs were 1.3, 1.5 and 2.5 for 4.5mg, 10mg and 25mg dose groups, respectively.

NIRF guided surgery in patients with suspect PDAC using bevacizumab-IRDye800CW is safe and feasible. However, suboptimal TBRs were obtained because no clear distinction between pancreatic cancer from normal or inflamed pancreatic tissue was achieved.

INTRODUCTION

Currently, the only curative treatment of pancreatic cancer is radical surgery (R0 resection). Only in the minority of the patients, who appear to have a resectable tumor before surgery, a radical resection is achieved with long-term survival. Patient outcome mainly depends on the radicality of the surgical resection and the absence of metastases during surgery.(1, 2) Due to the quick spread of pancreatic cancer cells via perineural and perivascular pathways occult metastases and ingrowth in resection margins can easily be missed.(3) At this moment, surgeons have to rely solely on visual inspection and palpation to distinguish between tumorous and benign tissue and to detect remaining small tumor deposits. Because of these limitations positive resection margin rates are reported as high as 50%-75%.(4)

Improved visualization of resection margins and detection of small tumor deposits is highly desirable in pancreatic cancer surgery. A relatively new technique that can fulfill this unmet need is intraoperative near-infrared fluorescence (NIRF) imaging.(5) The main advantages of NIRF imaging are the real-time and tumor-specific visual feedback to the surgeon, thereby enabling differentiation between benign and malignant tissue during surgery and enhancing visualization of small tumor deposits.(6) A fluorescent tracer will accumulate in/bind to the tumor after intravenous administration. Subsequently, fluorescent signals can be detected using dedicated imaging systems. Recent studies showed promising results using tumor-specific NIRF imaging for the visualization of several cancer types.(7-10) However, successful and tumor-specific visualization of pancreatic cancer using NIRF imaging remains challenging.

Vascular Endothelial Growth Factor (VEGF) is involved in tumor-induced angiogenesis and lymphangiogenesis in most solid tumors.(11) Several studies report an overexpression of VEGF in pancreatic cancer tissue compared to normal pancreatic tissue.(12, 13) Bevacizumab is an antibody directed towards VEGF-overexpressing tumors and by coupling the compound to the organic fluorophore IRDye800CW a tumor-specific near-infrared fluorescent tracer (bevacizumab-800CW) was developed. Bevacizumab-800CW has already shown to be a valid tracer for molecular imaging in several cancer types.(8, 14, 15)

The aim of this study was to determine whether intraoperative tumor-specific imaging of pancreatic cancer is feasible and safe using the fluorescent tracer bevacizumab-800CW.

METHODS

This study was approved by the certified medical ethics review board of the University Medical Center Groningen (UMCG) and Leiden University Medical Center (LUMC) (clinicaltrials.gov ID: NCT02743975). This study was performed in accordance to the principles of Helsinki, the International Conference on Harmonisation of Good Medical Practices and

the laws and regulations of the Netherlands. All patients provided written informed consent before participation in the study. A safety monitoring board was appointed before start of the clinical trial. All serious adverse events occurring during or after surgery were reported immediately to the investigational review board of the UMCG, the data safety monitoring board, and the Dutch Central Committee on Research Involving Human Subjects.

Patients

For this non-randomised, open-label, multi-centre study, patients aged older than 18 years with a clinical suspicion of pancreatic ductal adenocarcinoma (PDAC), who were scheduled to undergo surgical intervention with curative intent were included. All patients had a WHO performance score of 0-2. Patients who underwent neoadjuvant treatment or had another invasive malignancy were not included. Other exclusion criteria were: medical or psychiatric conditions compromising the patient's ability to give informed consent, pregnant or lactating women, a history of infusion reactions to bevacizumab , inadequately controlled hypertension or a history of myocardial infarction, TIA, CVA, pulmonary embolism, uncontrolled chronic hepatic failure or unstable angina pectoris six months prior to inclusion.

Study design

The primary objective of this study was to determine whether bevacizumab-800CW could safely be used to identify pancreatic ductal adenocarcinoma with NIRF imaging. The secondary objective was to identify the optimal dose for the visualization of tumor tissue.

Therefore, a 4 x 3 dose-finding study design was used, consisting of two parts. In part I, four ascending doses of 4.5mg, 10mg, 25mg, and 50mg bevacizumab-800CW were intravenously administered three days prior to the planned surgery to three patients each. In part II, the cohort with the most optimal dose group will be supplemented to ten patients in order to obtain a sufficient number of data points. The most optimal dose group was to be chosen on the basis of tumor-to-background ratio (TBR).

Interim analyses were performed after completion of each cohort for the evaluation of intraoperative fluorescent signals, analyses of the *ex vivo* tumor-to-background ratios and safety outcomes.

Bevacizumab-IRDye800CW

Bevacizumab-IRDye800CW was produced in the GMP certified facility of the UMCG Hospital Pharmacy by conjugating bevacizumab (Roche AG, Basel, Switzerland) and IRDye-800CW-NHS (LI-COR Biosciences Inc, Lincoln, NE, USA) under regulated conditions. (16) IRDye800CW has excitation/emission maxima at 774 nm/789 nm.

Imaging systems

Intraoperative imaging was done with a fluorescence camera system dedicated to detect IRDye-800CW-NHS (SurgVision BV, 't Harde, the Netherlands). The system was configured with two LED lights for 800 nm illumination and one LED light for white light illumination. Real-time color and NIRF images were simultaneously collected. The imaging device was approved for intraoperative application in humans by the technical departments of the UMCG and LUMC.

Ex vivo imaging was performed using the Blackbox (SurgVision BV, 't Harde, the Netherlands) or the Pearl imager (LI-COR, Lincoln, NE, USA). For detection of fluorescence in Formalin-Fixed Paraffin-Embedded (FFPE) blocks the Odyssey® CLX fluorescence flatbed scanning system (LI-COR Biosciences Inc. Lincoln, NE, USA) was used.

Procedures

Figure 1 gives an overview of the workflow of NIRF imaging during all study steps.

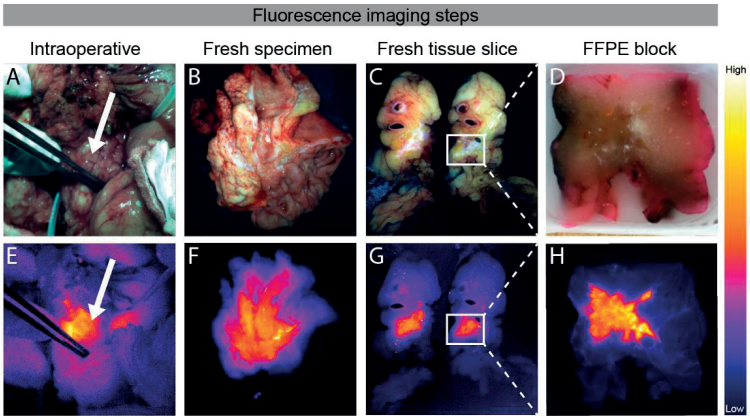

Figure 1. The workflow from intraoperative to FFPE blocks enabling correlation of intraoperative fluorescence signals with histopathology.
Intraoperative color images and corresponding fluorescence images are obtained *in vivo* during surgery. Then, imaging of the fresh surgical specimen, followed by serially slicing is performed. Imaging of the fresh tissue slices is followed by paraffin embedding. Imaging of formalin-fixed paraffin-embedded (FFPE) blocks is done to determine tumor-to-background ratio.

or to surgery, a staging laparoscopy (SL) was performed to exclude locally advanced or metastatic disease stage. In the UMCG, the SL was performed prior to the inclusion of patients, while in the LUMC, SL was performed immediately prior to the planned surgery. Patients received bevacizumab-800CW three days before surgery as an intravenous bolus injection. Tolerability assessments (ECG, blood pressure, pulse, peripheral oxygen satura-

tion, respiratory rate and temperature), were performed just before tracer injection, shortly after tracer injection and one hour after tracer injection.

Surgery was performed according to standard practice. Surgeons were not allowed to excise additional tissue based exclusively on fluorescence signals detected intraoperatively. NIRF imaging was performed at three predefined time points: 1) after laparotomy during which all surrounding organs were imaged and fluorescence intensity was determined, and in case nonspecific background fluorescent signals were present these were noted, 2) after full preparation of the specimen just before resection, the fluorescence intensity of the expected tumor and the normal pancreatic tissue was noted, and 3) after resection of the specimen, during which the remaining tissue was imaged. If additional lesions were detected with the near infrared camera system that were not part of intended resection, the surgeon was allowed to perform a biopsy for postoperative pathological analysis.

After resection, the gross specimen was imaged and subsequently sliced in 0.3 - 0.5 cm-thick slices according to the preferred grossing protocol.(4, 17) After formalin fixation, all slices were macroscopically examined. Those slices considered relevant for the pathologist were processed for histological assessment. The selection of tissue for embedding in FFPE blocks was not altered by fluorescence signal. However, after the pathologist completed the selection of slices for diagnostic purposes, an additional slice with high fluorescent signal that was not initially selected by the pathologist as relevant, could be embedded apart from standard-of-care. After microscopic evaluation and the final pathology report, the FFPE blocks were imaged and the TBRs were determined on the fluorescence images of the FFPE blocks after correlation of regions of interest on the corresponding histological slice. Additional information about the tracer, imaging procedures and pathological processing is provided in the Supplementary Information.

Statistics

Descriptive statistics were reported as means with standard deviation (SD), whereas median with range was used in case of a skewed distribution. TBR was defined as the mean fluorescence intensity (MFI, arbitrary unit) measured in pancreatic cancer tissue divided by the MFI in surrounding healthy tissue and was reported as mean. Fluorescent signals in tumor and normal tissue was compared using the Mann-Whitney test. A p-value of <0.05 was considered statistically significant. For descriptive statistics SPSS (version 23.0) was used, graphs were designed with Graphpad Prism (version 7.0).

RESULTS

Patient and safety data

Between December 1, 2016, and February 26, 2018, ten patients were enrolled in the study with suspected pancreatic ductal carcinoma. After completion of cohort III (25 mg), the investigational review board mandated termination of the study, because of low TBRs. Table 1 provides an overview of patient characteristics and tumor characteristics per patient (patient 01-10). Based on the histological assessment of the resected specimens, various malignancies were included in the study: pancreatic ductal adenocarcinoma (n=4), distal cholangiocarcinoma (n=1), carcinoma of the papilla (n=2), well differentiated grade 3 neuro-endocrine tumor of the pancreas (n=1) and a low-grade intraductal papillary mucinous neoplasm (n=1). In patient 04, no malignancy was present but an auto-immune pancreatitis based on histological assessment. In nine patients, the tracer was administered three days before exploratory laparotomy. In patient 03 imaging was performed 10 days after administration of 4.5mg tracer due to a postponed exploration because the patient developed ascending cholangitis the day before surgery. Therefore, one additional patient was included in cohort I (4.5mg). No allergic or anaphylactic reactions to bevacizumab-IRDye800CW were noted. Two serious adverse events were reported, both of which developed in patient 05 and were attributed to the pancreatoduodenectomy. These included a pancreatic fistula requiring percutaneous drainage and antibiotic treatment, and bleeding of the gastroduodenal artery stump 27 days postoperative requiring radiological coiling. Additional safety data is provided in the Suppnr. menagey dsex

Table 1. Patient and tumor characteristics.

	Patient					Tumor		
	Nr.	**Age**	**Sex**	**WHO**	**preop FNA**	**histology**	**TN stage**	**adicality**
4.5 mg	1	64	F	0	HGD	dist chol carc	T3N1	R0
	2	67	M	1		PDAC	T3N1	R0
	3	75	M	0		PDAC	T3N0	R0
	4	69	M	1	inconcl.	auto-immune pancreatitis		
10 mg	5	56	M	1		ampul carc	T3N1	R0
	6	73	F	0		PDAC	T3N1	R1
	7	74	F	0		IPMN: LG		R0
25 mg	8	47	F	0	HGD	PDAC	T2N2	R0
	9	74	F	0	HGD	ampul carc	T3N1	R1
	10	67	M	0		NET: grade 3	T3N0	

Preop: preoperative, FNA: fine needle aspiration, F: female, M: male, HGD: high grade dysplasia, dist chol carc: distal cholangiocarcinoma, PDAC: pancreatic ductal adenocarcinoma, inconcl.: inconclusive, ampul carc: ampul carcinoma, IPMN: LG: low grade intrapapillair mucinous neoplasm, NET: neuroendocrine tumor, R0: radical, R1: irradical

In- and ex vivo imaging per tumor type

PDAC: *in vivo* the location of the expected primary tumor could be visualized with NIRF imaging with all employed doses of the tracer compound. After resection of the pancreatic head (patient 06), the tail of the pancreas was suspect for residual tumor and also showed high fluorescence. The suspicion of malignancy was confirmed by intraoperative ultrasound, and therefore the pancreatic tail was resected. Histological assessment showed a poor differentiated tumor in the head, body and tail of the pancreas with the latter nog diagnosed during the preoperative work-up. In the other PDAC patients, nonspecific fluorescent signals remained visible after resection of the pancreatic head. No additional resection was performed based on these signals because it seemed clinically highly unlikely that this was due to any residual tumor. Histological assessment confirmed radical resection. The MFI increased per dose group between tumor and normal tissue which resulted in TBRs of 1.4, 1.7 and 2.1 per dose group, respectively (Figure 2A). Figure 2B demonstrates the contrast between tumorous and other types of tissue based on the difference in fluorescence intensity. Representative fluorescence images per dose group of specimen slices and FFPE blocks of PDAC are shown in Figure 3.

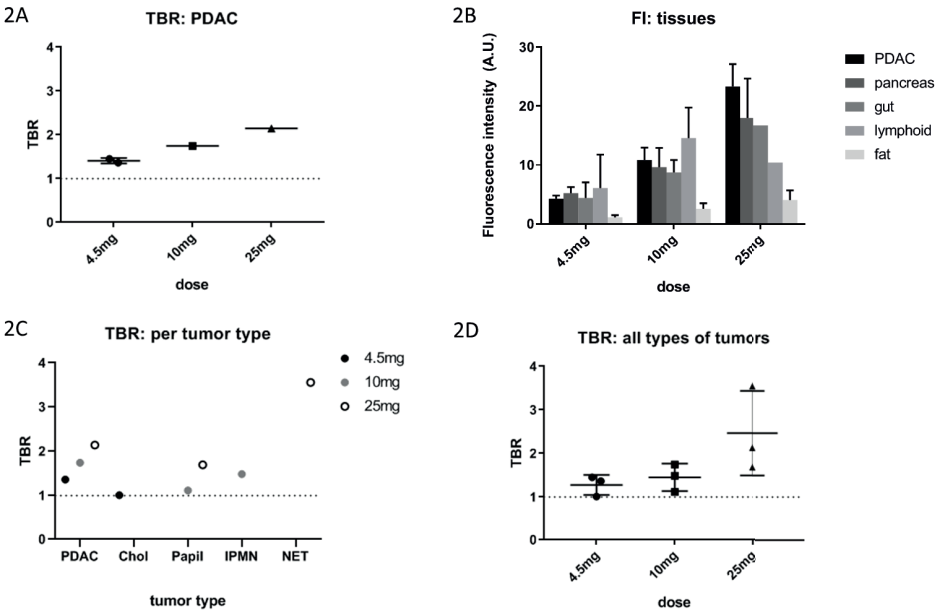

Figure 2. Tumor-to-background ratio's (TBR) and fluorescence intensity (FI).
2A: TBRs of all pancreatic ductal adenocarcinomas (PDAC) distributed per dose group. 2B: FI of different tissue types in patients with PDAC. 2C: mean TBR per tumor type distributed per dose group. 2D: mean TBRs of all types of tumors distributed per dose group.

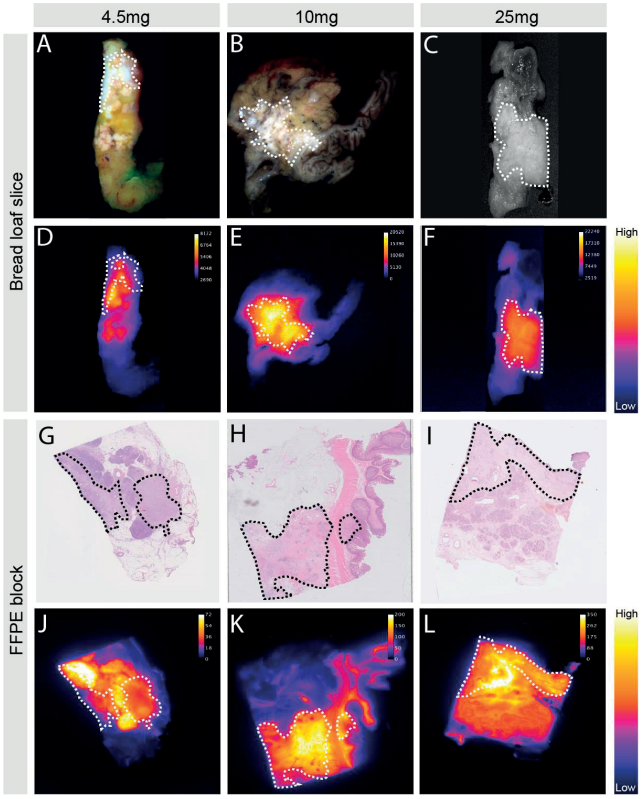

Figure 3: Representative images per dose group of pancreatic ductal adenocarcinoma.
Columns represent the three dose groups: 4.5 mg, 10 mg and 25 mg. Rows represent the imaging modality, in the upper part a white light image and in the lower part the representative fluorescence image. Tumor tissue is delineated with a white dashed line.

Distal cholangiocarcinoma: In vivo there was no fluorescent signal of the tumor (patient 01, 4.5mg). On the specimen slices and FFPE blocks the MFI was similar between tumor and normal tissue which resulted in a TBR of 1.0 (MFI 48.7 Vs. 48.1) (Figure 2C).

Carcinoma of the papilla: *in vivo* the location of the expected primary tumor could be visualized with NIRF imaging in two patients (10mg and 25mg). In patient 08, there was clinical suspicion of tumor in-growth in the superior mesenteric vein (SMV), and therefore, a wedge resection of the SMV was performed. NIRF imaging of the wedge was positive. Histologic assessment of the wedge confirmed ingrowth of malignant cells in the vascular wall. On the specimen slices and FFPE blocks the MFI was similar between tumor and normal tissue which resulted in a TBR of 1.1 and 1.7 for 10mg and 25mg, respectively. (Figure 2C).

Neuro-endocrine neoplasm: *in vivo* the expected location of the tumor was clearly visible with NIRF imaging and after resection fluorescent signals diminished strongly. On the

specimen slices and FFPE blocks the MFI was significantly different between tumor and normal tissue which resulted in a TBR of 3.6 (MFI 27.6 Vs. 7.8, P = 0.04) (Figure 2C).

Intraductal papillary mucinous neoplasm: in patient 07 the location of the expected primary tumor could be visualized with NIRF imaging (10mg), although clear distinction between pancreatic and tumorous tissue could not be made. On the specimen slices and FFPE blocks the MFI did not differ much between IPMN and normal tissue which resulted in a TBR of 1.5 (MFI 84.5 Vs. 56.7, P = 0.4) (Figure 2C).

Auto-immune pancreatitis: in patient 04 the location of the expected 'tumor' could be visualized with fluorescence imaging (4.5mg). *Ex vivo* extensive fibrotic and inflammatory tissue was seen and no normal pancreatic tissue remained. Therefore, there was no difference in fluorescence intensity in the resected specimen of the patient with pancreatitis (MFI 50.7).

Ex vivo TBRs of all types of tumors together, divided per dose group, are demonstrated in Figure 2D. TBRs were 1.3, 1.5 and 2.5 for 4.5mg, 10mg and 25mg, respectively. Fluorescent images of all different types of tumors are displayed in Figure 4.

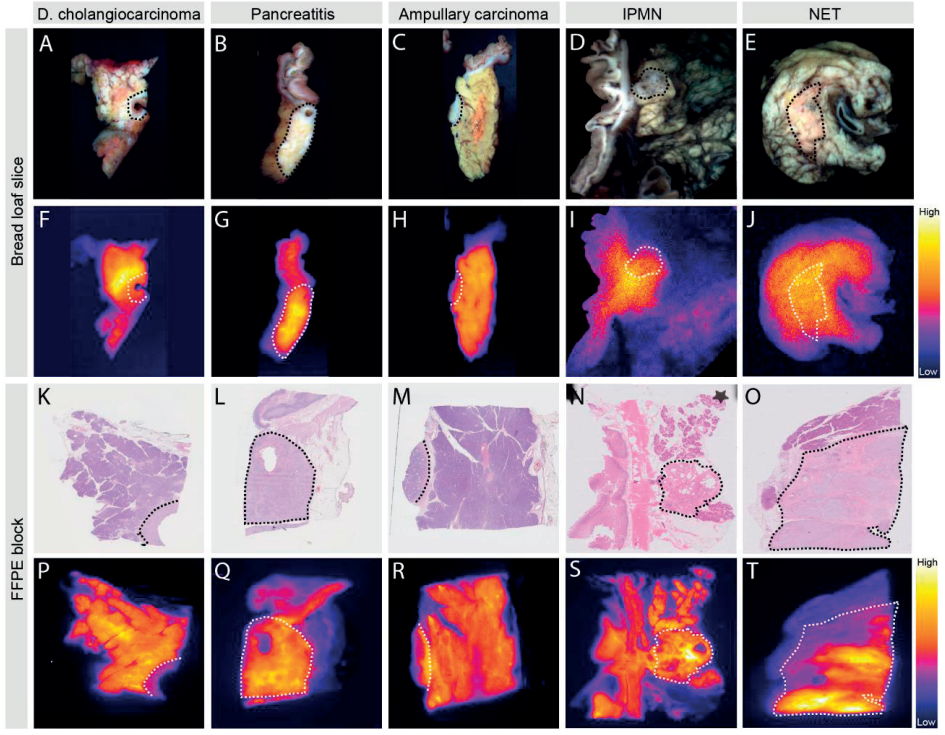

Figure 4: Representative images per tumor type.
Columns represent different tumor types: ductal adenocarcinoma, auto-immune pancreatitis, ampullay carcinoma, intraductal papillary mucinous neoplasm (IPMN) and neuro-endocrine tumor (NET). Rows represent the imaging modality, in the upper part a white light image and in the lower part the representative fluorescence image. Tumor tissue is delineated with a dashed line.

DISCUSSION

In this study, the safety and feasibility of visualizing pancreatic cancer tissue with bevacuzimab-800CW was assessed. Intravenous administration of bevacuzimab-800CW (4.5, 10 and 25mg) three days before appeared safe as no changes in safety parameters including vital signs and ECG and no related adverse events occurred. Both in vivo and ex vivo NIRF imaging of pancreatic cancer tissue was feasible with bevacizumab-800CW, as fluorescence signal could be detected in tumor tissue. However, suboptimal TBRs were obtained and distinguishing pancreatic cancer tissue from normal pancreatic tissue remains challenging.

NIRF imaging with other tracers in previous clinical trials had similar results. The feasibility of SGM-101, a 700nm antibody against carcinoembryonic antigen (CEA), was assessed for intraoperative NIRF imaging of PDAC. SGM-101 could reach and bind CEA-expressing tumor cells, but with modest TBRs (1.6 for primary tumors).(18) With cetuximab-IRDye800 it was also feasible to detect pancreatic cancer tissue and tumor-bearing lymph nodes. Studies with larger patient number must show if this tracer indeed is suitable for in vivo NIRF imaging of pancreatic cancer.(19) Limited success rates for treating PDAC with systemically administered agents are commonly attributed to the desmoplastic stroma of PDAC, which is thought to severely reduce the delivery of these therapies. Interestingly, both cetuximab and bevacizumab are large monoclonal antibodies and both managed to penetrate through the dense desmoplastic stroma and to bind pancreatic cancer cells and endothelial cells.

The results of these NIRF imaging studies for detection of pancreatic cancer suggest that pancreatic tumor tissue might be a difficult type to detect. The yield of tumor-specific imaging in the current study was lower than expected, and therefore, the study was terminated early. The most obvious reasons for suboptimal pancreatic cancer visualization with NIRF are unfavorable intrinsic characteristics of pancreatic cancer. Due to the previously mentioned desmoplastic stroma, poor vascularization and high intratumoral pressure, the antibody-based tracers might not accumulate optimally in the tumor compared to the surrounding tissue. This makes it difficult to distinguish normal tissue from tumorous tissue. In this study, the difficulty to demonstrate tumor-specific fluorescent imaging could also be due to a suboptimal choice of the target VEGF, an endothelial cell-specific key regulator of angiogenesis. A tracer targeting stroma, or a combination of tracers, could be the solution.(20) An FGmRNA profiling study on a set of normal pancreatic tissue and PDAC tissue identified THY1, CTSE, GGT5 and MUC1 as potential targets for pancreatic cancer imaging.(21) Other targets that are potentially suitable for NIRF imaging of pancreatic tumors are integrin $\alpha v\beta 6$ and uPAR.(22) Furthermore, future studies should focus on a tracer that can differentiate between chemotherapy-induced fibrotic tissue and vital cancer cells, because an increased number of patients will be treated with neoadjuvant therapy.

Moreover, the detection of metastases is important in optimal treatment strategy assessment for pancreatic cancer patients. Identification of preoperatively missed metastases via preoperative SL with NIRF imaging could be of great value for these patients. Since resection of the primary tumor does not increase the prognosis in metastasized patients and only delays appropriate treatment.(23) Therefore, a tumor-specific tracer should be used that is not metabolized by the liver, because pancreatic cancer preferably metastasizes to the liver. A potential tracer could be cRGD-ZW800-1, which is renally cleared. Preclinical studies showed promising results for pancreatic cancer detection.(24) cRGD-ZW800-1 is currently being tested in patients with colorectal tumors and if promising will be expanded to pancreatic cancer patients (clinicaltrials.gov ID:NL6250805817).

A unique aspect of our study is the variety of cancer types that were included; besides pancreatic ductal adenocarcinoma, also neuroendocrine tumors, distal cholangiocarcinoma, IPMNs and ampullary tumors were visualized with bevacuzimab-800CW. Tumor targeted NIRF imaging of these tumors has not yet been described. The tracer also bound to the vessels in these tumors and most had comparable TBRs to PDACs. An exception was noted with neuroendocrine tumors for which we observed a 3-fold higher signal intensity from the tumor compared to the background signal. This likely reflects the hypervascular characteristics of these tumors that are able to synthesize and secrete high amounts of VEGF.(25)

In conclusion, NIRF guided surgery in patients with suspect pancreatic cancer using bevacizumab-IRDye800CW is safe and feasible. However, suboptimal TBRs were obtained and distinguishing pancreatic cancer tissue from normal pancreatic tissue remains challenging.

REFERENCES

1. Campbell F, Smith RA, Whelan P, Sutton R, Raraty M, Neoptolemos JP, et al. Classification of R1 resections for pancreatic cancer: the prognostic relevance of tumor involvement within 1 mm of a resection margin. Histopathology. 2009;55(3):277-83.
2. Ghaneh P, Kleeff J, Halloran CM, Raraty M, Jackson R, Melling J, et al. The Impact of Positive Resection Margins on Survival and Recurrence Following Resection and Adjuvant Chemotherapy for Pancreatic Ductal Adenocarcinoma. Ann Surg. 2017.
3. Zhang JF, Hua R, Sun YW, Liu W, Huo YM, Liu DJ, et al. Influence of perineural invasion on survival and recurrence in patients with resected pancreatic cancer. Asian Pac J Cancer Prev. 2013;14(9):5133-9.
4. Verbeke CS, Gladhaug IP. Resection margin involvement and tumor origin in pancreatic head cancer. Br J Surg. 2012;99(8):1036-49.
5. Vahrmeijer AL, Hutteman M, van der Vorst JR, van de Velde CJ, Frangioni JV. Image-guided cancer surgery using near-infrared fluorescence. Nat Rev Clin Oncol. 2013;10(9):507-18.
6. Tipirneni KE, Warram JM, Moore LS, Prince AC, de Boer E, Jani AH, et al. Oncologic Procedures Amenable to Fluorescence-guided Surgery. Ann Surg. 2017;266(1):36-47.
7. Rosenthal EL, Warram JM, de Boer E, Chung TK, Korb ML, Brandwein-Gensler M, et al. Safety and Tumor Specificity of Cetuximab-IRDye800 for Surgical Navigation in Head and Neck Cancer. Clin Cancer Res. 2015;21(16):3658-66.
8. Harlaar NJ, Koller M, de Jongh SJ, van Leeuwen BL, Hemmer PH, Kruijff S, et al. Molecular fluorescence-guided surgery of peritoneal carcinomatosis of colorectal origin: a single-centre feasibility study. Lancet Gastroenterol Hepatol. 2016;1(4):283-90.
9. Koller M, Qiu SQ, Linssen MD, Jansen L, Kelder W, de Vries J, et al. Implementation and benchmarking of a novel analytical framework to clinically evaluate tumor-specific fluorescent tracers. Nat Commun. 2018;9(1):3739.
10. van Dam GM, Themelis G, Crane LM, Harlaar NJ, Pleijhuis RG, Kelder W, et al. Intraoperative tumor-specific fluorescence imaging in ovarian cancer by folate receptor-alpha targeting: first in-human results. Nat Med. 2011;17(10):1315-9.
11. Ellis LM, Hicklin DJ. VEGF-targeted therapy: mechanisms of anti-tumor activity. Nat Rev Cancer. 2008;8(8):579-91.
12. Tang RF, Wang SX, Peng L, Wang SX, Zhang M, Li ZF, et al. Expression of vascular endothelial growth factors A and C in human pancreatic cancer. World J Gastroenterol. 2006;12(2):280-6.
13. Nagakawa Y, Aoki T, Kasuya K, Tsuchida A, Koyanagi Y. Histologic features of venous invasion, expression of vascular endothelial growth factor and matrix metalloproteinase-2 and matrix metalloproteinase-9, and the relation with liver metastasis in pancreatic cancer. Pancreas. 2002;24(2):169-78.
14. Lamberts LE, Koch M, de Jong JS, Adams ALL, Glatz J, Kranendonk MEG, et al. Tumor-Specific Uptake of Fluorescent Bevacizumab-IRDye800CW Microdosing in Patients with Primary Breast Cancer: A Phase I Feasibility Study. Clin Cancer Res. 2017;23(11):2730-41.
15. Hartmans E, Tjalma JJJ, Linssen MD, Allende PBG, Koller M, Jorritsma-Smit A, et al. Potential Red-Flag Identification of Colorectal Adenomas with Wide-Field Fluorescence Molecular Endoscopy. Theranostics. 2018;8(6):1458-67.

16. Ter Weele EJ, Terwisscha van Scheltinga AG, Linssen MD, Nagengast WB, Lindner I, Jorritsma-Smit A, et al. Development, preclinical safety, formulation, and stability of clinical grade bevacizumab-800CW, a new near infrared fluorescent imaging agent for first in human use. Eur J Pharm Biopharm. 2016;104:226-34.
17. Adsay NV, Basturk O, Saka B, Bagci P, Ozdemir D, Balci S, et al. Whipple made simple for surgical pathologists: orientation, dissection, and sampling of pancreaticoduodenectomy specimens for a more practical and accurate evaluation of pancreatic, distal common bile duct, and ampullary tumors. Am J Surg Pathol. 2014;38(4):480-93.
18. Charlotte E.S. Hoogstins LSFB, Babs G. Sibinga Mulder, J. Sven D. Mieog, Rutger Jan Swijnenburg, Cornelis J.H. van de Velde, Arantza Farina Sarasqueta, Bert A. Bonsing, Berenice Framery, André Pèlegrin, Marian Gutowski, Françoise Cailler, Jacobus Burggraaf, Alexander L. Vahrmeijer. Image-guided surgery in patients with pancreatic cancer: a clinical trial using SGM-101, a novel carcinoembryonic antigen-targeting, near-infrared fluorescent agent in process. 2017.
19. Tummers WS, Miller SE, Teraphongphom NT, Gomez A, Steinberg I, Huland DM, et al. Intraoperative Pancreatic Cancer Detection using Tumor-Specific Multimodality Molecular Imaging. Ann Surg Oncol. 2018;25(7):1880-8.
20. Boonstra MC, Prakash J, Van De Velde CJ, Mesker WE, Kuppen PJ, Vahrmeijer AL, et al. Stromal Targets for Fluorescent-Guided Oncologic Surgery. Front Oncol. 2015;5:254.
21. Koller M, Hartmans E, de Groot DJA, Zhao XJ, van Dam GM, Nagengast WB, et al. Data-Driven Prioritization and Review of Targets for Molecular-Based Theranostic Approaches in Pancreatic Cancer. J Nucl Med. 2017;58(12):1899-903.
22. de Geus SW, Boogerd LS, Swijnenburg RJ, Mieog JS, Tummers WS, Prevoo HA, et al. Selecting Tumor-Specific Molecular Targets in Pancreatic Adenocarcinoma: Paving the Way for Image-Guided Pancreatic Surgery. Mol Imaging Biol. 2016;18(6):807-19.
23. Parsons CM, Sutcliffe JL, Bold RJ. Preoperative evaluation of pancreatic adenocarcinoma. J Hepatobiliary Pancreat Surg. 2008;15(4):429-35.
24. Handgraaf HJM, Boonstra MC, Prevoo H, Kuil J, Bordo MW, Boogerd LSF, et al. Real-time near-infrared fluorescence imaging using cRGD-ZW800-1 for intraoperative visualization of multiple cancer types. Oncotarget. 2017;8(13):21054-66.
25. Villaume K, Blanc M, Gouysse G, Walter T, Couderc C, Nejjari M, et al. VEGF secretion by neuroendocrine tumor cells is inhibited by octreotide and by inhibitors of the PI3K/AKT/mTOR pathway. Neuroendocrinology. 2010;91(3):268-78.

10

A Prospective Clinical Trial to Determine the Effect of Intraoperative Ultrasound on Surgical Strategy and Resection Outcome in Patients with Pancreatic Cancer

B.G. Sibinga Mulder, S. Feshtali, A. Farina Sarasqueta,
R.J. Swijnenburg, A.L. Vahrmeijer, B.A. Bonsing, J.S.D. Mieog

Journal of Ultrasound in Medicine and Biology, 2019 Aug. Supplementary data available online.

ABSTRACT

Surgical exploration in patients with pancreatic or periampullary cancer is often performed without intraoperative image-guidance. Although intraoperative ultrasound (IOUS) may enhance visualization during resection, this tool has not been investigated in detail until now. Here, we performed a prospective cohort study to evaluate the effect of IOUS on surgical strategy and to evaluate whether vascular involvement and radicality of the resection could be correctly assessed with IOUS.

IOUS was performed by an experienced abdominal radiologist during surgical exploration in 31 consecutive procedures. The effect of IOUS on surgical strategy was determined as having 1) no effect, 2) determination of tumor localization, 3) evaluation of vascular involvement, or 4) ability to waive surgery. Radicality of the resections and vascular contact was determined during pathological analysis and compared to preoperative imaging and during IOUS.

Overall, IOUS influenced surgical strategy in 61% of procedures. In 21 out of 27 malignant tumors a radical resection was achieved (78%). Vascular contact was assessed correctly using IOUS in 89% compared to 74% using preoperative imaging.

IOUS can help the surgical team to assess the resectability and to visualize the tumor and possible vascular contact in real time during resection. IOUS may therefore increase the likelihood of achieving a radical resection.

INTRODUCTION

The prognosis for patients with pancreatic cancer who undergo surgery with curative intend depends largely on the ability to achieve a radical resection.(1) Typically, preoperative computed tomography (CT) imaging is used to determine the local extent of the tumor.(2) Factors that determine local resectability include contact with surrounding structures, vascular involvement and the absence of distant metastases.(3) To improve outcome, neoadjuvant chemotherapy is often administered to patients who present with a borderline resectable or locally advanced tumor.(4) However, neoadjuvant chemotherapy can complicate the ability to assess the resectability of the tumor using CT imaging, largely due to the difficulties associated with distinguishing between chemotherapy-induced fibrosis and viable tumor tissue.(5, 6)

Surgical treatment for pancreatic cancer generally begins with surgical exploration to identify occult metastases and to assess the tumor's resectability. During this procedure, the surgeon must rely solely on visual inspection and palpation in order to distinguish between tumor and normal tissue. This can be challenging, particularly in the presence of peritumoral inflammation. Moreover, in up to 60% of patients who undergo a resection of their pancreatic tumor, histological microscopic assessment reveals tumor infiltration into the borders of the resected specimen, resulting in a high rate of local recurrence.(7-9) On the other hand, approximately half the patients who underwent venous resection due to suspected tumor invasion are found to have no tumor infiltration based on a pathological examination in the resected vascular patch.(10) Given these factors, the current state-of-the-art is to perform high-risk surgery, despite a suboptimal success rate and the fact that resection is often performed without the benefit of intraoperative guidance and visualization.

Ultrasound, mostly endoscopic, has gained an important role in diagnosing patients with a suspicion of pancreatic cancer, with the benefit of performing fine needle aspirations during the same procedure.(11) Laparoscopic ultrasound can be performed during staging laparoscopy prior to surgical exploration.(12) During surgery, intraoperative ultrasound (IOUS) can be useful in helping to determine vascular involvement in patients with borderline resectable pancreatic cancer.(13, 14) By offering real-time imaging data, IOUS provides direct feedback regarding the lesion's extent and vascular involvement. This information can then be used to guide the surgical strategy and approach. In addition, because it uses a high-frequency probe in direct contact with the organ, IOUS provides superior spatial resolution and contrast compared to CT and MRI scans.(15) Although IOUS may be useful during surgical exploration and resection of pancreatic cancer, few studies have used this technique to assess tumor extension and subsequent IOUS-guided resection.(16) The study of Kolesknik *et al.* retrospectively examined the effect of IOUS on surgical interventions, reporting that their surgical strategy changed due to IOUS in 30% of the patients, most of them due to the detection of hepatic metastases.(17) Except for this study, IOUS is not

routinely applied during resections of pancreatic cancer and the added value is scarcely described.

Here, the benefits of performing IOUS with respect to surgical strategy in patients with a pancreatic or periampullary tumor undergoing surgical exploration was evaluated. In addition, the results of preoperative radiological imaging, IOUS, and pathological evaluation of the resected specimen were compared.

METHODS

Patients

In the Leiden University Medical Center (LUMC), preoperative radiological imaging was performed on all patients with a suspect lesion in the pancreas. A CT scan was present of all patients, in some patients an additional MRI scan was made. If it was deemed necessary, a preoperative cytology sample was obtained and used for histopathological confirmation of a malignancy. The patients were evaluated by the multidisciplinary pancreatic team in order to determine whether surgery was a treatment option, and if so, whether a vascular resection should be considered. Each resection began with a staging laparoscopy in order to exclude the presence of metastases. In patients who went on for an explorative laparotomy, IOUS was performed. In this study consecutive patients who underwent surgical explorative laparotomy for pancreatic or periampullary cancer (including duodenal, distal bile duct, or ampulla of Vater cancer) at the LUMC from June 2016 through June 2017 were included. Patients who underwent surgery for a neuroendocrine tumor were excluded from this study. The use of IOUS during the surgical procedure is standard of care in the LUMC and in this study only the impact of IOUS was evaluated, therefore, a waiver was given for the need for informed consent by the Medical Ethics Committee of the LUMC.

Outcomes

The primary objective was to evaluate the effect of IOUS on surgical strategy, therefore, the effect of IOUS on the surgical strategy and/or any additional information obtained from IOUS was defined as follows: 1) no value, 2) additional information regarding tumor localization, 3) additional information regarding vascular contact or 4) the ability to waive surgery.

The secondary objective was to compare the IOUS assessment with the pathological assessment, including the radicality of the resection.

The tertiary objective was to evaluate the assessment of vascular involvement, therefore, both the preoperative imaging results and IOUS assessment of vascular contact was compared with the pathological examination, which is the current golden standard. The contact

between the tumor and any vessel was evaluated, and in particularly, contact between the tumor and the superior mesenteric vein (SMV), including the portal vein (PV) and confluens.

Description of different modalities

Preoperative imaging

The preoperative CT scans were acquired using an Aquilion ONE 160-detector row helical CT (Toshiba Medical Systems Europe, Zoetermeer, the Netherlands). Intravenous contrast (Glucagen 0.5mg) was administered with automatic power injection prior to obtaining the scan. Axial, coronal and sagittal slices were obtained during the pancreatic phase (20 s after injection) and during the portal venous phase (50 s after injection). MR images were acquired with a Philips Ingenia 3.0T scanner (Philips, Amsterdam, the Netherlands), after intravenous injection with the contrast medium Dotarem (0.2 ml/kg). In addition, a magnetic resonance cholangiopancreatography was performed. Detailed scanning protocols for both CT and MRI scans are provided in Supplementary Information S1.

Evaluation of the preoperative imaging was initially performed by a specialized abdomen radiologist, subsequently, the scans were viewed and discussed during the multidisciplinary pancreatic team meeting. The patient's most recent preoperative scan was evaluated for: direct or indirect signs of the tumor, the tumor's maximum diameter, density, and localization. The vascular contact was assessed and the resectability was determined based on the DPCG (Dutch Pancreatic Cancer Group) 2012 guidelines, an overview of these guidelines is given in the Supplementary Information S2.(18) Vascular resection was suggested if deemed necessary. Lymph node status of the tumor was determined. The number of days between the last preoperative scan and surgery were noted. For this study, the final evaluation of the scans during the multidisciplinary pancreatic team meeting was used.

Intraoperative ultrasound

After completion of the staging laparoscopy, subsequent laparotomy, Kocher maneuver and exposition of the ventral side of the pancreas, IOUS was performed and read by the same specialized radiologist (author SF) as who assessed the preoperative imaging. The role of the surgeons during the IOUS assessment was supportive. The Toshiba Aplio 300 (Toshiba Medical Systems Europe, Zoetermeer, the Netherlands) equipped with a 7.0-MHz linear T-shaped transducer (frequency range: 4.0-11.0 MHz; radius: 46 mm) was used.

First, the entire pancreas was imaged in order to obtain a global overview and to identify additional potential lesions. Second, the tumor was imaged, and the visibility, echogenicity, border, margin, and maximum diameter were noted. Third, the relationship of the tumor with the surrounding tissues/structures was assessed. Fourth, the contact between the tumor and the surrounding vessels was evaluated and the length and extension of the vascular involvement was determined. Vascular involvement was assessed according to the preoperative

imaging guidelines, and the same consequences for resectability were used (Supplementary Information S2). In case the tumor grows into a vessel the vessel is mostly distorted or stenosed by the tumor, which can be observed with ultrasound. In addition, the distance of involvement and surrounding component can assessed.

The IOUS findings were directly discussed with the surgical team, potentially resulting in a different resection margin determination or leading to an extended vascular reconstruction, either by patch or segment resection. In addition, the margin(s) that had the highest risk of R1 (irradical) resection were designated. In the event that vascular involvement and/or invasion into surrounding structures was too extensive, the surgeons could opt to refrain from a surgical resection. In addition, the radiologist schematically drew the tumor relative to the pancreas, ducts, vessels, and all surrounding structures. The duration of the entire IOUS assessment was noted, and relevant images were saved for post-procedure evaluation.

Pathological examination (PA)

The resected specimens were histologically examined according to the Verbeke protocol, by a specialized pathologist (author AFS) who noted the tumor's characteristics, including the origin, differentiation grade, maximum diameter, the presence of perineural invasion and lymphatic and/or vascular invasion, and extension in peripancreatic soft tissue.(19) Margins to all pancreatic surfaces were measured. Radicality was assessed as follows: R0, tumor-free; R1, tumor extension <1 mm; or R2, macroscopically non-radical. In the event that a vascular reconstruction was performed, the borders of the vascular patch and the depth of invasion in the vascular patch or segment were also assessed for tumor involvement. All resected lymph nodes were scored for tumor positivity.

Statistics

Assuming that the surgical strategy would be changed in > 30% of the patients due to the IOUS assessment, 31 patients should be included. A sample size of 31 patients achieves 80% power using the two-sided McNemar's test with a significance level of 0.05.

Differences between correct assessment of vascular contact between preoperative imaging and IOUS were assessed with a McNemar test.

RESULTS

Patient characteristics

During the study period, IOUS was performed in 31 surgical explorations (Table 1). One patient underwent two explorations: six months after a pancreatic head resection, she underwent a pancreatic tail resection for a second primary malignancy. Vascular contact was suspected on nine preoperative scans and vascular involvement on one scan, therefore, vas-

Table 1. Patient characteristics.

			n	*%*
total			31	
age*	**mean (SD)**		64.3	9.8 (SD)
sex*	**male**		16	53%
	female		14	47%
endoscopic ultrasound	**yes**		22	71%
	no		9	29%
stent in situ	**yes**		5	16%
	no		26	84%
neo-adjuvant treatment	**gemcitabine**		3	10%
	FOLFIRINOX		1	3%
	none		27	87%
last imaging before surgery	**CT scan**		24	77%
	visibility:	*direct sign*	*11*	*46%*
		indirect sign	*13*	*54%*
	density:	*hypodens*	*9*	*37%*
		isodens	*15*	*63%*
	MRI scan		7	23%
	visibility:	*direct sign*	*7*	*100%*
		indirect sign	*0*	*0*
	best sequence:	*T1*	*3*	*43%*
		DWI	*2*	*29%*
		dynamic	*2*	*29%*
size (max diameter; mm)	**% measurable**		17	55%
	median (IQR)		24	14-28 (IQR)
origin and localisation of tumor	**ampulla of Vater**		3	10%
	distal bile duct		4	13%
	duodenum		4	13%
	pancreas		20	64%
		head/neck	*12*	*60%*
		proc. uncinatus	*2*	*10%*
		corpus	*4*	*20%*
		tail	*2*	*10%*
vascular contact of tumor	**no vascular contact**		17	55%
	contact with vessel		9	29%
	involvement of vessel		1	3%
	contact not judgeable		4	13%
clinical lymph node status	**N0**		24	77%
	N1		7	23%

Table 1. Patient characteristics. (*continued*)

		n	*%*
days between scan and surgery	**median (IQR)**	31	21-36 (IQR)
type of surgery	**PPPD/whipple**	21	67%
	tail resection	3	10%
	total pancreatectomy	3	10%
	duodenum resection	1	3%
	no resection	3	10%

**one patient was operated on twice. only included once. IQR: inter quartile range*

cular resection was suggested for this patient. Vascular contact could not be determined from four preoperative scans (13%) due to the isodense appearance on the scans. Twenty-seven malignant tumors and one benign lesion were resected, of which four included a vascular resection. During three explorations, resection was abandoned because of irresectable disease.

Primary outcome: effect of IOUS assessment on surgical strategy

The IOUS-based characteristics of the tumors are summarized in Table 2. The use of IOUS extended the average procedure by 11 (±5) minutes. All tumors (100%) were detected with IOUS and vascular contact was detected in 14 patients (45%). The majority of the tumors was clearly visible, hypoechogenic, and had an irregular border.

Next, the effect of IOUS assessment on the surgical procedure was examined. A detailed overview of the effect of IOUS assessment on surgical strategy and the information that was provided based on the IOUS assessment are provided in Table 3. Example IOUS images corresponding to the findings are shown in Figure 1.

Secondary outcome: correlation with pathological findings

Resection was cancelled twice based on the IOUS assessment during surgical exploration, in addition, surgery was also cancelled during a third procedure; however, this decision was based on inspection followed by confirmation of malignancy in a frozen section, rather than on the IOUS assessment. In one case, the pathological analysis (PA) revealed a serous cystadenoma in the resected specimen, instead of a malignant tumor. Thus, a total of 27 malignancies were resected, which are summarized in Supplementary Table S3. Of these 27 resected malignancies, 6 (22%) were irradical (R1), with the following resection margins involved: superior mesenteric artery (SMA) (n=2 tumors), tumor growth in a resected segment of the SMV (n=2), gastroduodenal artery resection margin (n=1), and both the pancreatic resection margin and the common bile duct margin (n=1). The surgical strategy was influenced by the IOUS assessment in four of the patients with a R1 resection.

Table 2. Tumor characteristics of IOUS assessment.

		N=31	*%*
duration IOUS (min)	**median (IQR)**	10	7-15 (IQR)
size (max diameter; mm)	**% measurable**	22	71%
	median (IQR)	22	18-34 (IQR)
origin and localisation of tumor	**ampulla of Vater**	3	10%
	distal bile duct	2	6%
	duodenum	2	6%
	pancreas	24	78%
	head/neck	*14*	*58%*
	proc. uncinatus	*4*	*17%*
	corpus	*3*	*13%*
	tail	*2*	*8%*
	diffuse	*1*	*4%*
vascular contact of tumor	**no vascular contact**	16	52%
	contact with vessel	9	29%
	involvement of vessel	5	16%
	contact not judgeable	1	3%
visibility	**clear**	21	68%
	moderate	6	19%
	poor	4	13%
echogenicity	**hypoechogenic**	29	94%
	isoechogenic	2	6%
border	**distinct**	12	39%
	indistinct	19	61%
margin	**sharp**	7	23%
	irregular	24	77%

IQR: inter quartile range

Tertiary outcome: comparison of the preoperative imaging, IOUS and PA assessments about vascular involvement

Next, the results of the IOUS and final PA assessment for the 27 resected malignancies with respect to any vascular involvement were compared. Specifically, the tumor contact with the SMV or SMA resection margins as assessed by microscopic examination was compared with both the preoperative imaging and the IOUS assessment; these results are summarized in Table 4. In four patients, the vascular contact could not be assessed on preoperative imaging, in one of these patients the vascular contact could also not be assessed with IOUS.

Table 3. Influence of IOUS on surgical strategy.

No Influence	**12**	**39%**
Tumor localisation	**8**	**26%**
Identification of lesions with IOUS, compared to preoperative diagnostics	4	
One malignant lesion was retrieved with IOUS, instead of multiple lesions	*2*	
An additional or larger lesion was retrieved, leading to total pancreatectomy	*2*	
Determination resection margin	4	
Based on location of tumor a duodenal, PPPD or tail resection was performed	*2*	
After neoadjuvant therapy, and preoperative scan was suboptimal judgeable	*2*	
Vascular involvement	**9**	**29%**
Vascular contact during IOUS was more extensive than on preoperative scan, leading to vascular reconstruction	4	
Vascular contact on preoperative scan was suboptimal, but visible with IOUS	4	
Vascular contact on preoperative scan was not present during IOUS	1	
Waivement of resection	**2**	**6%**
Due to extensive vascular contact during IOUS, not present on preoperative scan and histopathologically confirmed by a frozen section	2	

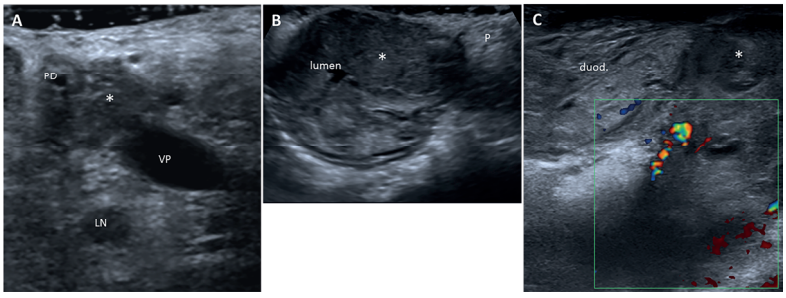

Figure 1. IOUS images corresponding to influences on surgical strategy.
Panel A) vascular involvement: vena porta (VP) >120^0 contact with tumor (*), therefore, resection with VP patch. *LN: lymph node, PD: ductus pancreaticus.*
Panel B) tumor localization: tumor (*) in anterior duodenal wall, caudal from papilla. The duodenal border is intact, only minimal edema in pancreatic fat (P), therefore, only a duodenum resection was performed. *Lumen: lumen of duodenum.*
Panel C) waivement of resection: ingrowth of conglomerate of the tumor (*) in branches of superior mesenteric artery, which was not identified on preoperative imaging.

Table 4. Vascular contact as assessed during pathological examination compared to preoperative imaging and IOUS assessment.

		preoperative Imaging		
		no contact	**vascular contact**	**contact not judgeable**
PA	**no contact**	14	1	2
	vascular contact	2	5	2

		IOUS		
		no contact	**vascular contact**	**contact not judgeable**
PA	**no contact**	16	0	1
	vascular contact	1	8	0

In one patient, pathological evaluation revealed contact of both the SMA margin and the SMV margin, but during the preoperative imaging and IOUS assessment only contact with the SMV was established. Therefore, this patient is not included in the table.

The analysis revealed that contact (or lack of contact) between the tumor and the vascular groove (including SMA and SMV resection margins) was correctly assessed using preoperative imaging in 20 of the 27 procedures (74%) and IOUS assessment was correct in 24 of the 27 procedures (89%), which did not significantly differed from each other (p-value: 0.21). Moreover, contact (or lack of contact) between the tumor and solely the SMV (including PV and confluens) was assessed correctly using preoperative imaging in 21 of the 27 procedures (78%), and IOUS assessment was correct in 25 out of 27 tumors (93%), this also did not significantly differed from each other (p-value: 0.06). All of the tumors that had no vascular contact were radically resected (R0).

Neoadjuvant chemotherapy

Finally, the four patients that received neoadjuvant chemotherapy were evaluated on an individual basis. In one patient, no vascular contact or vascular involvement was visible using either preoperative imaging or IOUS. Unfortunately, as tumor involvement was found at the gastroduodenal artery resection margin; this resection margin was not assessed using IOUS, and during microscopic examination only a small cluster of tumor cells was identified. In the second patient, neither vascular contact nor vascular involvement could be determined using preoperative imaging; in contrast, IOUS revealed contact between the tumor and the PV. It remained however unclear whether this was tumor tissue or fibrotic tissue. Eventually, the tumor was peeled away from the PV and was radically resected; therefore, the tissue was likely fibrotic tissue. In the third patient, no vascular contact or vascular involvement was visible using preoperative imaging; IOUS showed a mass with characteristics suggestive of

a complete response (Figure 2). Since the tumor responded completely to the neoadjuvant chemotherapy the fibrotic mass is hard to distinguish on Figure 2. The complete response was confirmed by microscopic examination. Lastly, in the fourth patient, vascular contact between the tumor and the SMV and/or PV could not be determined reliably based on preoperative imaging. In this case, IOUS revealed that the distance between the tumor and the SMV/PV was 16 mm; thus, the tumor could be removed radically without vascular resection as was confirmed with PA.

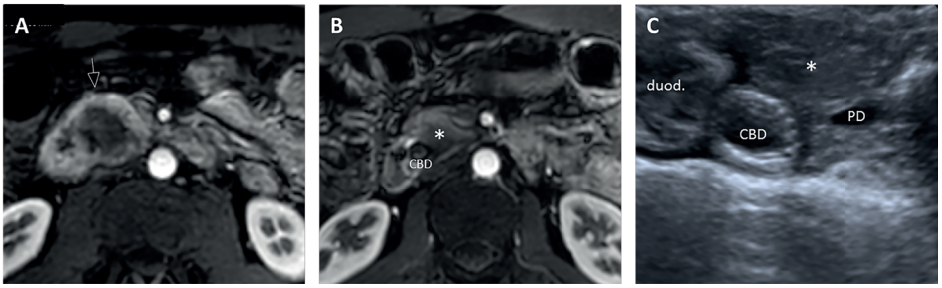

Figure 2. Example of preoperative MRI images and IOUS images of complete response on Folfirinox.

Panel A) scan: dynamic (post-contrast) MRI scan showing a borderline resectable tumor. *Arrow: ductal pancreatic adenocarcinoma, definable mass.*

Panel B) scan: dynamic (post-contrast) MRI scan showing the remnant of the tumor (*), no visible mass and without contrast signal, only fibrotic irregular tissue. A stent is present in the ductus choledochus (CBD).

Panel C) ultrasound: a hypoechoic irregular area (*) in the neck of the pancreas without a definable mass. A stent is present in the ductus choledochus (CBD). *PD: ductus pancreaticus, duod.: duodenum.*

DISCUSSION

In our prospective cohort study of 31 surgical explorations, IOUS was of significant clinical value in 61% of the procedures by providing additional information at an early stage during the exploration. The vascular contact (or lack of contact) was correctly assessed with IOUS in 89% of the procedures; a 15% increase compared to the preoperative imaging. Although this increase is not significantly, IOUS shows a trend towards better evaluation of vascular involvement. Due to the direct feedback of the radiologist to the surgeons during the procedures, surgeons were generally prepared earlier in the surgery with respect to what they could expect. Not only the extensiveness of the resection could be altered due to the IOUS assessment, also vascular reconstruction could be advised and tumors treated with neoadjuvant therapy, as well as their responses, could be visualized with IOUS.

The use of IOUS during surgery for pancreatic cancer is not a new application, but IOUS is not routinely used during these procedures and has, surprisingly, scarcely been

studied in the last few years. Therefore, the added value of IOUS is not recorded. In an Ukrainian study, 76 patients were retrospectively included and the IOUS assessment changed the surgical strategy in 30%.(17) However, these changes were retrospectively determined, and consisted mainly in the identification of additional hepatic metastases. In contrast, all our procedures started with laparoscopic staging immediately prior to surgical exploration thereby potentially identifying occult superficial liver metastases. Thereafter, patients were included in our prospective study for evaluation of their primary tumor with IOUS. In our group, no occult metastases were found during the open exploration following laparoscopy.

IOUS can yield more information than the preoperative imaging scan by providing direct contact with the tissue and real-time imaging data. On the preoperative CT scan, the majority of tumors (63%) in our cohort appeared isodense, preventing direct visibility of the tumor using this imaging modality. In contrast, all tumors could be visualized with IOUS, and only 13% was suboptimal visualized. In addition, the rate of discordance between preoperative imaging and microscopic examination was higher than between IOUS and microscopic examination with respect to vascular involvement. Interestingly, De Werra *et al.* reported an even higher discordance rate between preoperative imaging and pathology reports compared to our cohort (64% versus 44%, respectively).(13)

In our patient cohort, the rate of R1 (non-radical) resection was 22%, which is lower than the global reported rate of approximately 60%.(8) The resulting increase in the rate of R0 (radical) resection may have been the result of IOUS, thereby increasing the surgeon's ability to directly visualize vascular involvement and/or ingrowth during surgical exploration. One factor that may explain the discordance rate between IOUS and the microscopy findings in our study is that IOUS failed to reveal the positive resection margins of the gastroduodenal artery and the common bile duct in two patients, because these margins were not assessed with IOUS and besides that, only a cluster of a few tumor cells was present. The two non-radically resected SMV segments can be explained due to tumor growth through the SMV wall, whilst the segment borders were tumor negative. In addition, the remaining two non-radically resected tumors may be explained by the tumor grade and the way the tumor grew in small nests and individual cells. The limitation of IOUS is the incapability of visualization of small clusters of tumor cells or individual cells.

Another aspect in which IOUS can have added value is assessing pancreatic cancer in patients who receive neoadjuvant chemotherapy and patients who have extensive pancreatitis. In these patients, preoperative imaging cannot necessarily be used to reliably determine the extent of the tumor and/or vascular involvement. Even with IOUS it can be sometimes difficult to discriminate between chemotherapy-induced fibrosis and vital tumor tissue, although vascular involvement and the extent of the tumor can be determined better with IOUS than with a preoperative scan as is suggested by our results. Despite that only four patients in our cohort were treated with neoadjuvant chemotherapy, IOUS was in 50% of additional value and could visualize the tumor whereas preoperative imaging was shortcoming. With

the upcoming neoadjuvant treatment administration in this patient population it is of great importance to further investigate the added value of IOUS for these patient; therefore, larger studies are needed in order to determine whether IOUS can provide a superior assessment in these patients.

A requirement for maximizing the benefits of IOUS is to have a trained and experienced specialist to perform and interpret the IOUS during surgery, which has the added advantage of allowing close collaboration between the radiologist and the surgical team, providing real-time information regarding the tumor's characteristics, which can immediately be compared with the preoperative imaging findings. This specialized radiologist performs the preoperative assessment of the scan and also assesses the tumor intraoperatively with ultrasound. This is of importance because the radiologist is than better prepared for what to encounter during surgery. Furthermore, the radiologist is able to detect differences between the imaging modalities and compare the preoperative findings with the intraoperative findings. This contributes to optimizing the peri-operative imaging process and feedback to the MDT. In our study, the postoperative microscopic findings were evaluated by the pathologist in collaboration with the involved radiologists and surgeons, with the goal of improving both the preoperative and intraoperative staging and assessment of the tumor.

Although this describing study consists of relatively low patient numbers, strong trends towards benefit of IOUS was observed. IOUS was helpful in terms of determining the resection margins, assessing vascular involvement, identifying additional lesions, and determining whether surgery should be waived. Contrast-enhanced ultrasound could improve IOUS-guided pancreatic or periampullary cancer resection even further as it has already demonstrated its use in the detection of pancreatic liver metastases.(20)

Based on our results, we would advise IOUS for specific patients for the highest possible yield of additional findings. For example, IOUS may be of value in patients who received neoadjuvant chemotherapy or for patients in which vascular involvement is (dubious) present on a preoperative scan.

In summary, we report that IOUS plays an important role at our medical center in assessing the resectability, the extent of the tumors and the vascular involvement with the goal of achieving radical resections. This is based on experience and the positive results of this describing study. In the near future IOUS will probably also be of greater importance for the evaluation of neoadjuvantly treated tumors. At our hospital, a specialized radiologist now performs IOUS routinely in all patients who undergo surgery with the intention to achieve radical resections, thereby providing direct feedback to the surgeon.

REFERENCES

1. Kim KS, Kwon J, Kim K, Chie EK. Impact of Resection Margin Distance on Survival of Pancreatic Cancer: a Systematic Review and Meta-Analysis. Cancer Res Treat. 2016.
2. Ichikawa T, Erturk SM, Sou H, Nakajima H, Tsukamoto T, Motosugi U, et al. MDCT of pancreatic adenocarcinoma: optimal imaging phases and multiplanar reformatted imaging. AJR Am J Roentgenol. 2006;187(6):1513-20.
3. Feldman MK, Gandhi NS. Imaging Evaluation of Pancreatic Cancer. Surg Clin North Am. 2016;96(6):1235-56.
4. Liao M, Zhong X, Zhang J, Liu Y, Zhu Z, Wu H, et al. Radiofrequency ablation using a 10-mm target margin for small hepatocellular carcinoma in patients with liver cirrhosis: A prospective randomized trial. J Surg Oncol. 2017;115(8):971-9.
5. Donahue TR, Isacoff WH, Hines OJ, Tomlinson JS, Farrell JJ, Bhat YM, et al. Downstaging chemotherapy and alteration in the classic computed tomography/magnetic resonance imaging signs of vascular involvement in patients with pancreaticobiliary malignant tumors: influence on patient selection for surgery. Arch Surg. 2011;146(7):836-43.
6. Katz MH, Fleming JB, Bhosale P, Varadhachary G, Lee JE, Wolff R, et al. Response of borderline resectable pancreatic cancer to neoadjuvant therapy is not reflected by radiographic indicators. Cancer. 2012;118(23):5749-56.
7. Campbell F, Smith RA, Whelan P, Sutton R, Raraty M, Neoptolemos JP, et al. Classification of R1 resections for pancreatic cancer: the prognostic relevance of tumor involvement within 1 mm of a resection margin. Histopathology. 2009;55(3):277-83.
8. Neoptolemos JP, Palmer DH, Ghaneh P, Psarelli EE, Valle JW, Halloran CM, et al. Comparison of adjuvant gemcitabine and capecitabine with gemcitabine monotherapy in patients with resected pancreatic cancer (ESPAC-4): a multicentre, open-label, randomised, phase 3 trial. Lancet. 2017;389(10073):1011-24.
9. Ghaneh P, Kleeff J, Halloran CM, Raraty M, Jackson R, Melling J, et al. The Impact of Positive Resection Margins on Survival and Recurrence Following Resection and Adjuvant Chemotherapy for Pancreatic Ductal Adenocarcinoma. Ann Surg. 2017.
10. Giovinazzo F, Turri G, Katz MH, Heaton N, Ahmed I. Meta-analysis of benefits of portal-superior mesenteric vein resection in pancreatic resection for ductal adenocarcinoma. Br J Surg. 2016;103(3):179-91.
11. Iqbal S, Friedel D, Gupta M, Ogden L, Stavropoulos SN. Endoscopic-ultrasound-guided fine-needle aspiration and the role of the cytopathologist in solid pancreatic lesion diagnosis. Patholog Res Int. 2012;2012:317167.
12. Allen VB, Gurusamy KS, Takwoingi Y, Kalia A, Davidson BR. Diagnostic accuracy of laparoscopy following computed tomography (CT) scanning for assessing the resectability with curative intent in pancreatic and periampullary cancer. Cochrane Database Syst Rev. 2016;7:CD009323.
13. de Werra C, Quarto G, Aloia S, Perrotta S, Del Giudice R, Di Filippo G, et al. The use of intraoperative ultrasound for diagnosis and stadiation in pancreatic head neoformations. Int J Surg. 2015;21 Suppl 1:S55-8.
14. D'Onofrio M, Vecchiato F, Faccioli N, Falconi M, Pozzi Mucelli R. Ultrasonography of the pancreas. 7. Intraoperative imaging. Abdom Imaging. 2007;32(2):200-6.

15. Sun MR, Brennan DD, Kruskal JB, Kane RA. Intraoperative ultrasonography of the pancreas. Radiographics. 2010;30(7):1935-53.
16. Tamm EP, Bhosale PR, Vikram R, de Almeida Marcal LP, Balachandran A. Imaging of pancreatic ductal adenocarcinoma: State of the art. World J Radiol. 2013;5(3):98-105.
17. Kolesnik O, Lukashenko A, Shudrak A, Golovko T, Lavryk G, Huralevych J. Intraoperative ultrasonography in pancreatic surgery: staging and resection guidance. Exp Oncol. 2015;37(4):285-91.
18. DPCG. DPCG-definities resectabiliteit pancreascarcinoom (PREOPANC trial, DPCG 2012) 2012 [Available from: http://dpcg.nl/images/Criteria_resectabiliteit.pdf.
19. Verbeke CS, Leitch D, Menon KV, McMahon MJ, Guillou PJ, Anthoney A. Redefining the R1 resection in pancreatic cancer. Br J Surg. 2006;93(10):1232-7.
20. Taimr P, Jongerius VL, Pek CJ, Krak NC, Hansen BE, Janssen HL, et al. Liver Contrast-Enhanced Ultrasound Improves Detection of Liver Metastases in Patients with Pancreatic or Periampullary Cancer. Ultrasound Med Biol. 2015;41(12):3063-9.

11

Quantitative margin assessment of radiofrequency ablation of a solitary colorectal hepatic metastasis using Mirada RTx: A feasibility study

B.G. Sibinga Mulder, P. Hendriks, T.R. Baetens, A. van Erkel,
C.J.H. van de Velde, A.L. Vahrmeijer, J.S.D. Mieog, M.C. Burgmans

BMC Medical Imaging, 2019 Sep. Supplementary data available online.

ABSTRACT

Compared to surgery, radiofrequency ablation (RFA) for colorectal liver metastasis(CRLM) is associated with higher local recurrence (LR) rates. A wide margin (at least 5mm) is generally recommended to prevent LR, but the optimal method to assess ablation margins is yet to be established. The aim of our study was to evaluate the feasibility and reproducibility of CT-CT scan co-registration, using Mirada RTx software, in order to assess ablation margins of patients with CRLM.

In this retrospective study, pre- and post-ablation contrast-enhanced CT scans of 29 patients, treated with percutaneous RFA for a solitary CRLM, were co-registered. Co-registration was performed by two independent radiologist, based on venous structures in proximity to the tumor. Feasibility of CT-CT scan co-registration and inter-observer agreement for reproducibility and ablation margins was determined. Furthermore, the minimal ablation margin was compared with the occurrence of LR during follow-up.

Co-registration was considered feasible in 18 patients (61% male, 63.1(±10.9) year), with a perfect inter-observer agreement for completeness of ablation: $\varkappa = 1.0$ ($p<0.001$). And substantial inter-observer agreement for measurement of the minimal margin (≤ 0mm, 1-5mm, ≥ 5 mm): $\varkappa = 0.723$(p-value < 0.001). LR occurred in eight of nine (88.9%) incompletely ablated CRLM and in one of the nine completely ablated CRLM (11.1%).

Co-registration using Mirada RTx software is reproducible and potentially a valuable tool in defining technical success. Feasibility of co-registration of pre- and post-ablation CT scans is suboptimal if scans are not acquired concordantly. Co-registration may potentially aid in the prediction of LR after percutaneous ablation.

INTRODUCTION

Radiofrequency ablation is an established minimally invasive treatment for patients with unresectable liver metastases from colorectal cancer.(1) Compared to surgery, RFA is associated with higher rates of local recurrence (LR).(2, 3) Histological confirmation of treatment success is not possible, therefore, technical success of ablation is generally defined as having successfully delivered a certain amount of energy that is considered to create an ablation zone with sufficient margins.(4) In clinical practice, CT scans most commonly used for margin evaluation based on visual qualitative assessment without quantitative determination of the ablation margin. Generally, a margin of at least 5 mm is advised.(5) This seems intuitively correct, but there is only limited evidence to support this assumption and no standardized and validated method to assess ablation margins.(6, 7)

Co-registration of pre- and post-ablation cross-sectional images allows three-dimensional quantitative assessment of ablation margins. Several studies investigating different techniques for quantitative assessment of RFA procedures for hepatocellular carcinoma (HCC) using CT-CT scan co-registration have been performed and are found to be superior to qualitative visual assessment in determining ablation margins and predicting local tumor recurrence.(7-9) Although, different results are obtained between experienced readers and less experienced readers. Quantitative assessment offers a more objective and reproducible method to evaluate technical success of ablation.(8)

Co-registration of pre- and post-ablation CT scans is challenging, as shape and position of the liver may differ between the two scans as a result of differences in patient positioning, breathing related liver motion and liver deformation due to the ablation or previous surgery.(10) Most common co-registration algorithms are rigid, and/or need manual manipulation. By using a semi-automatic, non-rigid registration algorithm, an automatic correction for difference in liver position and morphology can be applied.

In this retrospective study, we evaluated feasibility and reproducibility of quantitative ablation margin assessment of patients with a solitary CRLM, using the described CT-CT scan co-registration software from Mirada RTx. Furthermore, we correlated the minimal ablation margins to local tumor recurrence.

METHODS

The study was designed as a retrospective cohort study to investigate the feasibility and reproducibility of co-registration of pre- and post-ablation CT scans of patients with a solitary CLRM. Two independent readers assessed the co-registration and a scoring model was used to determine feasibility and reproducibility. Furthermore, the minimal margins obtained after ablation were measured and correlated to local recurrence.

Medical Ethical Approval

For this study medical ethical approval was obtained. All patient gave informed consent to undergo RFA. Informed consent was waived for the conduct of the study. Patient confidentiality was guaranteed using anonymized data and radiologic images, and all data was entered into an encrypted and secured database.

Patients

Between January 2009 and March 2014, 313 patients underwent a first thermal ablation procedure of the liver in our institution (re-ablations were not included). Of the 313 patients, 284 patients were excluded from the analyses for the following reasons: hepatocellular carcinoma (n=112), liver metastases other than CRLM (n=25), a pre-ablation MRI scan (n=100), microwave ablation (n=8), ablation during open surgery (n=19), multifocality (n=13), technical failure (n=3) or a missing post-ablation CT (n=4). Co-registration of liver images of two scans is often challenging due to alterations in liver shape and position: accurate co-registration of a liver area often results in a mismatch in other areas. In order not to increase the complexity of co-registration, patients with more than one lesion were not included in this feasibility study. Finally, we included 29 patients who underwent percutaneous radiofrequency ablation (RFA) of a solitary CRLM. Patient and lesion characteristics are shown in Supplementary Table S1. Pre- and post-ablation contrast-enhanced CT scan, including at least an portal-venous phase, was available in all patients with the baseline CT scan being performed within two months prior to the procedure.

RFA procedure

Three interventional radiologists specialized in RFA of the liver performed the RFA procedures and had at start of the inclusion period an experience of at least two years. Percutaneous RFA was performed under general anesthesia under ultrasound guidance and in case of suboptimal ultrasonic guidance the procedure was performed with CT guidance. A single electrode was used (3 cm exposed tip Cooltip (Covidien, Gosport Hamspire, United Kingdom) or StarBurst XL (AngioDynamics, Amsterdam, Netherlands)) or multiple electrodes with a switch-control system (3 or 4 cm exposed tip Cooltip). Ablation was performed for 12 (single Cooltip electrode) or 16 minutes (multiple Cooltip electrodes) using standard impedance controlled ablation. Temperature-based ablation was performed with the StarBurst XL electrode.

Contrast-enhanced CT was performed immediately after ablation on a 16-slice spiral CT (Aquillion-16, Toshiba, Tokyo, Japan) using the following scanning parameters: 16x1 mm scanning, 120 KV, rotation 0.5 s, contrast Ultravist 370 (dose weight depended) with a delay of 75 s for portal venous phase. In the supplementary Table S2 the scanning protocol is included.

All RFA procedures were deemed to be technically successful at the time of the procedure if 1) a predefined amount of energy (based on information provided by vendors on the ablation size at different settings) was successfully delivered to the tumor and 2) the coagulation area was thought to fully encompass the tumor based on visual qualitative assessment and 3) residual tumor enhancement on immediate post-ablation CT was absent. Visual assessment was performed by eye-balling and two-dimensional measurements. Pre- and post-ablation CT scans were projected side-by-side on the computer screen. By scrolling up and down both scans the interventional radiologist assessed whether the ablation area was correctly located and was thought to fully encompass the tumor with a margin of at least 5mm. Also, the post-ablation scan was assessed to rule out residual tumor enhancement. In addition to this, the distance was measured of the tumor and ablation zone to anatomical landmarks such as the liver edges and veins in order to confirm that the ablation zone was in a correct position and ablation margins were considered to be sufficient.

Mirada RTx Software

Mirada RTx is a software application developed for radiation therapy treatment planning. The software is integrated into Vitrea Advanced Visualisation (Vital Images, Minnetonka, U.S.A) and designed for rigid and deformable registration of medical image datasets including PET, CT, MR, and SPECT scans. In our study, we used Mirada RTx to perform CT-CT scan co-registration with a semi-automated deformable registration algorithm with manual alteration when necessary. These manual alterations were either done by rotation and translation of a scan, or with use of a landmark algorithm that interpolates a deformable transformation by manually selecting corresponding anatomical landmarks in both scans. Delineation of the tumor volume and ablation area was done using a greyscale-based semi-automatic delineation tool with manual adjustments for accurate segmentation. In a fused-imaging view, RFA margins were quantitatively assessed by expanding the tumor's contour until line intersection with the delineated ablation area. In case the tumor was not located completely within the ablation area, negative margin size was determined in the same way by expanding the ablation area delineation. Besides the narrowest margin in millimeters (mm), the anatomical location of the narrowest margin was determined as well. In case the tumor exceeded the tumor ablation area, the anatomical location of the highest tumor excess was recorded.

Scoring

Two interventional radiologists of the LUMC staff, experienced in RFA of liver lesions, who were blinded to follow-up data, independently performed co-registration of the pre- and postablation CT scans. Pre- and post-ablation portal venous phase CT scans were loaded into Mirada RTx. First, manual co-registration of the pre- and post-ablation CE-CT scans (venous phase) was based on venous structures and other liver landmarks in proximity to

the tumor, such as cysts or calcifications. Landmarks were placed on bi- or trifurcation of the portal vein to co-register the pre- and post-ablation CT scan. At the start of the co-registration process landmarks were placed centrally. Then, peripheral landmarks were chosen that were located closer to the tumor. After co-registration was performed a grading system from 1-5 was used to assess the reliability of co-registration: 1 = co-registration completely unreliable due to large differences in liver shape and position between pre- and post-ablation CT, 2 = suboptimal co-registration, 3 = sufficient co-registration, but not accurate for measurement in mm, 4 = good co-registration or 5 = perfect co-registration. If the quality of co-registration in a patient was graded 4 or 5 by both radiologists, tumor and ablation volumes were delineated on both scans using automatic contour detection. In case the observers graded co-registration of the patient different, a consensus reading was applied.

Secondly, the automatic contour detection was evaluated by the radiologist and manually altered in case contour detection was not considered to be inaccurate. Both delineations (tumor and ablation zone) were projected in one scan, resulting in an overlay of pre- and post-ablation CT scans. This overlay allowed assessment of ablation margins. The side of the minimal margin was noted, and the margin was measured in millimeters by both observers. In case of incomplete ablation, the extension of the tumor beyond the ablation zone was recorded in millimeters (negative margin). Inter-observer agreement was calculated for two different outcomes: 1) total encompassment of the tumor by the ablation zone; meaning that the tumor was inside the ablation zone, or without total encompassment of the tumor; meaning that the ablation zone did not cover the tumor completely, and 2) negative or no margin (≤0 mm), a minimal margin of 1-5 mm or a minimal margin of ≥ 5 mm. In case the observers measured different margins for the same patient, resulting in a difference in category grouping, a consensus reading was applied.

Local recurrence

Follow-up was performed according to standard local protocol, including a visit every three months to the surgical outpatient clinic, carcinoembryonic antigen (CEA) determination, and a CE-CT scan of the chest and abdomen. The follow-up scans were evaluated by an independent radiologist unaware of the ablation margin that was obtained during the ablation. In case of reported recurrence, the side of insufficient or minimal margin was compared with the localization of LR during follow-up. Patient and lesion characteristics of the patients without LR were compared with the patients with LR. The average of the minimal obtained margin determined by both observers was compared to development of LR.

Statistics

The level of agreement in margins between the two observers was estimated using unweighted Kappa $\varkappa$ statistics. The agreement was interpreted as poor (0), slight (≤ 0 to 0.20), fair (0.21 to 0.40), moderate (0.41 to 0.60), substantial (0.61 to 0.80), almost perfect (≥ 0.80 to 0.99)

and perfect (1.00).(11) For continuous data, groups were compared using the independent *t*-test; categorical data were compared using the chi-square test. Data were analyzed using SPSS version 23.0. The statistical results were considered to indicate significance if the *p*-value was less than 0.05.

RESULTS

All tumor ablations (n=29) (median size 21mm (range 8-42mm)) were considered to be technically successful at the time of the procedure, as judged qualitatively by the radiologist performing the procedure. Twenty tumors were ablated ultrasound guided, in nine patients the tumors could not be visualized with ultrasound, their ablation was performed CT guided.

Scoring

The co-registration of pre- and post-ablation CT scans was good (4) or perfect (5) in 18 (62%) patients. These patients were included in further analyses and for correlation with local recurrence. Patient and lesion characteristics of the patients are presented in Table 1. No significant differences in patient and lesion characteristics were observed between the patients who developed LR and who did not develop LR (Table 1).

The cause for suboptimal co-registration (grade 1, 2 or 3) was the difference in liver position during the pre- and post-ablation scan. This could be due to a difference in position of the patient (diagnostics scans were acquired with the patient in a supine position, whereas some RFA procedures were performed with the patient in a left lateral position to allow a lateral intercostal approach) or because the scans were obtained during a different breathing phase (in- or expiration). In two of the excluded patients there were artefacts in the post-ablation scans, therefore co-registration was not possible (grade 1).

Eventually, 10 patients were graded 4 and 8 patients were graded 5. In 8 patients consensus reading was performed.

Based on quantitative analysis using CT-CT scan fusion imaging, coverage of the tumor by the coagulation area was found to be incomplete in tumors of 9 patients (50%). In the other 9 patients complete ablation was achieved with a mean ablation margin of 2.2 ± 1.9 mm.

The inter observer agreement was perfect for completeness of the ablations of the 18 CRLM patients: $\varkappa = 1.0$ (p-value < 0.001). Agreement for measurement of the minimal margin (mm), divided in three groups (≤ 0mm, 1-5mm, ≥ 5 mm), was substantial: $\varkappa = 0.723$ (p-value < 0.001). Eventually, 13 patients were in the ≤ 0mm group, six in the 1-5mm group, and two in the ≥ 5 mm group. In three a consensus reading was performed.

Table 1. Patient characteristics

		total		no LR		LR		
		n		*n*		*n*		*p-value*
total		**18**		9		9		
age	mean (SD)	**63.1**	**±10.9**	61.8	±7.6	64.3	±13.8	*0.64*
sex	male	**11**	**61%**	6	67%	5	56%	*0.63*
	female	**7**	**39%**	3	33%	4	44%	
previous CRLM surgery	yes	**9**	**50%**	5	56%	4	44%	*0.64*
	no	**9**	**50%**	4	44%	5	56%	
occurrence of CRLM	metachronous	**7**	**39%**	3	33%	4	44%	*0.63*
	synchronous	**11**	**61%**	6	67%	5	56%	
days preoperative CT scan - RFA procedure	mean (SD)	**32.2**	**±17.2**	27.9	±15.8	36.4	±18.4	*0.31*
year of RFA	2009-2011	**7**	**39%**	4	44%	3	33%	*0.63*
	2012-2014	**11**	**61%**	5	56%	6	67%	
lesion size (mm)	median (range)	**22**	**8-42**	22	8-31	25	11-42	*0.17*
categorized lesion size	<21 mm	**8**	**44%**	4	44%	4	44%	*1.00*
	>20 mm	**10**	**56%**	5	56%	5	56%	
liver half / segment **left**	segment 2	**1**	**6%**			1	11%	*0.14*
	segment 3	**1**	**6%**	1	11%			
	segment 4	**5**	**27%**	1	11%	4	45%	
right	segment 5	**2**	**11%**	1	11%	1	11%	
	segment 6	**1**	**6%**			1	11%	
	segment 7	**4**	**22%**	3	33%	1	11%	
	segment 8	**4**	**22%**	3	33%	1	11%	
follow-up (months)	mean (SD)	**44.7**	**±20.5**	52.3	±14.8	37.3	±23.5	*0.13*
survival	death	**5**	**28%**	1	11%	4	44%	*0.11*

LR: local recurrence, CRLM: colorectal liver metastasis; RFA: radiofrequency ablation

Local recurrence rate

A schematic overview of the technique and the real-life implementation, including an example of a patient with LR four months after ablation is given in Figure 1. In Figure 2 an overview is demonstrated of the delineation of a tumor and ablation zone after co-registration was performed.

Patients with incomplete tumor ablation based on quantitative assessment were at a significantly higher risk of LR: 88.9% compared to 11.1% patients in whom complete ablation was successfully achieved (p-value = 0.003). LR occurred after a median of 7 months (range 3 – 9).

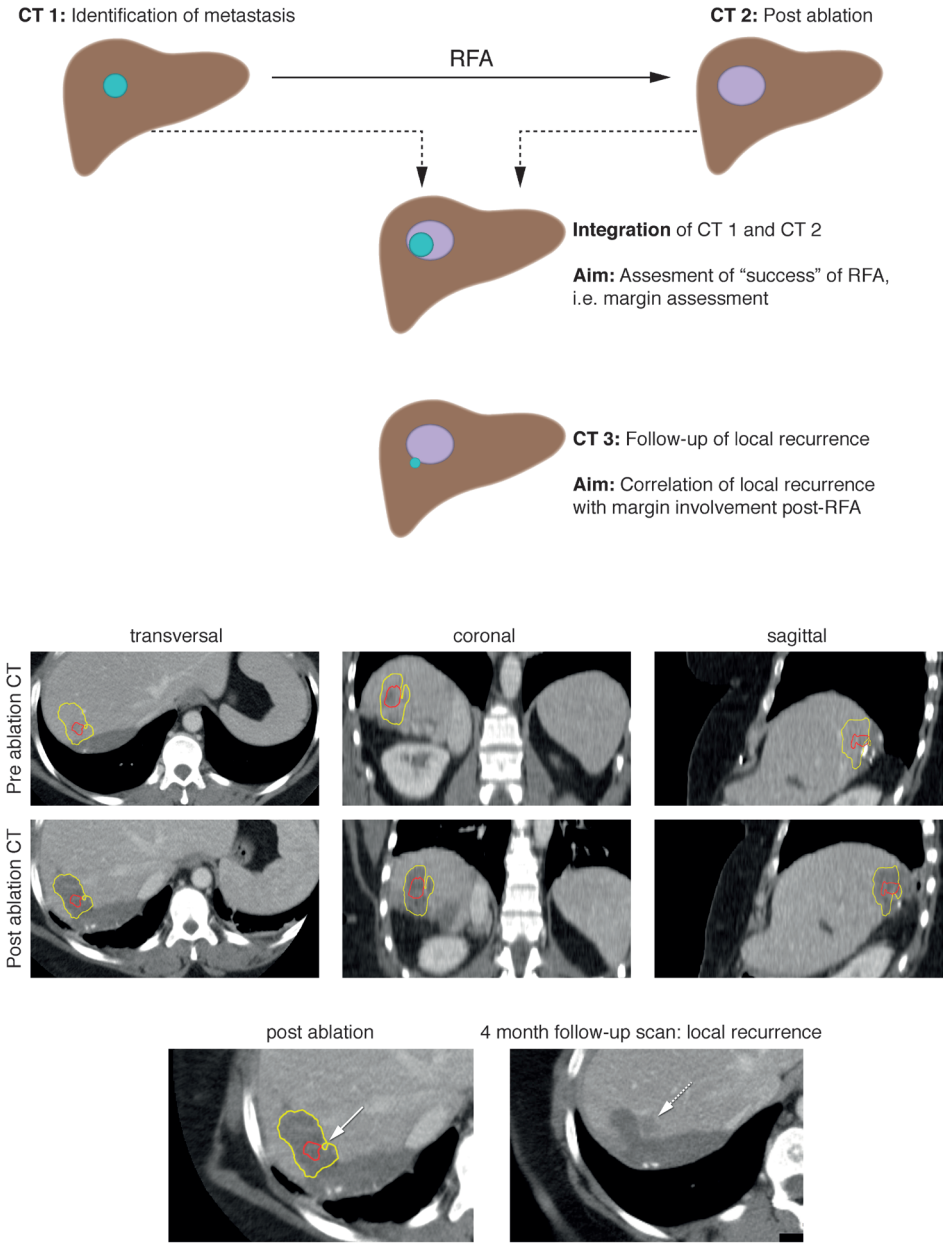

Figure 1. Schematic overview and real-life implementation of the used technique for assessment of successful ablation.

Panel above: schematic overview of technique.

Panel below: example of a patient who developed local recurrence (dashed arrow) of her colorectal liver metastasis four months after ablation, precisely on the spot of the minimal obtained margin (arrow). The patient has undergone previous liver surgery, the clips are used as landmark.

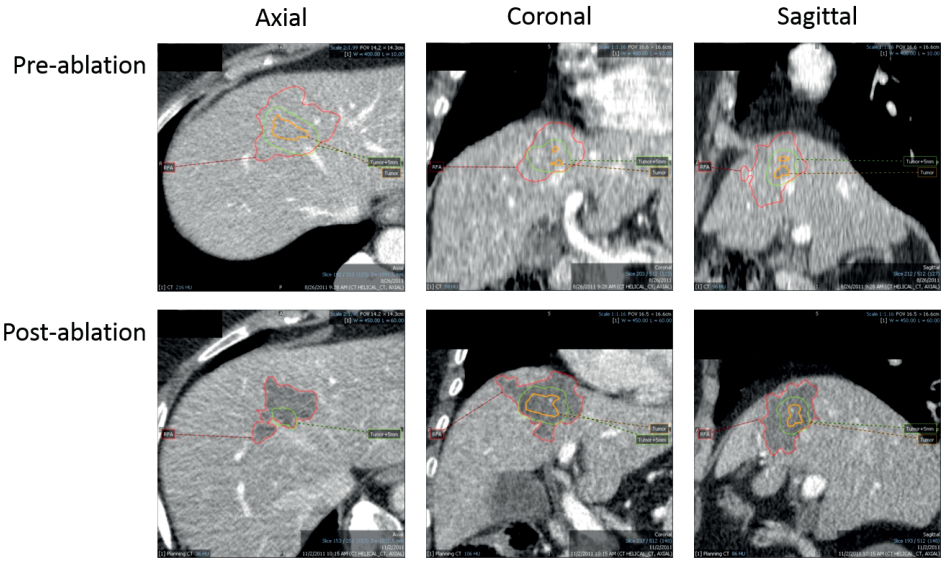

Figure 2. Overview in all dimensions after co-registration and delineation of the tumor and ablated zones.
Orange delineation: tumor; green delineation: tumor + 5mm; red delineation: ablation zone.

The correlation between the minimal obtained margin and the presence of LR was also determined: the average obtained margin of patients without LR was 2.1 mm compared to an average obtained margin of -2.6 mm for patients with LR (p-value < 0.001). The minimal obtained margins (average of the measured margins by the observers) correlated to the presence of LR is demonstrated in Figure 3.

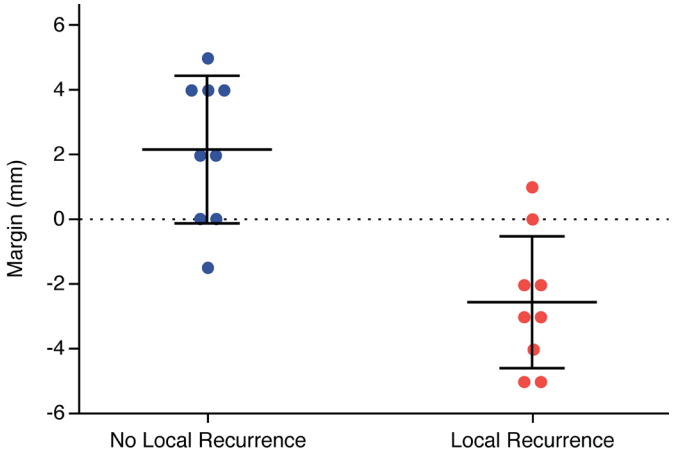

Figure 3. The obtained average minimal margin (in mm) correlated to the presence of local recurrence.

DISCUSSION

In our study the obtained percutaneous RFA margins in patients with a solitary CRLM were analyzed using CT-CT scan co-registration software with Mirada RTx. The main objective of this study was to evaluate the feasibility and reproducibility of this technique. From the 29 patients that were included, sufficient co-registration was only possible in 18 patients (62%). The reason for suboptimal co-registration in the remaining 11 patients is due to difference in liver position and/or shape. This can be explained by the retrospective study design, in which patient positioning and breathing related liver motion were not taken into account during CT acquirement. Despite the limited feasibility, our results demonstrate that quantitative analyses of ablation margins with Mirada RTx software may be a valuable method to determine the end-point of ablation. In those patients in whom co-registration was feasible, the inter-observer agreement for completeness of the ablation of the patients whose scan were co-registered adequately, was perfect. In addition, a correlation was found between completeness of ablation and local recurrence. The good reproducibility of this technique and trend to the possibility of predicting local recurrence is an important finding for future prospective studies.

Overall, this quantitative method of margin measurement was accurate for patients who had scans with concordant liver positions. Against our expectations, half of the evaluated patients were unsuccessfully ablated when re-assessed using quantitative co-registration software. By using CT-CT scan co-registration to determine technical success, we were able to identify a possible trend in the differentiation between patients with a very high risk (88.9%) of tumor recurrence and patients with low risk of recurrence (11.1%).

The superiority of quantitative assessment of minimal margins over qualitative visual assessment has also been demonstrated in patients with HCC. Kim *et al.* compared retrospectively qualitative visual assessment with quantitative, CT-CT scan fusion imaging, assessment in 103 patients undergoing RFA for 110 HCC lesions.(7) All 110 tumors were ablated with the intention to achieve a margin of >5 mm. Yet, quantitative assessment using CT-CT scan fusion showed an ablation margin of >5 mm in only 2.7% of the tumors, whereas based on visual assessment the percentage of ablations with >5mm margins was deemed to be 34.5%. The inaccuracy of visual assessment has also been demonstrated in a study by Park *et al.*, in which qualitative assessment was compared with quantitative assessment in HCC patients by fusion of pre-ablation magnetic resonance imaging (MRI) scan and a post-ablation CT scan.(8) Quantitative assessments proved to be more accurately than qualitative assessment, especially when assessment was performed by radiologists with limited experience.

Against our expectations, in the patients in whom complete tumor ablation was achieved, the margin was below 5 mm (mean 2.2 ± 1.9 mm). These findings are in concordance with the previously mentioned study of Kim *et al.* They found that a margin of ≥ 2 mm was

sufficient to achieve LR of <10% in patients with hepatocellular carcinomas. Although we cannot draw conclusions from our results due to the small patient number, this remarkable finding is in concordance with the data about LR and overall survival for surgical R0 resections of CRLM, for which a margin of 1 mm is required.(12) Another explanation might be that we did not take possible tumor shrinkage into account during measurements of the ablation and tumor borders. Therefore, obtained margins may have been wider in reality than how they were assessed in this study on the direct post-procedural CE-CT scan.

In future studies, quantitative analysis may be used to determine the endpoint of ablation and instigate immediate re-ablation when insufficient margins are obtained (while the patient is still under general anesthesia or sedation). In prospective studies mismatches between co-registration between pre- and post-ablation scans can be minimized by performing both scans immediately before and after ablation to ensure minimal difference in liver position and morphology. Minimizing breathing influences can be limited by using high-frequency jet ventilation or apnea during scanning.(13) Another feature that might increase the reliability of the Mirada RTx could be automatic evaluation of the delineated tumor and ablation zone. Since complete tumor ablation was in this study assessed by checking the projection of both borders in all scans visually.

In conclusion, we showed that co-registration of pre- and post-ablation CT scans using Mirada RX is frequently not feasible as a result of differences in shape and position of the liver. Yet, in patients in whom accurate co-registration was feasible determination of technical success of ablation is reproducible and ablation margins correlated with LR. Future prospective studies should focus on optimized scanning protocols to increase feasibility of co-registration of pre- and post-ablation scans as quantitative assessment of ablation may prove to be a valuable tool in determining technical success and predicting LR.

REFERENCES

1. McKay A, Dixon E, Taylor M. Current role of radiofrequency ablation for the treatment of colorectal liver metastases. Br J Surg. 2006;93(10):1192-201.
2. Sofocleous CT, Petre EN, Gonen M, Brown KT, Solomon SB, Covey AM, et al. CT-guided radiofrequency ablation as a salvage treatment of colorectal cancer hepatic metastases developing after hepatectomy. J Vasc Interv Radiol. 2011;22(6):755-61.
3. Hamada A, Yamakado K, Nakatsuka A, Uraki J, Kashima M, Takaki H, et al. Radiofrequency ablation for colorectal liver metastases: prognostic factors in non-surgical candidates. Jpn J Radiol. 2012;30(7):567-74.
4. Lee JM, Han JK, Lee JY, Kim SH, Choi JY, Lee MW, et al. Hepatic radiofrequency ablation using multiple probes: ex vivo and in vivo comparative studies of monopolar versus multipolar modes. Korean J Radiol. 2006;7(2):106-17.
5. Wang X, Sofocleous CT, Erinjeri JP, Petre EN, Gonen M, Do KG, et al. Margin size is an independent predictor of local tumor progression after ablation of colon cancer liver metastases. Cardiovasc Intervent Radiol. 2013;36(1):166-75.
6. Yedururi S, Terpenning S, Gupta S, Fox P, Martin SS, Conrad C, et al. Radiofrequency Ablation of Hepatic Tumor: Subjective Assessment of the Perilesional Vascular Network on Contrast-Enhanced Computed Tomography Before and After Ablation Can Reliably Predict the Risk of Local Recurrence. J Comput Assist Tomogr. 2017;41(4):607-13.
7. Kim YS, Lee WJ, Rhim H, Lim HK, Choi D, Lee JY. The minimal ablative margin of radiofrequency ablation of hepatocellular carcinoma (> 2 and < 5 cm) needed to prevent local tumor progression: 3D quantitative assessment using CT image fusion. AJR Am J Roentgenol. 2010;195(3):758-65.
8. Park J, Lee JM, Lee DH, Joo I, Yoon JH, Park JY, et al. Value of Nonrigid Registration of Pre-Procedure MR with Post-Procedure CT After Radiofrequency Ablation for Hepatocellular Carcinoma. Cardiovasc Intervent Radiol. 2017;40(6):873-83.
9. Makino Y, Imai Y, Igura T, Kogita S, Sawai Y, Fukuda K, et al. Feasibility of Extracted-Overlay Fusion Imaging for Intraoperative Treatment Evaluation of Radiofrequency Ablation for Hepatocellular Carcinoma. Liver Cancer. 2016;5(4):269-79.
10. El-Gamal FEA, Elmogy M, Atwan A. Current trends in medical image registration and fusion. Egypt Inform J. 2016;17(1):99-124.
11. Roberts C. Modelling patterns of agreement for nominal scales. Stat Med. 2008;27(6):810-30.
12. Bhutiani N, Philips P, Martin RC, 2nd, Scoggins CR. Impact of surgical margin clearance for resection of secondary hepatic malignancies. J Surg Oncol. 2016;113(3):289-95.
13. Engstrand J, Toporek G, Harbut P, Jonas E, Nilsson H, Freedman J. Stereotactic CT-Guided Percutaneous Microwave Ablation of Liver Tumors With the Use of High-Frequency Jet Ventilation: An Accuracy and Procedural Safety Study. AJR Am J Roentgenol. 2017;208(1):193-200.

IV

Summary and future perspectives

12

Summary and future perspectives

This thesis is focused on two main cancerous diseases: pancreatic and colorectal cancer. The peri-operative process of these two diseases was critically evaluated and new techniques were suggested to supplement this process. The main goal of the presented studies was to improve selection of patients with resectable tumors, determine the most suitable treatment plan, detect metastatic disease and improve radical resection rates. In this final part all results will be summarized and the future perspectives of the described techniques will be discussed.

DIAGNOSTIC PROCESS

Molecular diagnostics

Part I describes the implementation and validation of targeted Next-Generation Sequencing (NGS) in the diagnostic process of patients with a suspect pancreatic lesion. The value of NGS in pancreatic cancer was for the first time observed in a patient with a suspect recurrence that turned out to be a second primary tumor. This changed the treatment strategy from palliation to resection. Due to this promising result the technique was validated on DNA in cytology samples obtained from 70 patients with a suspect pancreatic lesion. The treatment plan was adjusted in 10% of the patients, preventing hazardous surgery for patients with benign conditions or suggesting resection of malignancies that were otherwise deemed as pancreatitis. This validation cohort consisted of consecutive included patients; all presented at the multidisciplinary pancreatic cancer team meetings, regardless of the probability of diagnosis based on the standard diagnostics.

In the follow-up multicenter study, the value of NGS in patients with a suspect pancreatic lesion without a conclusive cytology sample or probability diagnosis was determined. The treatment plan was changed in approximately one third of the patients. Also, repeated diagnostic biopsies could be prevented. Due to this multicenter study, NGS is integrated in the diagnostic process standardly in multiple hospitals, and might be expanded further nationally.

In the future NGS will be of special importance for patients with suspect lesions who could be treated with neoadjuvant therapy. Not only for confirmation of a malignancy, but also for systemic therapy response assessment. Diagnostic techniques focussing on molecular level are being optimized, and based on blood samples tumor response can be measured. For instance, *KRAS* pathogenic variations can be measured in circulating cell-free DNA (cfDNA) in the blood. Based on correlation of *KRAS* incidence in blood samples prior to start of neoadjuvant therapy and after, response can be determined. Furthermore, after treatment with curative intend, recurrence can be detected by taking blood samples and determining the genomic alterations in cfDNA of blood samples.(1) This might even lead to detection of early stage cancer and cancer screening.(2) NGS could gain a more prominent

role by optimizing the gene panel for ductal adenocarcinoma, enabling to sequence ultra-deep in a very low amount of tumor DNA.

Molecular diagnostics in patients with colorectal liver metastases (CRLM) should be shortly mentioned. Several studies with large patient numbers have analysed growth patterns of CRLM for the determination of impact on prognosis or overall survival.(3) But, biological status of the tumor is of even greater importance in the diagnostic process, especially for treatment proposal. Mutational status, mainly *KRAS* and *BRAF*, and studies investigating micro-RNA's could eventually help the clinicians during the multidisciplinary team meetings to determine the best therapeutic approach, timing and type of chemotherapy and whether to perform a resection or not.(4-7) For example, *BRAF* mutations are associated with poor prognosis.(8) NGS is gaining a more prominent role in the treatment of colorectal cancer, since this relatively easy technique can distinguish different types of mutations and predict response to treatment and metastatic spread.(9-11) Biological profiles should be further analysed and investigated in future studies in order to improve prediction of prognosis and patient based treatment.

Preoperative imaging

This part discusses mainly the role of preoperative imaging in CRLM. As described in **chapter 5,** the influence of MRI scanning with Primovist contrast (P-MRI) has a direct effect on treatment strategy proposal in a clinical setting. P-MRI scans lead to better differentiation, resulting in prevention of unnecessary surgeries, improved preoperative planning and prevention of repeated interventions by early identification of small lesions. During surgery of patients with resectable CRLM, several intraoperative techniques aid in the detection and resection of CRLM.(12, 13)

Pre- and intraoperative imaging techniques partly overlap, making each other superfluous. Future studies should focus on bundling of these techniques, aiming for tumor identification and radical tumor removal resulting in prevention of reinterventions and improved overall survival. For example, P-MRI scans might not be of value in all patients since livers are intraoperatively also assessed with intraoperative ultrasound (IOUS) and/or near-infrared fluorescence (NIRF) imaging. Based on multivariate analysis of large patient cohorts predictive factors can be identified indicating who will benefit from additional P-MRI scanning, like multiple lesions or synchronous development. This results in prevention of costly and time-consuming scanning without much yield. Furthermore, P-MRI scanning and NIRF imaging with indocyanine green (ICG) have both proven to identify additional lesions. But, P-MRI scanning is insufficient for the detection of superficial lesions, whereas NIRF imaging can only assess the outer 1 cm layer of the liver, so these techniques supplement each other. Based on nationwide multicenter studies guidelines should be updated, and recommendations should be made about which imaging modality should be used during the diagnostic and therapeutic process.

Although, pancreatic cancer is not discussed in this part, it will be addressed shortly. Current international and Dutch guidelines for pancreatic cancer still suggest CT scanning.(14-16) However, there's a need for optimization of preoperative imaging in patients with suspect pancreatic cancer. Not only is differentiation between cancer, inflamed and (chemotherapy induced) fibrosis tissue difficult on CT (or MRI) scans, the assessment of extent of vascular contact also gives hurdles.(17, 18) Furthermore, due to the large incidence of patients presenting with metastatic disease or developing metastatic spread just after surgery, preoperative imaging should also be more focused on detecting metastases.(19, 20) Preoperative MRI scanning, including a DWI sequence, might prevent surgery in patients who already developed small (hepatic) metastases.(21, 22) Unpublished data of 93 patients who underwent intended curative surgery for pancreatic cancer in the LUMC between January 2016 and July 2017, shows an incidence of metastastic disease in 21.5% of the patients during surgery or within 3 months after surgery. In an ongoing clinical trial from Radboud MC (NCT03469726), all patients with (suspect) pancreatic cancer will undergo an additional Contrast-enhanced Diffusion-weighted MRI (CE-DWI-MRI) can within two weeks from the Contrast-enhanced CT (CECT) scan. All suspect metastatic lesions will be biopsied to obtain pathological confirmation. Follow-up CE-DW-MRI and CECT scans will be made at 3, 6 and 12 months. Future prospective studies, like the study of Radboud MC, should focus more improving patient selection, so patients will not undergo unnecessary hazardous surgery. Since detection of metastatic disease during exploration immediately prior to planned resection is related to very poor prognosis of patients, sufficient preoperative imaging is of vital importance for this patient population.(23)

Another solution for detection of metastatic disease and for evaluation of the local extend of the primary pancreatic tumor, could be in PET imaging. So far, PET is not standard in the diagnostic process of pancreatic cancer, but various upcoming and ongoing studies are investigating tumor-specific tracers for PET imaging. In the near future a tumor-specific αvβ6 PET tracer will be investigated in patients with pancreatic cancer.

Hybrid tracer: preoperative and intraoperative imaging

Chapter 6 describes the value of hybrid tracer use in patients with colorectal cancer, namely cRGD. This tracer is based on the tripeptide Arg-Gly-Asp (RGD), which targets various integrins (e.g. αvβ6) overexpressed on tumor cells and correlating with neoangiogenesis. With one single molecular imaging agent preoperative PET and NIRF imaging can be realized. Several advantages of hybrid tracer use are improved patient selection, preoperative surgical planning, intraoperative surgical guidance and optimisation of radical resection rates. Time management is of importance for hybrid tracers, tumor-specific nuclear signals should be detectable quickly and the NIRF signals should remain stable over time. The interval between preoperative imaging and surgery could be shortened by using hybrid tracers, increasing the probability of concordance between preoperative planning and surgery. In the future, tracers

will probably be increasingly developed in a hybrid form, since obtaining market approval for a single drug is very costly and time consuming (22) There is a great need to develop single contrast agents (drugs) that have more than one indication. A cRGD-based tracer can be used for the detection of several cancer sorts, and a hybrid tracer can be used for both pre- and intraoperative imaging. Development of future tracers should take both into account.

The clinically available near-infrared cRGD-ZW800-1 tracer is currently being tested in patients with colorectal cancer in a clinical trial (NL6250805817). Depending on the clinical trial results, cRGD-ZW800-1 will also be used for the intraoperative detection of pancreatic cancer. *In vivo* pre-clinical studies have already shown that NIRF imaging of pancreatic cancer with cRGD-ZW800-1 is sufficient.(24) A great advantage of cRGD-ZW800 tracers is the renal clearance of the isotopes. Pancreatic, or colorectal, liver metastases can be detected, because the liver remains dark.

INTRA-OPERATIVE TECHNIQUES

Staging laparoscopy using NIRF imaging

Performing staging laparoscopy immediately prior to curative intended surgery in pancreatic cancer patients is now performed standardly in the LUMC as described in **chapter 7**. But, addition of NIRF imaging using indocyanine green (ICG) for the detection of hepatic metastasized spread yielded less than expected. Using tumor-specific NIRF imaging could overcome drawbacks from the aspecific ICG, since extrahepatic lesions can also be identified, like peritoneal spread. Tumor-specific imaging could improve evaluation of the primary tumor during the laparoscopy. This will be of special value for neoadjuvantly treated patients in whom distinction between chemotherapy induces fibrosis, viable tumor cells and healthy tissue is hard.(17, 18) Although ultrasound was of no added value in the described study, contrast-enhanced ultrasound might be of more value.(25)

Future studies should focus on developing tumor-specific tracers, resulting in optimal NIRF imaging during staging laparoscopy for the evaluation of metastatic or locally advanced disease. This will become of special value since the number of neoadjuvantly treated patients will increase and tumor response evaluation on preoperative imaging is suboptimal.

NIRF imaging in colorectal liver metastases

NIRF imaging is most frequently applied during liver surgery, since real-time demarcation of liver lesions can be easily performed using ICG. This technique proved to be feasible for detection and resection of HCC as well as metastases, all with different fluorescence patterns.(26) Lesions can be detected, additional lesions can be identified and CRLM can be radically resected based on the characteristic fluorescent rim present around the lesion. With the introduction of clinically available laparoscopic systems equipped with a NIRF

channel and the possibility to project the fluorescence signals over the white light images, this technique is applied increasingly as standard of care.

In **chapter 8** the use of NIRF imaging with ICG for resection of CRLM is extensively described, focusing on technical aspects. Reports like these will become of special interest to be able to implement NIRF imaging widely in a standardized manner. Future studies about NIRF imaging should focus on expanding, and making surgeons comfortable with this technique. The MIMIC trial (NTR7674) is an example of a Dutch multicenter study, during which NIRF imaging using ICG will be used during laparoscopic resection of CRLM. The added value of NIRF imaging for liver surgery is already proven, but the focus of this study is on radical tumor removal and stimulating the learning curve of surgeons by using NIRF imaging. Afterwards, when clinical tumor specific tracers become available in the future, surgeons are already used to NIRF guided surgeries.

As described earlier, a disadvantage of the use of NIRF imaging with ICG is the limitation for liver use only, due to the non-specific properties of ICG. Also causing potential non-specific fluorescence signals in the liver, resulting in a relative increased false-positive ratio. Tumor-specific tracers can overcome this drawbacks. But still, the maximal depth penetration of a fluorescence signal is limited to 1 cm (25), therefore NIRF imaging should be combined with other techniques, such as radionuclides. Preoperative PET/SPECT scans provide information about tumor extension and allow surgical planning. Deeper seated tumors could be visualized using intraoperative ultrasound, preferably contrast-enhanced ultrasound. In the far future the limited depth penetration problem might even be solved with the use of multispectral optoacoustic tomography (MSOT) or photoacoustic imaging. (26-27) Depth penetration is extended to approximately 5cm, but these techniques are still in an early stage.

Tumor-specific NIRF imaging in pancreatic cancer

Sufficient tumor-specific tracers for pancreatic cancer are not yet clinically available. Several studies have been done trying to visualize pancreatic cancer cells using fluorescent tracers, with suboptimal results.(27, 28) As **chapter 9** describes, bevacizumab-800CW is disappointing for tumor specific NIRF imaging of pancreatic cancer. This can be due a variety of reasons. Firstly, shedding of vascular endothelial growth factor (VEGF) which is targeted by bevacizumab-800CW, in the microenvironment and surrounding tissue results in diffused VEGF binding and increased background signals. Another reason can be the large amount of abundant desmoplastic stroma, resulting in sparser fluorescent patterns compared to other tumor types. Due to the size of antibody tracers, antibodies are probably not the most suitable fluorescent tracers for targeting of pancreatic cancer.

In the future a tracer targeting stroma, or using a combination of tracers, could be the solution.(29) Primary pancreatic tumors already are highly heterogenous and are therefore hard to target completely. Targeting both the primary tumor including potential metastases,

for example during staging laparoscopy, is even harder. Due to homing of the tumor cells in other microenvironments such as the liver, novel mutations occur, consequently leading to even larger heterogeneity, also between the metastases and the primary tumor. All current studies are performed with fluorescent labelled antibodies. Smaller tracers like integrins or nanobodies will be better tracers for targeting of pancreatic cancer. Targets should be evaluated for being able to distinct between inflammation, chemotherapy adjusted tissue and viable cancer cells, since neoadjuvant therapy will probably become standard-of-care. CEA and integrin αvβ6 seem to be promising targets, as is uPAR.(30)

Furthermore, with the upcoming minimally invasive procedures, laparoscopic and robot assisted surgeries, tracers should be developed for and adjusted to the NIRF channels with which these systems are equipped. NIRF imaging will be especially valuable for these kind of procedures because switching between the white light channels and NIRF channels can be done easily. Therefore, checking resection margins or assessing suspect (metastatic) lesions can be performed within seconds. Wide field NIRF imaging requires dimmed lights and displacements of camera systems, operation rooms should be optimized for quick and easy use of camera's during open surgery.

Intraoperative ultrasound

Endoscopic ultrasound has gained an important role in the diagnostic process of patients with pancreatic cancer. But ultrasound during surgery is not standardly performed, whilst IOUS has multiple benefits: easy access, direct feedback and low costs are a few examples. In **chapter 10** IOUS was used for the assessment of pancreatic tumors. In this prospective cohort study the focus was on assessment of vascular contact and resection margins compared to histopathological assessment. IOUS assessment was superior to preoperative imaging for the assessment of vascular contact. Furthermore, in more than half of the patients the initial surgical strategy was adjusted based on findings with the IOUS. Surgeons were in general prepared earlier during the procedure for what to encounter with regards to: vascular contact, additional lesions or a too extensive disease. Additionally, high radical resections rates were obtained in this cohort, almost 80% was resected radical. Compared to an overall radical resection rate of 40% worldwide.(31) With the use of a high-frequency probe in direct contact with the organ, IOUS provides superior spatial resolution and contrast compared to preoperative imaging.

In an ongoing multicenter study, UltraPanc, (NTR7621) the use of IOUS during resections of pancreatic cancer is investigated more extensively. Changes in surgical strategy due to IOUS assessment will be determined during this follow-up study. The most important objective of this study will be the standardization of IOUS use, especially for assessment of vascular contact with the tumor. By standardization of IOUS assessment radical resection rates could be increased and unnecessary vascular reconstructions or irradical resected tumors due to vascular involvement can be prevented.(32) Since neoadjuvant therapy will gain a more

prominent role in the therapy of pancreatic cancer patients, all future studies investigating the surgical process of pancreatic cancer should emphasize also this aspect. IOUS might be of help in discriminating between benign and malignant tissue. By standardized IOUS assessments performed by experienced abdominal radiologist, the primary tumor might be assessed more accurately. Therefore, half of the patients in the UltraPanc study will be treated neaodjuvantly. After standardization and improving IOUS assessment by this study, tumor specific contrast-enhanced ultrasound for visualization of pancreatic cancer should be investigated.(33, 34) Contrast-enhanced ultrasound might yield even more, not only for assessment of metastastic spread or locally advanced disease, but also about primary tumor status after neoadjuvant therapy and involvement of surrounding vessels and structures.

POST-PROCEDURAL EVALUATION

Radio-frequency ablation

The primary objective of **chapter 11** was to evaluate the feasibility and reproducibility of CT-CT scan co-registration, using Mirada RTx software, in order to assess radio frequency ablation margins of patients with CRLM. Based on this retrospective cohort the feasibility was sub-optimal, but co-registration was reproducible. The secondary objective was to correlate the ablation margin to the occurrence of local recurrence. In future prospective studies, quantitative analysis using co-registration for instance, might be a valuable tool in defining technical success. Immediately after the percutaneously ablated tumors, the ablation margins can be assessed using this co-registration software, predicting if local recurrence might occur. If so, direct re-ablation can be performed, hopefully preventing local recurrence and re-interventions later on.

GENERAL FUTURE PERSPECTIVES AND CONCLUSIONS

Selecting patients suitable for undergoing hazardous pancreatic surgery, or resection of colorectal liver metastases, remains challenging. Molecular diagnostics will increasingly become an important factor in diagnosing patients with suspect lesions and will aid in choosing patient specific oncologic treatment. Optimizing preoperative imaging helps to determine the local expansion of the primary tumor and can also detect possible metastases, improving patient based treatment selection and surgical planning. NIRF imaging in the diagnostic process and during surgery can aid in detection of the primary cancer and possible metastases. Moreover, due to the ability to highlight specific structures surgeons can aim for optimal radical resections and can diminish iatrogenic damage and morbidity. Future studies investigating NIRF imaging should be focussed on distinguishing vital cancer cells

from chemotherapy induced fibrosis, since systemic treatment is increasingly administered. Another focus can be on a different type of tracer, for example conjugation of fluorophores to nanobodies, resulting in a shortened timeframe between injection of the tracer and intraoperative NIRF imaging.

Several other promising techniques might become of importance during surgery in the future. Like research focusing on the NIR-II optical window, which has a wavelength between 1000-1700nm, thereby extending the depth penetration for imaging.(35, 36) Photo-acoustic imaging also has the potency to visualize tissue up to several centimetres.(37) Spectroscopy is already used in the diagnostic process during EUS-FNA, but might also be of help to differentiate between different types of tissue during surgery.(38) Hyperspectral imaging systems are currently being developed, with the intention to differentiate between tissue types without the use of exogenic tracers.(39) Lastly, in addition to surgery, tumor-targeted photodynamic therapy can induce cell death using light activation of a photosensitizer. This might be used as additional intraoperative therapy after resection.(40)

To be able to broadly implement all the described and used techniques, large multicenter studies should be initialized. These studies should focus on new indications for NIRF imaging using ICG, in order to make surgeons familiar with the technique. Furthermore, studies focusing on tumor specific imaging should take patient outcome, like improved survival and reduction of morbidities, into account. Eventually, this will lead to wide-spread implementation in a standardized manner with quality assurance of intraoperative techniques like NIRF imaging.

REFERENCES

1. Oellerich M, Schutz E, Beck J, Kanzow P, Plowman PN, Weiss GJ, et al. Using circulating cell-free DNA to monitor personalized cancer therapy. Crit Rev Clin Lab Sci. 2017;54(3):205-18.
2. Cohen JD, Li L, Wang Y, Thoburn C, Afsari B, Danilova L, et al. Detection and localization of surgically resectable cancers with a multi-analyte blood test. Science. 2018;359(6378):926-30.
3. Fernandez Moro C, Bozoky B, Gerling M. Growth patterns of colorectal cancer liver metastases and their impact on prognosis: a systematic review. BMJ Open Gastroenterol. 2018;5(1):e000217.
4. Prasanna T, Karapetis CS, Roder D, Tie J, Padbury R, Price T, et al. The survival outcome of patients with metastatic colorectal cancer based on the site of metastases and the impact of molecular markers and site of primary cancer on metastatic pattern. Acta Oncol. 2018:1-7.
5. Tsilimigras DI, Ntanasis-Stathopoulos I, Bagante F, Moris D, Cloyd J, Spartalis E, et al. Clinical significance and prognostic relevance of KRAS, BRAF, PI3K and TP53 genetic mutation analysis for resectable and unresectable colorectal liver metastases: A systematic review of the current evidence. Surg Oncol. 2018;27(2):280-8.
6. Neerincx M, Sie DL, van de Wiel MA, van Grieken NC, Burggraaf JD, Dekker H, et al. MiR expression profiles of paired primary colorectal cancer and metastases by next-generation sequencing. Oncogenesis. 2015;4:e170.
7. Heublein S, Albertsmeier M, Pfeifer D, Loehrs L, Bazhin AV, Kirchner T, et al. Association of differential miRNA expression with hepatic vs. peritoneal metastatic spread in colorectal cancer. BMC Cancer. 2018;18(1):201.
8. De Roock W, De Vriendt V, Normanno N, Ciardiello F, Tejpar S. KRAS, BRAF, PIK3CA, and PTEN mutations: implications for targeted therapies in metastatic colorectal cancer. Lancet Oncol. 2011;12(6):594-603.
9. Capalbo C, Belardinilli F, Raimondo D, Milanetti E, Malapelle U, Pisapia P, et al. A Simplified Genomic Profiling Approach Predicts Outcome in Metastatic Colorectal Cancer. Cancers (Basel). 2019;11(2).
10. Osumi H, Shinozaki E, Takeda Y, Wakatsuki T, Ichimura T, Saiura A, et al. Clinical relevance of circulating tumor DNA assessed through deep sequencing in patients with metastatic colorectal cancer. Cancer Med. 2019;8(1):408-17.
11. Franczak C, Dubouis L, Gilson P, Husson M, Rouyer M, Demange J, et al. Integrated routine workflow using next-generation sequencing and a fully-automated platform for the detection of KRAS, NRAS and BRAF mutations in formalin-fixed paraffin embedded samples with poor DNA quality in patients with colorectal carcinoma. PLoS One. 2019;14(2):e0212801.
12. van der Vorst JR, Schaafsma BE, Hutteman M, Verbeek FP, Liefers GJ, Hartgrink HH, et al. Near-infrared fluorescence-guided resection of colorectal liver metastases. Cancer. 2013;119(18):3411-8.
13. Bonanni L, de'Liguori Carino N, Deshpande R, Ammori BJ, Sherlock DJ, Valle JW, et al. A comparison of diagnostic imaging modalities for colorectal liver metastases. Eur J Surg Oncol. 2014;40(5):545-50.
14. National Comprehensive Cancer Network website. NCCN Clinical Practice Guidelines in Oncology. 2015 [Pancreatic adenocarcinoma, version 2.2015:[Avail-

able from: http://www.nccn.org/professionals/physician_gls/f_guidelines.asp.
15. DPCG. DPCG-definities resectabiliteit pancreascarcinoom (PREOPANC trial, DPCG 2012) 2012 [Available from: http://dpcg.nl/images/Criteria_resectabiliteit.pdf.
16. Feldman MK, Gandhi NS. Imaging Evaluation of Pancreatic Cancer. Surg Clin North Am. 2016;96(6):1235-56.
17. Donahue TR, Isacoff WH, Hines OJ, Tomlinson JS, Farrell JJ, Bhat YM, et al. Downstaging chemotherapy and alteration in the classic computed tomography/magnetic resonance imaging signs of vascular involvement in patients with pancreaticobiliary malignant tumors: influence on patient selection for surgery. Arch Surg. 2011;146(7):836-43.
18. Katz MH, Fleming JB, Bhosale P, Varadhachary G, Lee JE, Wolff R, et al. Response of borderline resectable pancreatic cancer to neoadjuvant therapy is not reflected by radiographic indicators. Cancer. 2012;118(23):5749-56.
19. van der Geest LGM, Lemmens V, de Hingh I, van Laarhoven C, Bollen TL, Nio CY, et al. Nationwide outcomes in patients undergoing surgical exploration without resection for pancreatic cancer. Br J Surg. 2017;104(11):1568-77.
20. Gaujoux S, Allen PJ. Role of staging laparoscopy in peri-pancreatic and hepatobiliary malignancy. World J Gastrointest Surg. 2010;2(9):283-90.
21. Motosugi U, Ichikawa T, Morisaka H, Sou H, Muhi A, Kimura K, et al. Detection of pancreatic carcinoma and liver metastases with gadoxetic acid-enhanced MR imaging: comparison with contrast-enhanced multi-detector row CT. Radiology. 2011;260(2):446-53.
22. Luna A, Pahwa S, Bonini C, Alcala-Mata L, Wright KL, Gulani V. Multiparametric MR Imaging in Abdominal Malignancies. Magn Reson Imaging Clin N Am. 2016;24(1):157-86.
23. Tummers WS, Groen JV, Sibinga Mulder BG, Farina-Sarasqueta A, Morreau J, Putter H, et al. Impact of resection margin status on recurrence and survival in pancreatic cancer surgery. Br J Surg. 2019.
24. Handgraaf HJM, Boonstra MC, Prevoo H, Kuil J, Bordo MW, Boogerd LSF, et al. Real-time near-infrared fluorescence imaging using cRGD-ZW800-1 for intraoperative visualization of multiple cancer types. Oncotarget. 2017;8(13):21054-66.
25. Taimr P, Jongerius VL, Pek CJ, Krak NC, Hansen BE, Janssen HL, et al. Liver Contrast-Enhanced Ultrasound Improves Detection of Liver Metastases in Patients with Pancreatic or Periampullary Cancer. Ultrasound Med Biol. 2015;41(12):3063-9.
26. Boogerd LS, Handgraaf HJ, Lam HD, Huurman VA, Farina-Sarasqueta A, Frangioni JV, et al. Laparoscopic detection and resection of occult liver tumors of multiple cancer types using real-time near-infrared fluorescence guidance. Surg Endosc. 2017;31(2):952-61.
27. Tummers WS, Miller SE, Teraphongphom NT, Gomez A, Steinberg I, Huland DM, et al. Intraoperative Pancreatic Cancer Detection using Tumor-Specific Multimodality Molecular Imaging. Ann Surg Oncol. 2018;25(7):1880-8.
28. Charlotte E.S. Hoogstins LSFB, Babs G. Sibinga Mulder, J. Sven D. Mieog, Rutger Jan Swijnenburg, Cornelis J.H. van de Velde, Arantza Farina Sarasqueta, Bert A. Bonsing, Berenice Framery, André Pèlegrin, Marian Gutowski, Françoise Cailler, Jacobus Burggraaf, Alexander L. Vahrmeijer. Image-guided surgery in patients with pancreatic cancer: a clinical trial using SGM-101, a novel carcinoembryonic antigen-targeting, near-infrared fluorescent agent in process. 2017.

29. Boonstra MC, Prakash J, Van De Velde CJ, Mesker WE, Kuppen PJ, Vahrmeijer AL, et al. Stromal Targets for Fluorescent-Guided Oncologic Surgery. Front Oncol. 2015;5:254.
30. de Geus SW, Boogerd LS, Swijnenburg RJ, Mieog JS, Tummers WS, Prevoo HA, et al. Selecting Tumor-Specific Molecular Targets in Pancreatic Adenocarcinoma: Paving the Way for Image-Guided Pancreatic Surgery. Mol Imaging Biol. 2016;18(6):807-19.
31. Neoptolemos JP, Palmer DH, Ghaneh P, Psarelli EE, Valle JW, Halloran CM, et al. Comparison of adjuvant gemcitabine and capecitabine with gemcitabine monotherapy in patients with resected pancreatic cancer (ESPAC-4): a multicentre, open-label, randomised, phase 3 trial. Lancet. 2017;389(10073):1011-24.
32. Giovinazzo F, Turri G, Katz MH, Heaton N, Ahmed I. Meta-analysis of benefits of portal-superior mesenteric vein resection in pancreatic resection for ductal adenocarcinoma. Br J Surg. 2016;103(3):179-91.
33. Yuan HX, Wang WP, Wen JX, Lin LW, Exner AA, Guan PS, et al. Dual-Targeted Microbubbles Specific to Integrin alphaV-beta3 and Vascular Endothelial Growth Factor Receptor 2 for Ultrasonography Evaluation of Tumor Angiogenesis. Ultrasound Med Biol. 2018;44(7):1460-7.
34. Du J, Li XY, Hu H, Xu L, Yang SP, Li FH. Preparation and Imaging Investigation of Dual-targeted C3F8-filled PLGA Nanobubbles as a Novel Ultrasound Contrast Agent for Breast Cancer. Sci Rep. 2018;8(1):3887.
35. Harmsen S, Teraphongphom N, Tweedle MF, Basilion JP, Rosenthal EL. Optical Surgical Navigation for Precision in Tumor Resections. Mol Imaging Biol. 2017;19(3):357-62.
36. Antaris AL, Chen H, Cheng K, Sun Y, Hong G, Qu C, et al. A small-molecule dye for NIR-II imaging. Nat Mater. 2016;15(2):235-42.
37. Zackrisson S, van de Ven S, Gambhir SS. Light in and sound out: emerging translational strategies for photoacoustic imaging. Cancer Res. 2014;74(4):979-1004.
38. Stegehuis PL, Boogerd LS, Inderson A, Veenendaal RA, van Gerven P, Bonsing BA, et al. Toward optical guidance during endoscopic ultrasound-guided fine needle aspirations of pancreatic masses using single fiber reflectance spectroscopy: a feasibility study. J Biomed Opt. 2017;22(2):24001.
39. Lu G, Fei B. Medical hyperspectral imaging: a review. J Biomed Opt. 2014;19(1):10901.
40. Sarcan ET, Silindir-Gunay M, Ozer AY. Theranostic polymeric nanoparticles for NIR imaging and photodynamic therapy. Int J Pharm. 2018;551(1-2):329-38.

13

Nederlandse samenvatting

Momenteel is resectie de enige kans op lange termijn overleving voor patiënten met pancreaskanker. Indien er sprake is van gemetastaseerde ziekte of van lokaal uitgebreide tumorgroei hebben patiënten geen baat bij directe chirurgie, dan moet respectievelijk palliatieve of neoadjuvante behandeling nagestreefd worden. Het uitsluiten cq aantonen van irresectabiliteit is van groot belang tijdens het diagnostisch proces. Dit gebeurt aan de hand van preoperatieve beeldvorming en endoscopische echografie met als optie een diagnostische punctie, eventueel gevolgd door een stadiërings laparoscopie. Indien de primaire tumor resectabel lijkt moet een radicale resectie nagestreefd worden aangezien dit de beste prognose voor de patiënt oplevert. Tijdens de operatie kan de chirurg gebruik maken van verschillende intraoperatieve beeldvormende technieken om de tumor zo goed mogelijk in beeld te brengen en radicaal te verwijderen, dit gebeurt echter nog zeer beperkt en niet standaard.

Patiënten met levermetastasen van colorectale tumoren kunnen curatief behandeld worden, met een eventueel lange termijn overleving als resultaat. Metastasen worden indien mogelijk lokaal behandeld middels resectie of ablatie. Als er sprake is van een verder gedissemineerde ziekte is systemische therapie een optie. Preoperatieve beeldvorming is om verschillende redenen van belang: het afstemmen van de meest geschikte behandeling, het in kaart brengen van de metastasen en het opstellen van een chirurgisch plan. Om de prognose optimaal te houden is het noodzakelijk om de lokale behandeling radicaal uit te voeren. Verschillende intraoperatieve en postoperatieve technieken kunnen bijdragen aan een radicale resectie.

Dit proefschrift richt zich op het optimaliseren van het diagnostisch proces en de chirurgische behandeling van pancreas kanker en colorectale tumoren. Moleculaire diagnostiek, pre- en intraoperatieve beeldvormende technieken zullen aan bod komen. Een veel beschreven techniek in dit proefschrift is fluorescentie geleide chirurgie. Fluorescentie geleide chirurgie maakt gebruik van het nabij-infrarode licht om het visuele contrast tussen tumor en omliggend weefsel te vergroten.

DEEL 1: MOLECULAIRE DIAGNOSTIEK

In het eerste deel van dit proefschrift ligt de focus op moleculaire diagnostiek bij patiënten met een verdachte laesie van de pancreas. Moleculaire diagnostiek middels targeted Next-Generation Sequencing (NGS) kan tijdens het diagnostisch proces bijdragen aan het onderscheid maken tussen maligne en benigne aandoeningen. Diagnostische cytologische puncties worden met NGS geanalyseerd om pathogene varianten in het DNA aan te tonen. **Hoofdstuk 2** betreft een casus waaruit blijkt dat NGS een doorslaggevende factor kan zijn voor het kiezen van de juiste behandeling, en wordt de techniek uitvoerig beschreven. In **hoofdstuk 3** wordt beschreven hoe NGS gevalideerd is in een opeenvolgend patiënten cohort in het Leids Universitair Medisch Centrum (LUMC). Integratie van NGS in het

diagnostisch proces had een sensitiviteit en specificiteit van 93% en 100%, respectievelijk. Dankzij NGS veranderde het behandelplan in 10% van de patiënten. In **hoofdstuk 4** wordt een multicenter studie beschreven, waarbij NGS alleen wordt ingezet indien de diagnostiek moeizaam gaat en er veel twijfel blijft over de diagnose en passende behandelplan. NGS analyse resulteerde in het voorkomen van herhaling van een diagnostische punctie (n=7), het voorkomen van oncologische behandeling voor patiënten met een benigne conditie (n=8) en het aantonen van maligniteiten die anders gemist zouden worden (n=1).

DEEL 2: PREOPERATIEVE BEELDVORMENDE TECHNIEKEN

In **hoofdstuk 5** wordt de rol van de MRI scan, waarbij gadoxine-zuur (Primovist) als contrastmiddel wordt gebruikt, in patiënten met colorectale levermetastasen geanalyseerd. Tijdens het diagnostisch proces krijgen alle patiënten standaard een CT scan, indien het resectabele metastasen betreffen wordt sinds 2013 in het LUMC ook een MRI Primovist scan gemaakt. Differentiatie tussen maligne en benigne laesies met de MRI Primovist scan is sensitiever. Daarnaast is het ook mogelijk om op een MRI Primovist scan kleinere laesies (<1 cm) aan te tonen. Uit deze studie blijkt dat integratie van de MRI Primovist scans in het diagnostisch proces van patiënten met colorectale levermetastasen de ziekte nauwkeuriger in kaart brengt, de keuze voor behandelstrategie verbetert en korte-termijn reïnterventies vermindert.

Om tijdens pre-operatieve beeldvorming de tumor beter in beeld te brengen kan ook gebruikt gemaakt worden van tumor-specifieke beeldvorming, zoals PET scans met tumor-specifieke nucleaire tracers. **Hoofdstuk 6** beschrijft een pre-klinische studie waarin een hybride tracer getest wordt in proefdieren. Deze tumor-specifieke hybride tracer kan preoperatief gebruikt worden voor PET scans en intraoperatief voor fluorescentiebeeldvorming. De tracer, genaamd cRGD-ZW800-1-Forte-[^{89}Zr]Zr-DFO, bindt zich aan integrinen die tot overexpressie komen op tumorcellen en geassocieerd zijn met neoangiogenese. Door gebruik te maken van hybride tracers kan preoperatief de patiënten selectie verbeterd worden doordat metastasen of lokaal uitgebreide tumorgroei aangetoond kan worden. Vervolgens kan een chirurgische planning direct intraoperatief gerealiseerd worden. Bij het gebruik van hybride tracers is tijdsplanning van belang, echter is een groot voordeel dat maar één tracer toegediend wordt. Daarnaast kunnen twee technieken gerealiseerd worden met goedkeuring van maar één tracer. Bovendien is het door gebruik te maken van één tracer zeker dat pre-operatieve beeldvorming in overeenstemming is met intraoperatieve beeldvorming.

DEEL 3: INTRAOPERATIEVE BEELDVORMENDE TECHNIEKEN

Zoals boven beschreven, is het mogelijk om een stadiëringslaparoscopie uit te voeren om aanwezigheid bij levermetastasen van pancreaskanker uit te sluiten. Deze techniek kan aangevuld worden met laparoscopische echografie en fluorescentie beeldvorming, zoals in **hoofdstuk 7** is gedaan. In deze prospectieve cohort studie is gebruik gemaakt van indocyanine groen (ICG). ICG is een niet tumor-specifieke fluorescente tracer waarmee op een indirecte manier, metastasen succesvol in de lever worden aangetoond. Echografie had geen aanvullende waarde in deze studie. In toekomstige studies die zich richten op stadiëringslaparoscopie moet blijken of tumor-specifieke tracers van meerwaarde zijn. Dit kan met name van belang zijn om extra-hepatische metastasen en de primaire tumor in beeld te brengen. Verder is het noodzakelijk om onderscheid te maken tussen vitaal tumorweefsel en chemotherapie geïnduceerde fibrose na neoadjuvante therapie.

Het gebruik van ICG voor detectie van colorectale levermetastasen wordt beschreven in **hoofdstuk 8**. Het is al langere tijd bekend dat ICG van meerwaarde is voor de chirurgische behandeling van colorectale levermetastasen, aangezien (kleine) additionele levermetastasen die gemist waren op preoperatieve beeldvorming aangetoond kunnen worden. Deze studie richt zich op minimaal invasieve technieken waarbij fluorescentie beeldvorming toegepast kan worden. Hierdoor ontstaat de mogelijkheid om metastasen radicaal te reseceren op basis van de fluorescentie patronen. De technische aspecten van deze techniek worden belicht. Hiermee wordt de basis gelegd om tijdens minimaal-invasieve ingrepen metastasen te verwijderen op basis van de fluorescente feedback om hiermee het aantal radicale resecties te vergroten.

In **Hoofdstuk 9** wordt een eerste multicenter studie beschreven die zich richt op een tumor-specifieke fluorescentie tracer. De betreffende tracer, genaamd bevacuzimab-800CW, bindt aan vascular endothelial growth factor (VEGF). Ondanks succes bij andere tumortypen, werden suboptimale resultaten behaald met deze tracer voor het in beeld brengen van pancreaskanker. De mogelijke oorzaken hiervoor zijn de verdeling van de expressie van VEGF en de structuur van de tracer. Vanwege de grote stromale factor in pancreaskanker zullen toekomstige tumor-specifieke tracers zich ook moeten richten op het binden aan stroma. Verder zullen combinaties van verschillende tracers ingezet moeten worden vanwege het heterogene karakter van pancreaskanker.

Intraoperatieve echografie is een techniek die al jaren gebruikt wordt maar niet standaard wordt ingezet bij resectie van de tumor in de pancreas. Deze relatief makkelijk toepasbare en goedkope techniek, welke directe feedback verschaft aan de operateurs, wordt beschreven in **hoofdstuk 10**. In deze prospectieve cohort studie verschaft de intraoperatieve echo in de meerderheid van de patiënten extra informatie in vergelijking met de preoperatieve

beeldvorming. De vasculaire betrokkenheid kan goed in kaart worden gebracht, wat in een nieuwe lopende multicenter studie gestandaardiseerd wordt uitgezocht.

De laatst beschreven techniek is radio frequency ablation van colorectale levermetastasen, en wordt behandeld in **hoofdstuk 11**. Door directe co-registratie met behulp van de Mirada RTx software van de CT scan tijdens de ablatie en de CT scan meteen na de ablatie, kan het succes van de ablatie geëvalueerd worden. In dit hoofdstuk wordt deze techniek beschreven en gevalideerd in een retrospectief cohort. Vervolgstudies met directe co-registratie na ablatie moeten uitwijzen of lokaal recidief zo voorkomen kan worden.

LIST OF PUBLICATIONS

1. **Sibinga Mulder BG**, Hendriks P, Baetens TR, van Erkel AR, van Rijswijk CSP, van der Meer RW, van de Velde CJH, Vahrmeijer AL, Mieog JSD, Burgmans MC. Quantitative margin assessment of radiofrequency ablation of a solitary colorectal hepatic metastasis using MIRADA RTx on CT scans: a feasibility study. BMC Med Imaging. 2019 Aug 20;19(1):71. doi: 10.1186/s12880-019-0360-2. PMID: 31429708
2. de Valk KS, Handgraaf HJ, Deken MM, **Sibinga Mulder BG**, Valentijn AR, Terwisscha van Scheltinga AG, Kuil J, van Esdonk MJ, Vuijk J, Bevers RF, Peeters KC, Holman FA, Frangioni JV, Burggraaf J, Vahrmeijer AL. A zwitterionic near-infrared fluorophore for real-time ureter identification during laparoscopic abdominopelvic surgery. Nat Commun. 2019 Jul 16;10(1):3118. doi: 10.1038/s41467-019-11014-1. PMID: 31311922
3. **Sibinga Mulder BG**, Feshtali S, Fariña Sarasqueta A, Vahrmeijer AL, Swijnenburg RJ, Bonsing BA, Mieog JSD. A Prospective Clinical Trial to Determine the Effect of Intraoperative Ultrasound on Surgical Strategy and Resection Outcome in Patients with Pancreatic Cancer. Ultrasound Med Biol. 2019 Aug;45(8):2019-2026. doi: 10.1016/j.ultrasmedbio.2019.04.020. Epub 2019 May 24. PMID: 31130412
4. Tummers WS, Groen JV, **Sibinga Mulder BG**, Farina-Sarasqueta A, Morreau J, Putter H, van de Velde CJ, Vahrmeijer AL, Bonsing BA, Mieog JS, Swijnenburg RJ. Impact of resection margin status on recurrence and survival in pancreatic cancer surgery. Br J Surg. 2019 Jul;106(8):1055-1065. doi: 10.1002/bjs.11115. Epub 2019 Mar 18. PMID: 30883699.
5. **Sibinga Mulder BG**, Handgraaf HJ, Vugts DJ, Sewing C, Windhorst AD, Stammes M, de Geus-Oei LF, Bordo MW, Mieog JSD, van de Velde CJ, Frangioni JV, Vahrmeijer AL. A dual-labeled cRGD-based PET/optical tracer for pre-operative staging and intraoperative treatment of colorectal cancer. Am J Nucl Med Mol Imaging. 2018 Oct 20;8(5):282-291. eCollection 2018. PMID: 30510846
6. **Sibinga Mulder BG**, Visser K, Feshtali S, Vahrmeijer AL, Swijnenburg RJ, Hartgrink HH, van den Boom R, Burgmans MC, Mieog JSD. Gadoxetic acid-enhanced magnetic resonance imaging significantly influences the clinical course in patients with colorectal liver metastases. BMC Med Imaging. 2018 Nov 15;18(1):44. doi: 10.1186/s12880-018-0289-x. PMID: 30442100
7. Handgraaf HJM, **Sibinga Mulder BG**, Shahbazi Feshtali S, Boogerd LSF, van der Valk MJM, Fariña Sarasqueta A, Swijnenburg RJ, Bonsing BA, Vahrmeijer AL, Mieog JSD. Staging laparoscopy with ultrasound and near-infrared fluorescence imaging to detect occult metastases of pancreatic and periampullary cancer. PLoS One. 2018 Nov 1;13(11):e0205960. doi: 10.1371/journal.pone.0205960. eCollection 2018. PMID 30383818

8. Groen JV, **Sibinga Mulder BG**, van Eycken E, Valerianova Z, Borras JM, van der Geest LGM, Capretti G, Schlesinger-Raab A, Primic-Zakelj M, Ryzhov A, van de Velde CJH, Bonsing BA, Bastiaannet E, Mieog JSD. Differences in Treatment and Outcome of Pancreatic Adenocarcinoma Stage I and II in the EURECCA Pancreas Consortium. Ann Surg Oncol. 2018 Aug 27. doi: 10.1245/s10434-018-6705-1. PMID: 30151560
9. Hoogstins CES, Boogerd LSF, **Sibinga Mulder BG**, Mieog JSD, Swijnenburg RJ, van de Velde CJH, Farina Sarasqueta A, Bonsing BA, Framery B, Pèlegrin A, Gutowski M, Cailler F, Burggraaf J, Vahrmeijer AL. Image-Guided Surgery in Patients with Pancreatic Cancer: First Results of a Clinical Trial Using SGM-101, a Novel Carcinoembryonic Antigen-Targeting, Near-Infrared Fluorescent Agent. Ann Surg Oncol. 2018 Oct;25(11):3350-3357. doi: 10.1245/s10434-018-6655-7. Epub 2018 Jul 26. PMID: 30051369
10. Ibrahim I, **Sibinga Mulder BG**, Bonsing B, Morreau H, Farina Sarasqueta A, Inderson A, Luelmo S, Feshtali S, Potjer TP, de Vos Tot Nederveen Cappel W, Wasser M, Vasen HFA. Risk of multiple pancreatic cancers in CDKN2A-p16-Leiden mutation carriers. Eur J Hum Genet. 2018 May 16. doi: 10.1038/s41431-018-0170-y. PMID: 29769629
11. **Sibinga Mulder BG**, Vahrmeijer AL, Mieog JSD. Future applications of fusion-fluorescence imaging during laparoscopic procedures. Transl Gastroenterol Hepatol. 2017 Sep 21;2:76. doi: 10.21037/tgh.2017.09.03. eCollection 2017. PMID: 29034349
12. **Sibinga Mulder BG**, Mieog JSD, Farina Sarasqueta A, Handgraaf HJ, Vasen HFA, Swijnenburg RJ, Luelmo SAC, Feshtali S, Inderson A, Vahrmeijer AL, Bonsing BA, Wezel TV, Morreau H. Diagnostic value of Targeted Next-Generation Sequencing in patients with suspected pancreatic or periampullary cancer. J Clin Pathol. 2018 Mar;71(3):246-252. doi: 10.1136/jclinpath-2017-204607. Epub 2017 Aug 3. PMID: 28775172
13. Handgraaf HJM, Boogerd LSF, Höppener DJ, Peloso A, **Sibinga Mulder BG**, Hoogstins CES, Hartgrink HH, van de Velde CJH, Mieog JSD, Swijnenburg RJ, Putter H, Maestri M, Braat AE, Frangioni JV, Vahrmeijer AL. Long-term follow-up after near-infrared fluorescence-guided resection of colorectal liver metastases: A retrospective multicenter analysis. Eur J Surg Oncol. 2017 Aug;43(8):1463-1471. doi: 10.1016/j.ejso.2017.04.016. Epub 2017 May 6. PMID: 28528189
14. Handgraaf HJM, Boonstra MC, Prevoo HAJM, Kuil J, Bordo MW, Boogerd LSF, **Sibinga Mulder BG**, Sier CFM, Vinkenburg-van Slooten ML, Valentijn ARPM, Burggraaf J, van de Velde CJH, Frangioni JV, Vahrmeijer AL. Real-time near-infrared fluorescence imaging using cRGD-ZW800-1 for intraoperative visualization of multiple cancer types. Oncotarget. 2017 Mar 28;8(13):21054-21066. doi: 10.18632/oncotarget.15486. PMID: 28416744
15. Frouws MA, **Sibinga Mulder BG**, Bastiaannet E, Zanders MM, van Herk-Sukel MP, de Leede EM, Bonsing BA, Mieog JS, Van de Velde CJ, Liefers GJ. No association between metformin use and survival in patients with pancreatic cancer: An observa-

tional cohort study. Medicine (Baltimore). 2017 Mar;96(10):e6229. doi: 10.1097/MD.0000000000006229. PMID: 28272215

16. **Sibinga Mulder BG**, Mieog JS, Handgraaf HJ, Farina Sarasqueta A, Vasen HF, Potjer TP, Swijnenburg RJ, Luelmo SA, Feshtali S, Inderson A, Vahrmeijer AL, Bonsing BA, van Wezel T, Morreau H. Targeted Next-Generation Sequencing of FNA-derived DNA in pancreatic cancer. J Clin Pathol. 2017 Feb;70(2):174-178. doi: 10.1136/jclinpath-2016-203928. Epub 2016 Sep 26.
17. de Leede EM, **Sibinga Mulder BG**, Bastiaannet E, Poston GJ, Sahora K, Van Eycken E, Valerianova Z, Mortensen MB, Dralle H, Primic-Žakelj M, Borràs JM, Gasslander T, Ryzhov A, Lemmens VE, Mieog JS, Boelens PG, van de Velde CJ, Bonsing BA. Common variables in European pancreatic cancer registries: The introduction of the EURECCA pancreatic cancer project. Eur J Surg Oncol. 2016 Sep;42(9):1414-9. doi: 0.1016/j.ejso.2016.03.011. Epub 2016 Mar 28. PMID: 27061790

CURRICULUM VITAE

Babs Sibinga Mulder werd 29 juni 1992 geboren te Leiden. In 2010 behaalde zij haar eindexamen aan het Christelijk Gymnasium Utrecht, waarna zij fiscaal recht ging studeren aan de Universiteit Leiden. Zij behaalde haar propedeuse rechten en startte in 2011 met de studie Geneeskunde aan de Universiteit Leiden. Tijdens haar studie werkte zij bij Inzowijs om kinderen probleem gericht te begeleiden. Daarnaast was zij actief lid van de Leidse Studenten Vereniging Minerva. Haar wetenschappelijke stage liep zij op de afdeling Heelkunde van het Leids Universitair Medisch Centrum, en hier werd haar enthousiasme voor wetenschappelijk onderzoek gewekt. In 2015 heeft zij haar medische studie onderbroken om onderzoek te doen bij de Image-Guided Surgery groep van Dr. A.L. Vahrmeijer. Zij werd aangesteld als onderzoeker op de Bas Mulder Award onder begeleiding van Dr. J.S.D. Mieog om onderzoek te doen naar chirurgische technieken bij pancreas carcinoom. Tijdens haar onderzoeksperiode heeft zij meerdere poster- en podiumpresentaties gegeven op nationale en internationale congressen. Hierbij heeft zij een poster-award gewonnen (World Molecular Imaging Conference 2019) en tweemaal een reisstipendium (WMIC 2017 en 2019). In 2018 heeft zij haar medische studie hervat en is gestart met haar co-schappen. Naar alle waarschijnlijkheid zal zij haar artsenexamen in 2020 behalen.

DANKWOORD

Allereerst gaat mijn dank uit naar alle patiënten die hebben deelgenomen aan de wetenschappelijke onderzoeken. Zonder hen zou dit proefschrift er niet zijn.

Daarnaast wil ik alle andere mensen bedanken die hebben bijgedragen aan de totstandkoming van dit proefschrift, in het bijzonder:

Dr. Vahrmeijer, lieve Lex, jouw leiderschap maakt de Greenlight groep tot groot succes. Ik ben trots dat ik hiervoor heb kunnen werken en wil je bedanken voor de steun, inspiratie, jouw eeuwige vertrouwen en alle kansen die je mij hebt geboden tijdens mijn PhD traject. Zeker niet te vergeten alle bijkomende gezelligheid.

Dr. Mieog, allerbeste Sven, bedankt dat je me hebt aangenomen op de toepasselijke Bas Mulder award als jouw eerste promovenda. Met veel enthousiasme zijn we hier beiden aan begonnen, met mijn proefschrift als resultaat. Bedankt voor de begeleiding afgelopen jaren.

Prof. van de Velde, beste professor, jaren voor het begin van mijn PhD zijn we al gestart met het RFA onderzoek, dit lijkt me dan ook een toepasselijk laatste hoofdstuk van mijn proefschrift. Bedankt voor uw begeleiding.

Prof. Burggraaf, beste Koos, door jou heb ik me altijd welkom gevoeld op het CHDR en genoten van onze samenwerking bij de enkele gedeelde projecten, promotieborrels en congressen. Het is een ware inspiratie hoe jij naast alle verantwoordelijkheden als CEO van het CHDR begeleiding blijft geven aan onze groep.

De beste manier om te promoveren is samen met alle Greenlight collega's in het J3 hok gevuld met prachtige foto's, lussen, camerasystemen en roze Champagne! Ik wil alle oud-Greenlighters en de gehele huidige J3 hiervoor bedanken! Mark en Q, we hebben niet veel onderzocht samen maar wel veel geborreld! Opperhottie Char, dank voor het opleiden tot hottie! Hein, mijn muizen-opereer skills heb ik aan jou te danken! Willie, beste mede pancreas onderzoekster. Maxie, trouwe lebkov-ganger en eeuwig luisterend oor. Kim, totale match op gebied van lekker leven en champagne! Friso, wat een verademing toen jij startte en net zo enthousiast werd van groene levers als ik! Gelukkig ben je snel weer terug. Thomas, ik heb bijzonder veel aan jou gehad, dank voor alle dagelijkse therapeutische wandelingetjes, hepathotheetjes, jägerbombs, wijze lessen en het ophogen van het corporale gehalte! Allerliefste Nora, mijn grote voorbeeld! Dank voor onze heerlijke etentjes, roze Ginto's, feestjes, dansjes die we altijd gaan blijven doorzetten! Ik verheug me nu al op onze toekomstige maatschap!

Dank aan alle co-auteurs; het datacentrum, met in het bijzonder Elma; het Heelkunde lab, vooral Marieke, Shadhvi en Kees, zonder jullie was ik nergens in de wereld van cellen, kleuringen en gelletjes; mede pancreas collega's Jesse en Labrinus; mijn wetenschapsstage studenten Kim en Martijn. En JJ, ook al viel je niet onder mij, wel bedankt voor je toevoeging aan J3; Martine Frouws, met mijn wetenschappelijke stage is het allemaal begonnen.

Dank aan alle betrokken specialisten voor hun geduld en enthousiasme.
Rutger-Jan, veel dank voor de fijne samenwerking, jouw bijdragen aan mijn onderzoeken, alle gezelligheid tijdens congressen, skireis en borrels, ongetwijfeld blijft dit voortbestaan.
Henk, ik ken je al jaren, en mede dankzij jou heb ik een fijne tijd gehad in het LUMC. Wie had ooit gedacht dat we samen zouden publiceren. Dr. Bonsing, Bert, voor mij ben je een grote inspiratie, ik heb veel van je geleerd en hopelijk blijven we de wetenschapsweekenden in de boerderij in Friesland gewoon voortzetten.
Dr. Groot Koerkamp, Bas, met veel plezier luister ik naar jouw enthousiaste verhalen, inzichten en visie.
Prof. Morreau, zonder u zou een significant deel van mijn proefschrift er niet zijn geweest, hartelijk dank voor deze begeleiding. U heeft mijn wereld op het gebied van moleculaire diagnostiek zeer verbreed. Arantza, wat een geduld heb jij gehad met al onze opnames van de resectiepreparaten; bedankt voor alle pathologische ondersteuning en het trouw nakijken van mijn manuscripten.
Dr. Burgmans, Mark, bedankt voor de jarenlange prettige samenwerking en alles wat je mij op radiologisch gebied hebt bijgebracht. Shirin, door jou begrijp ik iets van MRI scans en echografie. Ik heb genoten van ons onderzoek samen en wat heb ik je daarna gemist tijdens de pancreas MDO's.
Plastisch chirurgie afdeling bedankt voor het genieten tijdens de niet-wetenschappelijke kant van mijn PhD traject. Piet en Marlies, ik ben extra trots op ons nieuw opgezette en veelbelovende onderzoek, hopelijk kunnen we dit met veel plezier voortzetten.

Al mijn lieve vriendjes en vriendinnen, teveel om op te noemen, ik ben gezegend met jullie. Parels, met jullie is het nog steeds zo'n feest als vroeger op de Schelpenkade. Oude Beursgang, het maakt niet uit hoe lang we elkaar niet zien, het blijft altijd hetzelfde. Maddy, ik ben zo blij met jou als nieuwe roomie! As, Gab, Stef, Lil, Car, Marge, Clara, Co, Sop, Mary, Laurens, Lau, Doon en Fer, jullie staan altijd voor mij klaar en ik heb ontzettend veel aan jullie gehad de afgelopen jaren!

Essie, dankzij jou harde werken is mijn werk nu vereeuwigd in een prachtig boek! Heel erg bedankt!

Liefste paranimfen, niemand die ik liever naast mijn zijde heb staan dan jullie. Yvette, wij delen een enthousiasme voor veel dezelfde passies wat vaak resulteert in enorme pieken en optimaal genieten, ik ben zo blij dat ik jou als vriendinnetje over heb gehouden aan mijn promotietijd. Lieve Eef, waar te beginnen, ik kan er een boek over schrijven. Jij hebt mijn leven op zoveel fronten verreikt, zonder jou kan ik me niet meer voorstellen. Wat ben ik blij dat ze ons hebben uitgevonden!

Lieve Elles, ik ben trots dat je het zo goed doet. Lieve Jet, ik had me geen betere zusterband kunnen wensen, je bent er altijd! Willem, lief broertje, jouw vrolijkheid en doorzettingsvermogen maken mij een trotse zus. Lieve mama, dank voor je onvoorwaardelijke steun en vertrouwen, ik kan altijd bij je terecht. Lieve pap, er is niemand met wie ik zo goed over de medische wereld kan sparren en daarvan kan genieten als met jou. Dank voor alle mogelijkheden die je me geeft. Zonder jullie zou ik nooit gekomen zijn waar ik nu ben.